UNIVERSIDADE DA BEIRA INTERIOR
Engenharia

Development of an UAV for the Air Cargo Challenge 2017 Competition

versão final após defesa

Alexandra Almeida Gomes

Dissertação para obtenção do Grau de Mestre em
Engenharia Aeronáutica
(Ciclo de estudos integrado)

Orientador: Prof. Doutor Miguel Ângelo Rodrigues Silvestre

Covilhã, dezembro de 2017

''The best view comes after the hardest climb''

(Unknown)

Acknowledgements

There are many people to whom I would like to thank for helping me over the last year in my research and studies and that have made this dissertation possible.

First, I would like to thank to my supervisor, PhD Miguel Silvestre for allowing me the opportunity to work and participate with you in several international projects along the last three years.

Further, I would like to thank those with whom I worked with during the Air Cargo Challenge 2017 project. This obviously includes the team AERO@UBI_MARS, for the commitment and dedication with which they have embraced this project.

At the same time, I would like to thank my life partner, Filipe Chaves, for everything you did for me and for helping me keep it all in perspective.

Finally, and most importantly, I would like to thank my parents for allowing me to realize my own potential. All the support they have provided me over the years was the greatest gift anyone has ever given me.

Abstract

The present dissertation reports the development of an unmanned remotely piloted aircraft for the Air Cargo Challenge 2017 competition. Air Cargo Challenge is a Design, Build, Fly Aeronautical Engineering competition held in Europe every two years. Given the frequent participation of the Department of Aerospace Sciences from University of Beira Interior in this competition and considering the lack of documentation regarding these participations, this Master of Science Dissertation aims to transmit the accumulated knowledge to future teams and the UAV development community.

The aircraft was developed using computer aided engineering tools in the greatest possible extent. The tools used for the development effort include: OpenFOAM®, XFOIL/XFLR5 for airfoil development and detailed wing design and analysis; 3D CAD software as Dassault Systems CATIA® V5 and SolidWorks®; CNC rapid prototyping like 3D printing and CNC hot wire foam core cutting. Experimental test rigs were developed for different studies regarding LiPo batteries for the propulsion and flight testing of high lift devices and roll control.

New low Reynolds number airfoils were designed as well as a Fowler flap with an innovative extension mechanism. This mechanism was built using 3D printing technology. Several tests were performed to different batteries to maximize propulsive system power. Furthermore, for the first time in an Air Cargo Challenge, a University of Beira Interior team used mould technology to build the aircraft in carbon fibre reinforced plastics.

Several delays and mishaps prevented the development of the aircraft from being completely ready for the competition.

Keywords

Aircraft, UAV, Air Cargo Challenge, Fowler Flap, Low Reynolds Number, Airfoil, XFOIL, XFLR5

Resumo

A presente Dissertação reporta o desenvolvimento de um veículo aéreo não tripulado para a competição Air Cargo Challenge 2017. O Air Cargo Challenge é uma competição de Engenharia Aeronáutica do tipo Design, Build, Fly, que acontece na Europa a cada dois anos. Dada a frequente participação do Departamento de Ciências Aeroespaciais da Universidade da Beira Interior nesta competição e considerando a falta de documentação relativa a estas participações, esta Dissertação de Mestrado pretende transmitir o conhecimento acumulado para futuras equipas e para a comunidade que desenvolve UAV.

A aeronave foi desenvolvida, tanto quanto possível, com ferramentas de engenharia assistida por computador. As ferramentas usadas incluem: OpenFOAM®, XFOIL/XFLR5 para o desenvolvimento de perfis, desenho e análise detalhados da asa; software CAD 3D Dassault Systems CATIA® V5 e SolidWorks®; ferramentas de prototipagem rápida como impressão 3D e máquina CNC de corte de espuma com fio quente. Foram desenvolvidas diferentes bancadas de teste para estudos de baterias LiPo para a propulsão e para ensaios de voo de dispositivos híper-sustentadores e de controlo de rolamento.

Foram desenhados novos perfis de baixo Reynolds bem como um flap Fowler com um inovador mecanismo de extensão. Este mecanismo foi construído com tecnologia de impressão 3D. Vários testes foram feitos para diferentes baterias de forma a maximizar a potência do sistema propulsivo. Além disso, pela primeira vez uma equipa da Universidade da Beira Interior utilizou tecnologia de moldes para construir o avião em plásticos reforçados com fibra de carbono.

Diversos atrasos e imprevistos levaram a que a aeronave não estivesse plenamente desenvolvida e pronta para participar na competição.

Palavras-Chave

Avião, UAV, Air Cargo Challenge, Flap Fowler, Baixo Número de Reynolds, Perfil Alar, XFOIL, XFLR5

Table of Contents

List of Figures

List of Tables

Nomenclature

ABS - Acrylonitrile Butadiene Styrene

ACC – Air Cargo Challenge

ACC15 – Air Cargo Challenge 2015 edition

ACC17 – Air Cargo Challenge 2017 edition

APAE – Portuguese Association of Aeronautics and Space

CFD – Computational Fluid Dynamics

CFRP – Carbon Fibre Reinforced Plastic

CNC – Computer Numerical Control

EPS - Pultruded Polystyrene Foam

ESC – Electronic Speed Controller

EUROAVIA – European Association of Aerospace Students

FCP – Flight Competition Points

GFRP – Glass Fibre Reinforced Plastic

IST – Instituto Superior Técnico

MOSFET - Metal Oxide Semiconductor Field Effect Transistor

MTOW – Maximum Take-Off Weight

PB – Prediction Bonus

PCP – Project Competition Points

PID – Proportional Integral Derivative Controller

PLA - Polylactic Acid

RANS – Reynolds Averaged Navier-Stokes

R/C – Radio Controller

SAW – Simple Additive Weighting

TB – Time Bonus

UHMWPE - Ultra High molecular weight polyethylene, Dyneema®

UHMW - Ultra High molecular weight polyethylene, Dyneema®

UAV - Unmanned Aerial Vehicle

UBI – University of Beira Interior

URANS - Unsteady RANS

List of Symbols

A_R – Aspect ratio

A_{RWing} – Wing aspect ratio

A_{R_V} – Vertical tail aspect ratio

A_{R_H} – Horizontal tail aspect ratio

b –Wing span

b_H –Horizontal tail span

b_V – Vertical tail span

b_{ref} – Reference span

c – Airfoil chord

c_{ref} – Reference chord

C_d – Drag coefficient of the airfoil

C_{D_p} – Total parasitic drag coefficient

$C_{D_{pi}}$ – Parasitic drag coefficient corrected for the Reynolds number

$C_{D_{p_{i_{Re_{ref}}}}}$ - Airfoil parasite drag coefficient at a known Reynolds

$C_{D_{ph}}$ - Horizontal tail airfoil drag

$C_{D_{pv}}$ – Vertical tail airfoil drag

$C_{D_{pW}}$ – Wing airfoil drag

C_{Di} – Total induced drag coefficient

$C_{D_{i_w}}$ – Wings induced drag coefficient

$C_{D_{i_h}}$ – Horizontal tail induced drag coefficient

C_{dmin} – Airfoil minimum drag coefficient

$C_{D_{mis}}$ – Miscellaneous drag coefficient

C_l – Airfoil lift coefficient

C_L - Aircraft lift coefficient

C_{L_h} - Lift coefficient of the horizontal tail

C_{Lmax} – Maximum lift coefficient of the wing

$C_{l\alpha max}$-Highest lift curve slope

$C_{l_{max}}$ – Airfoil maximum lift coefficient

$C_{l_{max\ Re_{Ref}}}$ – Maximum lift coefficient at reference Reynolds number

C_m – Pitching moment coefficient

$C_{Min_{Cap_{Battery}}}$ - Minimum capacity in the battery

D – Drag force

e – Oswald efficiency factor

F_{legs}- Flown legs

F_{TO}- Take-off force

g - Gravitational acceleration

GS – General Score

h_{CG}- Aircraft's longitudinal distance from center of gravity to the datum in number of number of wing mean geometric chords

h_h- Wings aerodynamic center longitudinal distance

h_H- Horizontal tail arm

h_V- Vertical tail arm

I- Current intensity

k – Turbulence kinetic energy [m^2/s^2]

k_i – Constant value

L – Lift Force

L/D – Lift-to-drag ratio

m – Mass [kg]

$m_{batteries}$ – Batteries mass [kg]

m_{EMPTY} – Empty mass [kg]

$m_{payload}$ – Payload mass

m_{total} – Total mass

MAC_{EH} – Horizontal tail mean aerodynamic chord

MAC_{EV} – Vertical tail mean aerodynamic chord

MAC_{Wing} – Wing mean aerodynamic chord

M – Pitching moment [N/m]

RC – Climb Rate

P – Penalties

$P_{pflight}$ – Points for each flight

Re – Reynolds number

$Re_{Cl_{ref}}$ – Lift coefficient at reference Reynolds number

Re_{Ref} – Reference Reynolds number

Re_{exp} – Correction exponent

S – Wing Area

S_H – Horizontal Tail Area

S_V – Vertical Tail Area

S_{fus} - Fuselage area

T – Thrust

$T_{available}$- Available thrust

T_{static} – Static thrust

TB – Time Bonus

T_R – Required Thrust

V_∞ – Airspeed $[m/s]$

V_{flight} - Flight speed

V_{LO} - Lift-off speed

x_{NP} - Neutral point position

x_{CG} - CG position

X_{TO} - Take-off distance

w- Proportionality function of the empty weight to the payload mass

W - Weight

W_{EMPTY} – Empty weight

W_{pay} – Arbitrated Payload weight

W_{sys} – Systems weight (motor, propeller, ESC, battery, receiver)

$W_{0_{ref}}$ - Reference airplane weight

Greek Symbols

α – Angle of attack

α_i - wings induced angle of attack correction

$\alpha_{C_{lmax}}$ – Angle of attack for maximum lift coefficient

μ – Dynamic viscosity $[N \cdot s/m^2]$

μ_0 – Dynamic viscosity at 0m altitude $[N \cdot s/m^2]$

ρ – Fluid density $[kg/m^3]$

ρ_0 – Fluid density at 0m altitude $[kg/m^3]$

γ – Climb Angle

π – Pi number

λ_{Wing} – Wing taper ratio

1 Introduction

1.1 Motivation

The motivation for this work was the need to transmit the accumulated knowledge gathered from Air Cargo Challenge (ACC) participations through a written document. To date, the University of Beira Interior (UBI) has a large track record (See Section 1.3 History of UBI's Participation in the Air Cargo Challenge) on the ACC, but documentation on these participations is scarce.

The main objective of this Master Degree dissertation is to document the development of the AERO@UBI_MARS aircraft for participation in the Air Cargo Challenge 2017 (ACC17) competition. Until now the knowledge that the teams had was transmitted by the faculty advisors, Dr. Miguel Ângelo Silvestre and Dr. Pedro Gamboa. The former also pilot of UBI ACC teams.

1.2 The Air Cargo Challenge Competition

The Air Cargo Challenge is an Aeronautical Engineering competition in Europe that is held every two years primarily directed to Aeronautical and Aerospace Engineering students [1]. It was founded by the Portuguese Association of Aeronautics and Space, in Portuguese *Associação Portuguesa de Aeronáutica e Espaço* (APAE). The first edition was in 2003 as a national competition but now is a worldwide event in aeronautics academia.

The Air Cargo Challenge offers students the unique opportunity to develop a challenging multidisciplinary project from the basic research to the finished product. By participating in the ACC, the teams can test their knowledge and, at the same time, get involved with a wide range of challenges which students will find in their future professional career: technical, interpersonal and financial skills as well as strict deadlines.

In 2007 the competition grew to an international level under the umbrella of EUROAVIA, the European Association of Aerospace Students, and the winning team got the possibility of organizing the next edition.

The competition has several punctuation items: design report, technical drawings, oral presentation, cargo loading time and flight task. The proof of flight is mandatory at the oral presentation, otherwise the team is disqualified by the organizing committee based on safety issues. A safety inspection is performed on every aircraft before the flight competition starts. The safety inspections include the following: Physical inspection of the aircraft to ensure

structural integrity and to verify compliance with the design report and technical drawings and before each flight a wing structural test is done (see Figure 1.1). To obtain points without penalties, the aircraft must take off in a 60m runway strip and has design restrictions such as the use of a specific motor and propeller and other limiting factors such as: limited span (2003, 2005 and 2007), limited lifting area (2009), limited empty weight (2011) and required to fit inside a transportation box (since 2009). Typically, the main objective was to take-off with the maximum possible payload; now, new and more specific tasks are required.

A major change began with the organization team of University of Stuttgart for ACC15. The team had to design, build and fly a remotely controlled airplane that could lift off in 60m with the maximum possible payload and fly as many 100 meter legs as possible in two minutes (see Figure 1.2) [2]. The number of points was determined using the formula given by (Equation 1.1.

$$FCP = \left(2F_{weight}\,[kg]\right)\left(F_{legs} + a\right)b \qquad \textbf{(Equation 1.1)}$$

Where FCP is Flight Competition Points, F_{Weight} the Flown payload mass in kg, F_{Legs} is Flown Legs.

a = 2 for a valid start + non-valid landing

a = 3 for a valid start + valid landing

b = 1 for a valid flight without crash

b = 0 for airplane losing parts or crashes or invalid start

The Maximum Take Off Weight (MTOW) was an important factor in the new flight task, but the speed and agility of the aircraft proved to be a major factor in the outcome of the competition. So, in the 2015 edition, the winning team was not the team that loaded the most weight. In ACC15, the AERO@UBI team reached the 5th place, distinguished by the fact that it was one of the lightest aircraft, about 2.2 kg and performed with a payload of 10.2kg for ten legs despite having flown with a payload of 11.2kg in an invalid flight, having the best result amongst the Portuguese teams. At the national level, a team from Instituto Superior Técnico (IST) - Olisipo, and a team from the University of Porto - Phoenix ranked in 12th and 23rd places, respectively.

Over the years, rules and regulations have been modified, however, maximizing take-off weight has remained one of the major goals. Typically, as in the current 2017 ACC edition, a bonus is added to the final score if the payload prediction is close to the actual payload flown in the competition. The payload Prediction Bonus (PB) is given according to Equation 1.2.

$$PB = 10\left(1 - \frac{|predicted\ payload - actual\ payload|}{predicted\ payload}\right) \qquad \textbf{(Equation 1.2)}$$

Further bonification points are added if, at the flight competition, the teams load the aircraft in under two minutes. For this Time Bonus (TB), the shorter the time a team uses to insert the payload in the aircraft, the more points it gains. The relation is according to Equation 1.3.

$$TB = 24\left(1 - \frac{t}{120}\right) \quad <= \quad t < 120s$$

$$TB = 0 \quad <= \quad t \geq 120s$$

(Equation 1.3)

If the team uses two minutes or more the bonus is zero, but there is no penalty if more than two minutes are needed.

In the current edition, ACC17, as in previous editions, there is a 3-minute time window for performing a successful take off and multiple attempts are possible during this time frame. After that, there is a 30 second time window for the aircraft to gain altitude and airspeed to prepare for taking the course before entering the 1st leg. Each leg is 100 meters long (see Figure 1.1). The countdown starts once the aircraft has passed the course start line (or after the 30 seconds for gaining altitude are over) and stops after 10 legs were fully flown [3].

According to the Requirements, Rules and Evaluation for the Air Cargo Challenge 2017 the General Score (GS) is according to Equation 1.4:

$$GS = FCP + PCP + P + Bonus$$

(Equation 1.4)

Where,
FCP are Flight Competition Points
PCP are Project Competition Points
P are the Penalties

The PCP score was:

- Detailed drawings = max. 30 points
- Report = max. 50 points
- Estimated Payload = max. 10 points
- Oral presentation = max. 30 points

Penalties would result from exceeding the oral presentation time or delays in delivery of reports and other documents. The reports, drawings, the estimated payload chart and the 3-view drawings should be delivered to the organization at or before the deadline. If the teams fail this deadline or have delays in delivering reports/drawings and delays during the competition,

they can lose points or even be disqualified. The oral presentation is restricted to 15 minutes and must include a movie that proves that the aircraft has previously flown, otherwise the team can be penalized. The teams can be disqualified if they disregard the regulations, if the video of proof of flight is missing, for breaking security rules or if aircraft parts are transported outside the transportation box. Flying outside a specified area and flying over spectators contributes to the team being disqualified in that round.

The biggest difference of ACC17 in respect to the 2015 edition is that it aimed to carry the maximum possible weight and fly in the minimum time 10 legs in the same 100m course (see Figure 1.2). The number of points are determined according to Equation 1.5.

$$P_{pflight} = 2\, m_{payload} \left(\frac{1000\ [m]}{t\ [s]} + a \right) b \qquad \textbf{(Equation 1.5)}$$

Where,
$P_{pflight}$ is points for each flight
$m_{payload}$ is payload mass
a = 0 for a valid start + on-valid landing
a = 0.5 for a valid start + valid landing
b = 1 for a valid flight without crash
b = 0 for airplane losing parts or crashes or invalid start

The most significant rule change compared to previous editions is that the final flight competition points correspond to the sum of the points of the two highest scored flights. The payload prediction and time bonus is the same as in previous editions, see (Equation 1.2 and Equation 1.3.).

In this edition, the aircraft must be able to perform the structure validation test before the flight competition. The wing will be supported at two points located at each wing tip as seen in Figure 1.1. The structural test consists of lifting by hand the fully loaded aircraft before each flight and it must be able to withstand this load without failure. This test is to simulate a load during the flight and it is done for safety reasons.

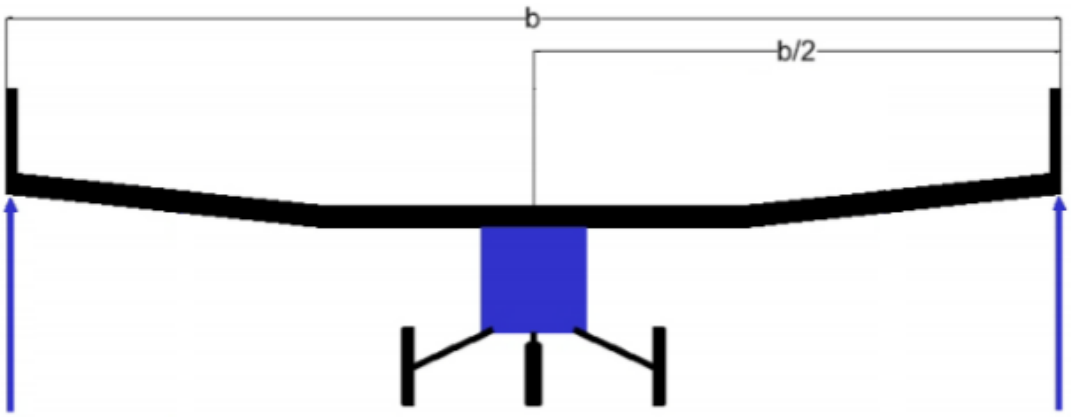

Figure 1.1 - Structural validation test [3].

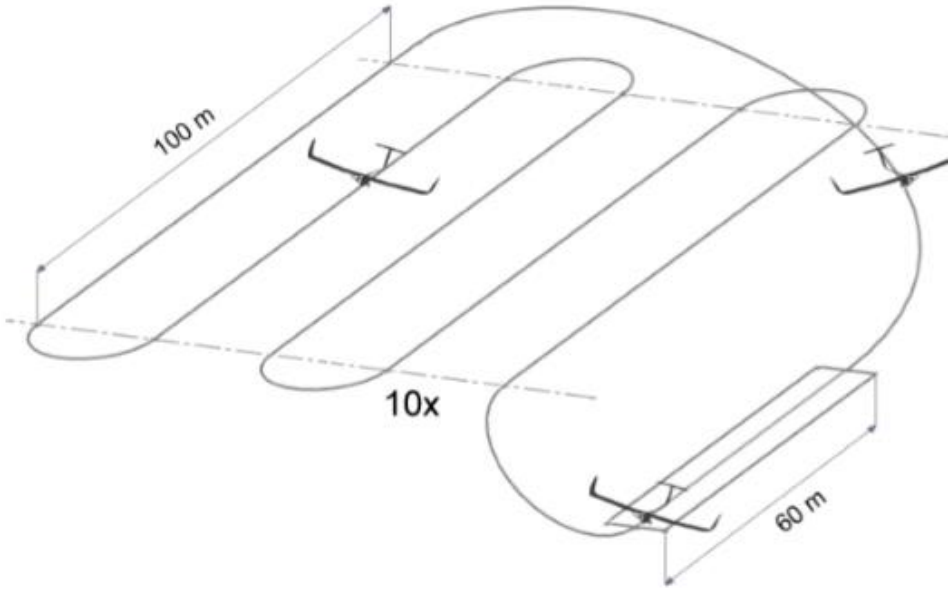

Figure 1.2 - 100 m legs [3].

1.3 History of UBI's Participation in the Air Cargo Challenge

UBI has participated in all editions of ACC, achieving an important record of results: 1st place and 3rd in 2003, again 3rd in 2005 and 1st place in 2007 and 2011. In the last edition, 2015 ACC the UBI team was fighting for victory but only got the 5th place after struggling with the difficulty of the new pylon race flight task.

Many designs have been tested over successive ACC editions making UBI a competitive player by the accumulated know-how. Various configurations (see Figure 1.3), structure types, materials, concepts regarding various solutions have been tested. A peculiar methodology of

development has been established based in research and experimentation. By winning the 2007 and 2011 editions, UBI has organized the 2009 and 2013 ACC events, giving Akamodell Stuttgart the opportunity to take the 1st place and host the last ACC, the 2015 edition. In 2015, the UBI team got the 5th place in the competition with a payload of 10.2kg but only 10 legs against the 10kg and 14 legs of the winner, the team from Zagreb.

Figure 1.3-UBI teams ACC participant designs over the years

In 2017 the current Air Cargo Challenge is being organized by EUROAVIA Zagreb from University of Zagreb. The University of Beira Interior is going to participate with two teams,

AERO@UBI_MARS and AERO@UBI_PVG, each with an aircraft of different configuration and design philosophy and construction technology.

1.4 Objectives

The present dissertation shares the same basic objective as those of the ACC competition, which is to stimulate student's interest in aeronautics. But in particular, the present document aims at:

- Describe the peculiar methodology of development that has been established based in research and experimentation for UBI's previous ACC participations;
- Share information for future teams;
- Contribute to the advancement of UAV development state of the art.

1.5 Overview

After this introductory chapter, in which the motivation, the essence of the Air Cargo Challenge competition, the history of University of Beira Interior at the Air Cargo Challenge and the objectives of this dissertation where described, the present dissertation is divided according to the following structure:

- Chapter 2 presents the literature review. Starting with a brief explanation of the fundamental theory behind the design of wings and airfoils for Low Reynolds numbers, the chapter closes with a state of the art presentation, were the most relevant airplanes, in respect to the current 2017 ACC edition, to take part on the competition are analysed.

- Chapter 3 presents the methodology. It begins by describing the research that fed the aircraft design. From the experiments regarding the propulsion system performance to the aerodynamics, including the development of the airfoil and the Fowler flap, roll control surfaces and the construction tests. The remainder of the Chapter is dedicated to the conceptual, preliminary and detailed design. The final Section is a description of the construction of the AERO@UBI_MARS Team aircraft for the ACC 2017.

- Chapter 4 presents the results and respective analyses.

- Chapter 5 concludes this dissertation with an overview of the work, main conclusions and some recommendations for future work.

2 Literature Review

2.1 Basic Theory

2.1.1 Wing Design

The wing may be considered as the most important component of the airplane. Wing geometry, with its basic characteristics, fundamentally span and mean chord, influences the aircraft configuration. *E.g.*, an airplane with high aspect ratio (high span and low mean wing chord) is more prone to have the horizontal tail in front of the vertical tail and *vice versa*. The primary function of the wing is to generate sufficient lift force (*L*). As consequences of generating lift, there is a drag force (*D*) occurrence and normally a nose-down pitching moment (*M*). While it is desired to maximize lift for a given dynamic pressure ($0.5\rho V^2$, with ρ being the air density and V the airspeed) the other two (drag and pitching moment) should be minimum for the sake of the airplane performance. This is why the ration *L*/*D* is known as aerodynamic efficiency. Wing pitching moment can be due to excessive wing sweep but for a straight wing it is mainly due to the airfoil pitching moment coefficient [4].

Wing drag is typically the highest share of the airplane's drag. Figure 2.1 shows the ACC2015 aircraft drag polar, it is seen that when going from a 2D airfoil to a 3D wing, the drag polar will be the sum of the profile drag of the airfoil, C_{dp} and the miscellaneous parasite drag from the rest of the aircraft and the induced drag, C_{Di}. Hence the importance of minimizing profile drag (i.e. pushing the profile drag curve to the left of the graph. Note that, as the lift coefficient gets lower, the profile drag becomes an increasingly higher proportion of the overall drag. So, the airfoil selection or design is an important stage of the aircraft development. For high aspect ratio ($A >> 6$) the wing behaviour (Lift) is closer to that of a 2D airfoil due to small tridimensional flow effect that is mostly concentrated on the wing tips.

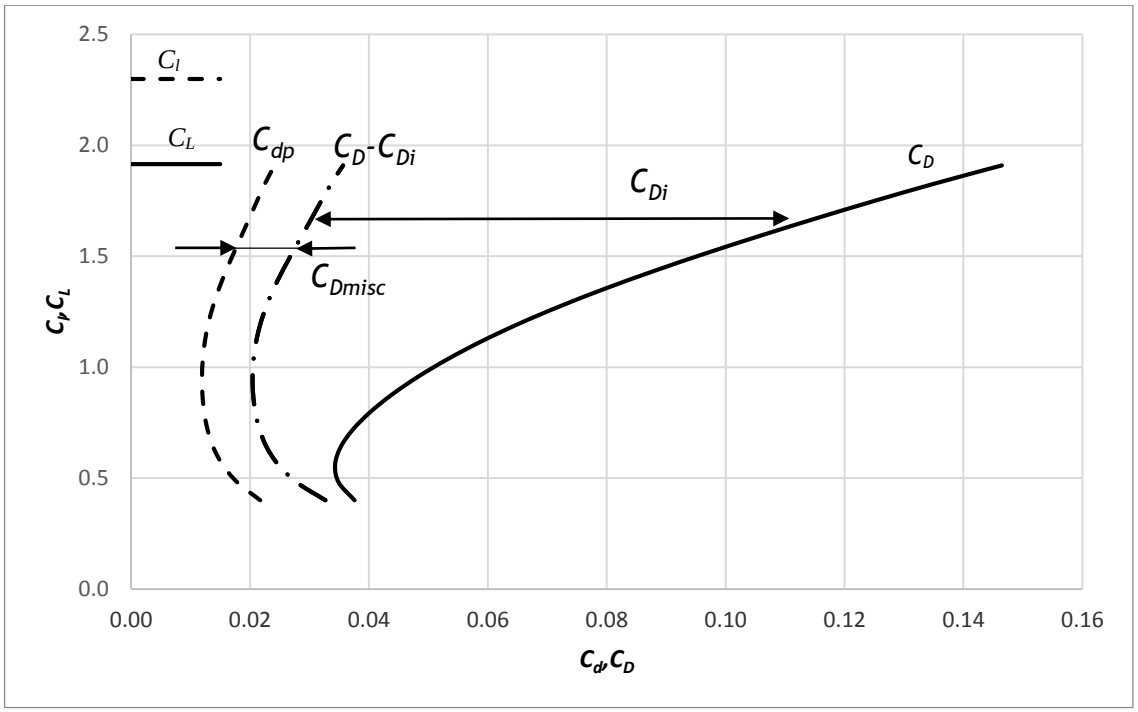

Figure 2.1 – Estimated drag polar of UBI ACC2015 Aircraft, respective wing airfoil drag and total drag minus the Induced Drag. Airfoil and aircraft maximum lift coefficients on the top.

The airplane's performance is determined by the excess of thrust, considering its mass, along the airspeed envelope. Excess thrust is the difference between the available propulsive thrust and the required thrust to maintain level flight. The required thrust must be equal to the airplane drag for permanent level flight as the lift must equal the weight in level flight.

In practice, the objective for any fixed wing aircraft design, *i.e.*, any airplane, is to maximize the aerodynamic efficiency, L/D, for any flight speed. Equation 2.1, gives the required thrust, T_R, for any airplane in level flight at constant airspeed. It is clear that the higher the aerodynamic efficiency, the smaller the required energy per unit of travelled distance. Equation 2.1 also shows that for a fixed available thrust versus airspeed, if you want to maximize the weight and the speed at which you fly, improving L/D becomes fundamental in increasing the payload and the cruise speed. The ACC flight competition score is directly proportional to both payload and cruise speed.

$$T_R = \frac{W}{L/D} \qquad \textbf{(Equation 2.1)}$$

Where $W = mg$ is the aircraft's weight, $g = 9.80665\ m/s^2$and m is the mass.

An aerodynamic force coefficient is defined for the aerodynamic force dividing the force by the dynamic pressure of the relative wind and also by the wing area. So, drag is given by Equation 2.2:

$$D = \frac{1}{2}\rho V^2 S C_D \quad \textbf{(Equation 2.2)}$$

Where,

$$C_D = C_{dp} + C_{Dmisc} + KC_L^2 \quad \textbf{(Equation 2.3)}$$

With C_{Dmisc} is the drag coefficient resulting from all other drag sources than the wing and KC_L^2 is the induced drag coefficient and *K* is referred to as induced drag factor and is modelled by Equation 2.4.

$$K = \frac{1}{\pi A_R e} \quad \textbf{(Equation 2.4)}$$

Where, e is the Oswald factor that is a function of the wing sweep, dihedral and chord distribution along the span, and the aspect ratio given by Equation 2.5:

$$A_R = \frac{b^2}{S} \quad \textbf{(Equation 2.5)}$$

In order to maximize L/D, one must consider that its value is the same in the nondimensional form: C_L/C_D. So, if the minimum value of C_D in reality tends to have a lower limit, the obvious way of improving C_L/C_D is to increase the C_L for the complete airspeed range. Considering that the lower limit of the speed range is also defined, in general aviation by a maximum stall speed limit but in ACC by the speed that can be reached in a 60 m take-off with a given mass and propulsive system thrust, Equation 2.6 shows that to increase C_L, the wing loading, W/S, also has to be maximized. On the other hand, Equation 2.7 shows that the D can increase significantly with C_L cancelling any gain in L/D. So, according to Equation 2.8 the span loading W/b must be kept constant. *I.e.*, a given weight must correspond to a constant span in the effort of maximising W/S. It becomes obvious that W/S must increase solelly by lowering the mean chord raising the problem of wing structure strength and rigidity on one perspective and also the problem of a lower Reynolds number effect in airfoil performance.

$$C_L = \frac{1}{0.5\rho V^2}\frac{W}{S} \quad \textbf{(Equation 2.6)}$$

$$D_i = WKC_L \quad \textbf{(Equation 2.7)}$$

$$D_i = \frac{1}{0.5\rho V^2 \pi e}\left(\frac{W}{b}\right)^2 \quad \textbf{(Equation 2.8)}$$

2.1.2 Low Reynolds Number Airfoils

The selection of an airfoil for the wing depends on the requirements of the airplane. For instance, freighter aircraft design requirements are quite different from an aerobatic airplane design objectives.

In general, the following are the criteria that some designers use to select an airfoil for the wing [5]:

1. Maximum lift coefficient ($C_{l_{\max}}$)
2. Lowest minimum drag coefficient ($C_{d_{\min}}$)
3. Highest lift-to-drag ratio ($(C_l/C_d)_{\max}$)
4. Highest lift curve slope ($C_{l_{\alpha\max}}$)
5. Lowest pitching moment coefficient (C_m)

In most of the cases, there is a compromise between these parameters and a weighting process, because all design parameters have not the same importance.

The Reynolds number (***Re***) is a measure of the ratio of inertial forces order of magnitude to viscous forces order of magnitude in a fluid flow. It is of great importance in the analysis of the boundary layer flow. It is defined as Equation 2.9:

$$Re = \frac{\rho V c}{\mu} \qquad \textbf{(Equation 2.9)}$$

Where c is reference length (e.g. wing chord being analysed) in m,
V is the airspeed in m/s,
ρ is the air density in kg/m^3,
μ is the air absolute viscosity in Pa.s .

For the SI system at mean sea-level conditions: $\rho_0 = 1.225\ kg.m^{-3}$ and $\mu_0 = 1.789 \times 10^{-5}\ Pa.s$, the expression becomes:

$$Re = 68500\ Vc \qquad \textbf{(Equation 2.10)}$$

For the ACC UAVs, for their typical airspeed and medium aerodynamic chord, a low number Reynolds (<500 000) will be present. However, for any given airplane in level flight, at constant altitude, the product of ***Re*** times the square root of the lift coefficient remains constant.

$$Re\sqrt{C_L} = \mathrm{k_i} \qquad \textbf{(Equation 2.11)}$$

Where, k_i is a constant value for a given aircraft mass, wing area and altitude.

Figure 2.2 shows the typical effect of *Re* number on an airfoil lift curve and drag polar. When the *Re* increases, the drag polar typically gets wider see right side of Figure 2.2 because for thick (t/c>0.06) airfoils, a higher *Re* delays the forward shift of the rear separation point with increasing angle of attack (α), ultimately delaying stall [5]. The slope and the intersection of the linear region to horizontal and vertical axes are usually unaffected by the Reynolds number. However, the higher the Reynolds number, the higher the stall angle of attack, α_1, α_2 and α_3, and respective maximum lift coefficients, $C_{L_{max\,1}}$, $C_{L_{max\,2}}$ and $C_{L_{max\,3}}$ in a nonlinear behaviour. This phenomena is more pronounced when the *Re* number gets below a given value known as the critical Reynolds number of the airfoil. This effect is purely viscous but it can be estimated with XFOIL [6][7] through XFLR5 [8].

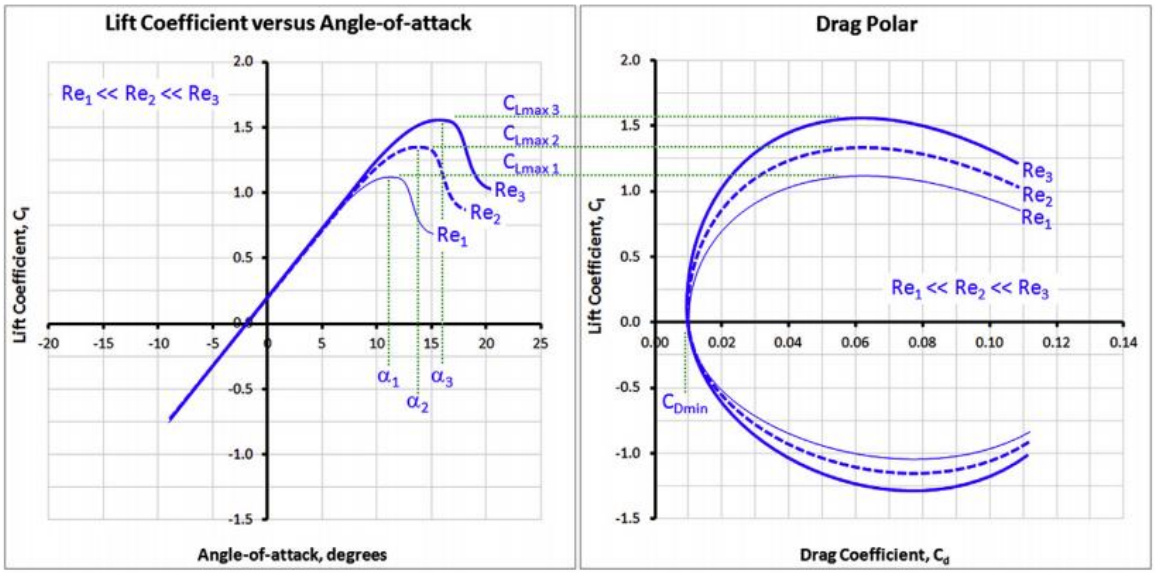

Figure 2.2 - The effect of Re number on lift curve and drag polar, [4].

Mark Drela was the author of XFOIL program, in the 80's with the objective of designing and analysing airfoils with the condition of subsonic Mach number. The program can calculate the pressure distribution, the lift, the drag in its pressure and friction parcels, the pitching moment as well as the boundary layer transition position in upper and lower surfaces of the airfoil by Computational Fluids Dynamics (CFD) with a viscous/inviscid two-dimensional panel method formulation code. XFOIL has been widely validated and its results follow closely the experimental data as shown in Figure 2.3. Nevertheless, as it is clear from the graph, XFOIL seems to underestimate the drag coefficient by about 5%.

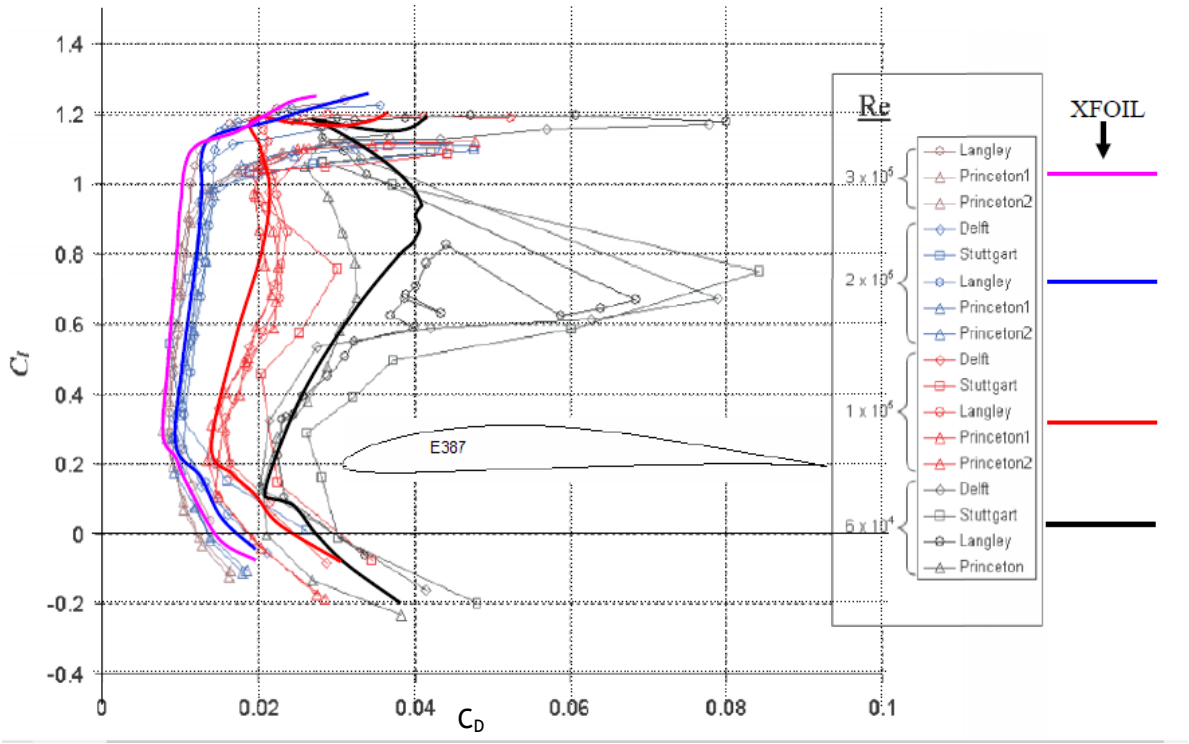

Figure 2.3 – XFOIL prediction performance (adapted from McArthur 2008), [9].

2.2 State of Art

In the present Section, the best ACC aircraft are described and analysed considering the requirements of the current ACC2017 edition.

In 2011, the team from UBI was the winner of the competition. The idea was to lift the maximum possible weight, but with a limitation on the Empty Weight (W_{EMPTY}) of 1.800 kg. The construction method (see Figure 2.4) was the most appropriated at the time. The tail surfaces were a skin on frame structure made of balsa wood on the spars and ribs with foam cores. The wing had a Carbon Fibre Reinforced Plastics (CFRP) tube spar with balsa wood ribs. The wing interfaces were based on aeronautical grade aluminium alloy for the hard points and pultruded CFRP. The wing surface was made from thermoplastic heat shrink film skin. The cargo bay was made from balsa wood and pultruded CFRP rod reinforcements. The tail cone was made from a CFRP tube from an off the shelf fishing rod. The payload in the cargo bay was locked in place by a pultruded CFRP rod that passed through two carbon fibre rings on the bottom of the fuselage side walls. The very light weight construction allowed for a very large wingspan with high aspect ratio, which maximized wing surface while maintaining low drag. This allowed for the lifting of a very large payload (by comparison with the other competitors). In 2011 the only goal was to lift as much weight as possible.

Figure 2.4 - UBI's Winner Airplane 2011.

Figure 2.5 shows the ACC09 aircraft from AkaModell Stuttgart. It was one of the first aircraft to use slotted Flaps because the regulations of 2009 limited the lifting surface to only $0.75m^2$. To lift the highest possible weight, one solution was to design an aircraft with high aspect ratio. At the very high lift coefficient allowed by the slotted Flaps (see Figure 2.1), the drag of the wings is mostly induced drag: $C_D \approx C_{Di}$ and $C_{Di} = KC_L^2$, so by increasing the aspect ratio, K decreases (see Equation 2.4) limiting the drag coefficient for those higher lift coefficients. This maximizes excess power.

The slotted flaps maintain the airflow attached to the deflected flap upper surface, increasing the lift compared to a conventional flap, and also allow the airflow on the main element of the airfoil to remain attached for a longer distance along the upper surface, helping even further to maximize the maximum lift coefficient. The aircraft seems to be built with CFRP in the fuselage tube, Glass fibre reinforced plastic (GFRP) in the payload bay structural skin and unidirectional CFRP stringers and transverse frames, and flexible skin on frame with heat shrink film in balsa wood frame on the tail surfaces construction. The wings seem to be built from bidirectional GFRP sandwich skins and unidirectional CFRP spar and the flaps from a sandwich of solid foam core and lightweight bidirectional GFRP skins.

The design of the ACC2013 aircraft Stuttgart AkaModell was similar but the wing shells were different. Figure 2.6 shows the construction method (materials) of the Stuttgart aircraft. The wing had a foam core with an embedded wing spar. The core and the wing spar were then covered with a layer of glass. On top of this glass layer, carbon roving was applied (in the wing spar area) and then another layer of glass and carbon fibre spread tow was applied. The wing is finished with a coat of paint.

Figure 2.5 - AkaModell Stuttgart 2009 [10].

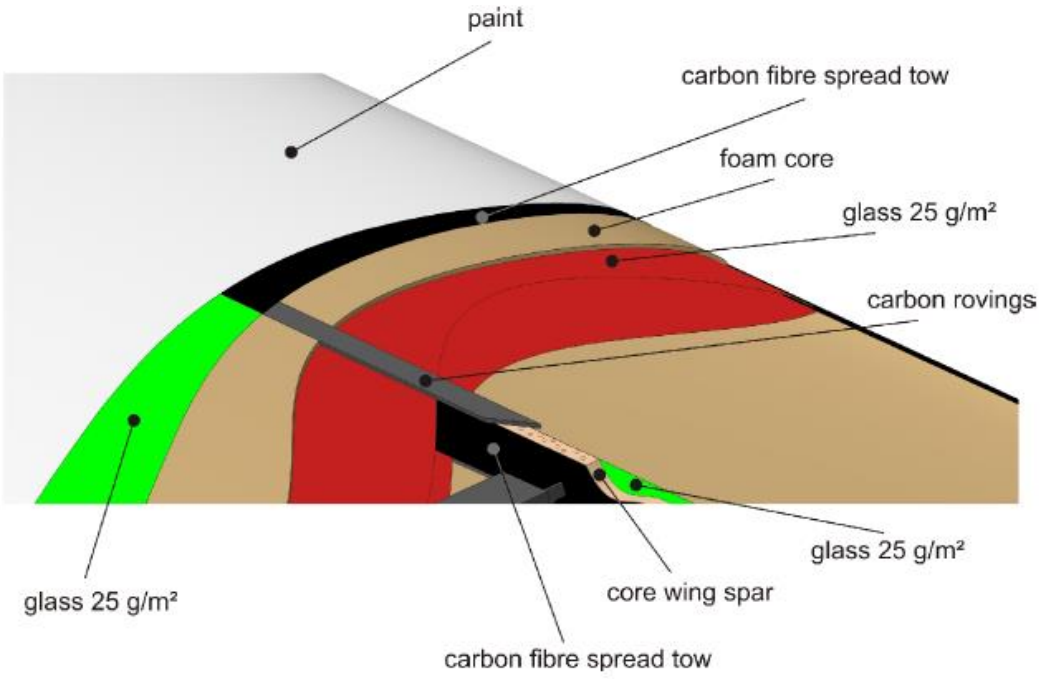

Figure 2.6 – AkaModell Stuttgart 2013 wing Shells, [10].

The aircraft shown in Figure 2.7 was built by Euroavia Zagreb team for ACC 2015. It is entirely made of bidirectional spread tow CFRP. They designed high relative chord slotted flaps to maximize the maximum lift coefficient and increase the wing loading while achieving the 60m take off run, [11]. To maximize the span fraction of the flaps, a rectangular wing planform was

used. The T tail was supported by a tail cone of apparent insufficient section as it wobbled during flight from lack of rigidity. In the last round, mostly due to the skills of the pilot, the Euroavia Zagreb team won the competition by lifting 10 kg and making 14 laps. They obtained 93.5 points in the oral presentation plus 370 points in the last flight, for a total of 463.5 points. In the 2nd place was the team Born TU Lift from Munich with 436.25 points (see Figure 2.8) and in 3rd place the EUROLIFTER team from Rzészow, Poland won with 379.15 (Figure 2.9).

For the conceptual design the winner of ACC15 used Simple Additive Weighting (SAW) method [11]. This method implies the study of all possible configurations of the components of the aircraft and then quantitatively evaluate these components in their positives and negative aspects. In the end the final configuration corresponds to configurations with highest score.

Figure 2.7 – Euroavia Zagreb Team 2015, [11].

The Team Born TU Lift participated in ACC 2015, with a very competitive biplane (see Figure 2.8) but they did not win, even though they lifted the highest payload weight. Apparently after a certain payload the more weight they lifted, the slower the airplane flew. Therefore, in their last flight they lifted more weight but performed fewer laps giving the chance for the team from Zagreb to do the last and victorious flight, going for first place. The airplane had a high aspect ratio, but because the total wing area is divided by two planes and in 2015 there was a wingspan limitation, each wing has a lower operating Reynolds number, leading to smaller airfoil efficiency of the wings' airfoil. On the other hand, they presented a remarkable full span two element flap that morphed the airfoil camber to adjust from the take off to the fast legs cruise and to the tight U turns high load factor flying condition at the end of each leg.

Figure 2.8 - Born TU Lift aircraft in ACC 2015, [12].

The Polish team got an honourable 3rd place with a high aspect ratio wing on the aircraft. Their aircraft was more focused on speed, thus lifting less weight while being able to perform more laps. The tail surfaces were skin on frame made out of the traditional balsa wood and heat shrink film covering. See Figure 2.9.

Figure 2.9 - EUROLIFTER team from Rzeszow, [13].

In the 2015 Edition, as shown in Figure 2.10, the UBI aircraft construction was very similar to the ACC 2011 winning airplane construction. The regulations limited the size of the aircraft to fit in a square of 2.5m side length, so the maximum possible wingspan was the diagonal of that square. The cargo bay was like the one of ACC 2011. In 2011, the payload was held in the cargo bay by a pultruded CFRP tube that passed through two unidirectional CFRP rings hanging from

the sides on the rear of the cargo bay. In 2015, the payload was locked in place by the landing gear itself which was placed on two hooks made from piano wire. These hooks design was problematic; the hooks proved not to be sufficiently resistant: bending by the landing gear load on them, which released the payload at the first take off in the competition. In subsequent flights the payload was locked in place by tying it with tape to the cargo bay body. Both UBI planes (ACC 2011 and ACC 2015) had a landing gear with only 2 wheels and a skid on the tail. This solution is lighter and provides a centre of gravity position check, since the airplane is balanced in the level position on the wheels, allowing a safe take off as long as the rudder has sufficient directional control while the tail ski allows the steering. However, the aircraft must gain sufficient speed for the rudder to become effective; this means that taking off with crosswinds is nearly impossible and the initial acceleration must be negotiated by the pilot, applying nose up command with the elevator and progressive throttle to prevent the drop of the nose to the ground. The wings' airfoil proved to be fundamental in the airplane's ability to lift 11.2 kg with a take-off in less than 60 meters in a non-valid flight. However, the aircraft suffered from flutter when flying at top speed, which compromised its safety and limited the speed in the legs. With the competition´s new focus on speed, the traditional full skin on frame wings construction that UBI used to employ is no longer adequate.

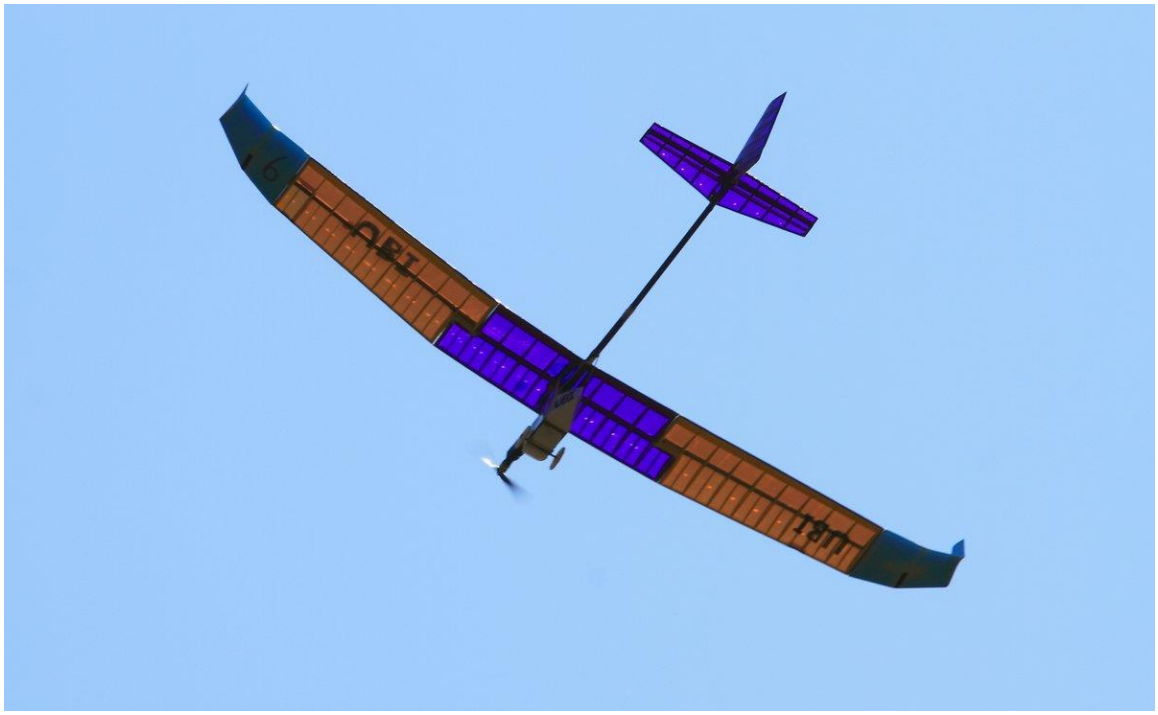

Figure 2.10 – AERO@UBI aircraft from 2015 edition.

3 Methodology

3.1 Research

For a competition such as the Air Cargo Challenge, the only way to achieve victory is to present the best concepts and solutions to all the details of the airplane. So, where it is possible to choose or innovate, the choice or the search for the innovation must take place as much as possible before the conceptual design stage of the aircraft development. So, an extensive research takes place very early in the development process. A propulsion system characterization took place in 2015 (Section 3.1.1) for the mandatory motor-propeller set to establish the propulsive system theoretical model and feed the conceptual and preliminary design calculations. Despite having already characterized the motor-propeller set at constant supply voltage, a study of the performance of most affordable Hi-End LiPo batteries available in the market was performed (Section 4.1).

3.1.1 Propulsion

3.1.1.1 Motor-propeller System Performance Testing

The APC 13x7 Sport propeller was tested in the wind tunnel at UBI low Reynolds propellers wind tunnel test facility [14]. The results for thrust versus airspeed are shown in Figure 3.1. It is seen that the thrust varies linearly with airspeed dropping about 0.5N for each m/s of increase in airspeed. The static thrust was 22.5 N. This allowed to identify the propulsive system theoretical model presented in Section 3.3.2.4 that was used in the preliminary design analyses.

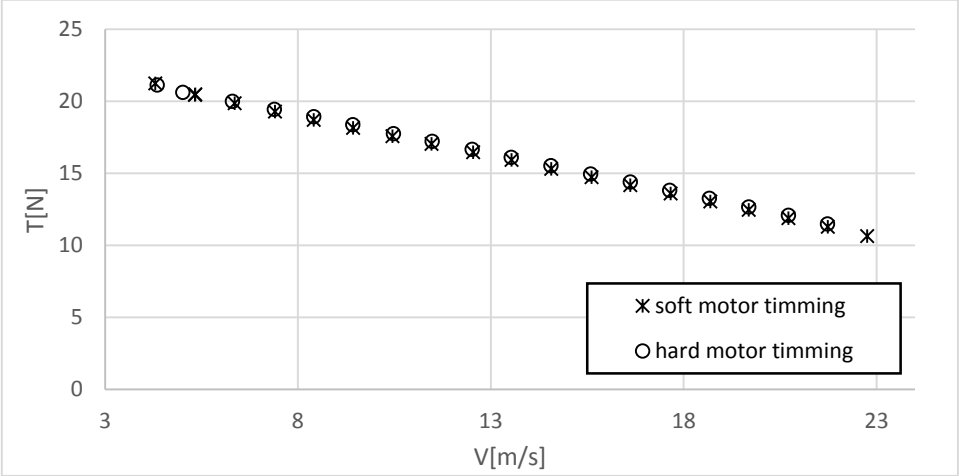

Figure 3.1 - Thrust versus airspeed for the AXI 2826/10 motor with the APC 13x7 Sport propeller for 11.7V in the electrical power supply.

3.1.1.2 Battery Testing and Selection

Batteries research is very important to maximise the performance of the propulsion system. The propulsive system power is roughly proportional to the battery voltage squared. This is explained by the fact that the electrical power is the product of current and the supply voltage. The current is proportional to the supply voltage. So, the battery supply voltage is squared in its correlation to the motor power. Therefore, the objective of this work was to identify the best battery to use in the ACC17 airplane. It needed to have the lowest voltage drop for the expected flight time. The battery temperature was expected to influence the battery voltage drop at the full power current. A set of highest specification discharge rate candidate 3S LiPo batteries were purchased and tested and a dedicated experimental setup was developed and put in place. The equipment to test the batteries included: two Arduino Nano, one MOSFET, three sensors of temperature, voltage and current, a power supply and one 3D printed box made from ABS to withstand the batteries heating temperature.

In Figure 3.2, the battery test diagram showing the basic system is presented. One Arduino Nano was used for the battery temperature versus time measurement, and the other Arduino Nano was used to measure the current and voltage of the battery. Heated battery tests were performed according to a purpose defined procedure, but using a temperature control device based on a PID controller, to maintain constant temperature.

Additionally, the actual ACC airplane motor and propeller, the Electronic Speed Controller (ESC) and R/C system were used to draw the battery current in realistic conditions. The test consisted in doing various discharges with the motor at full throttle (simulating the full throttle used in the competition flight). During each test, the time, voltage and current were measured. The procedure was repeated for battery at both room temperature and heated temperature. The results are presented in Section 4.1.

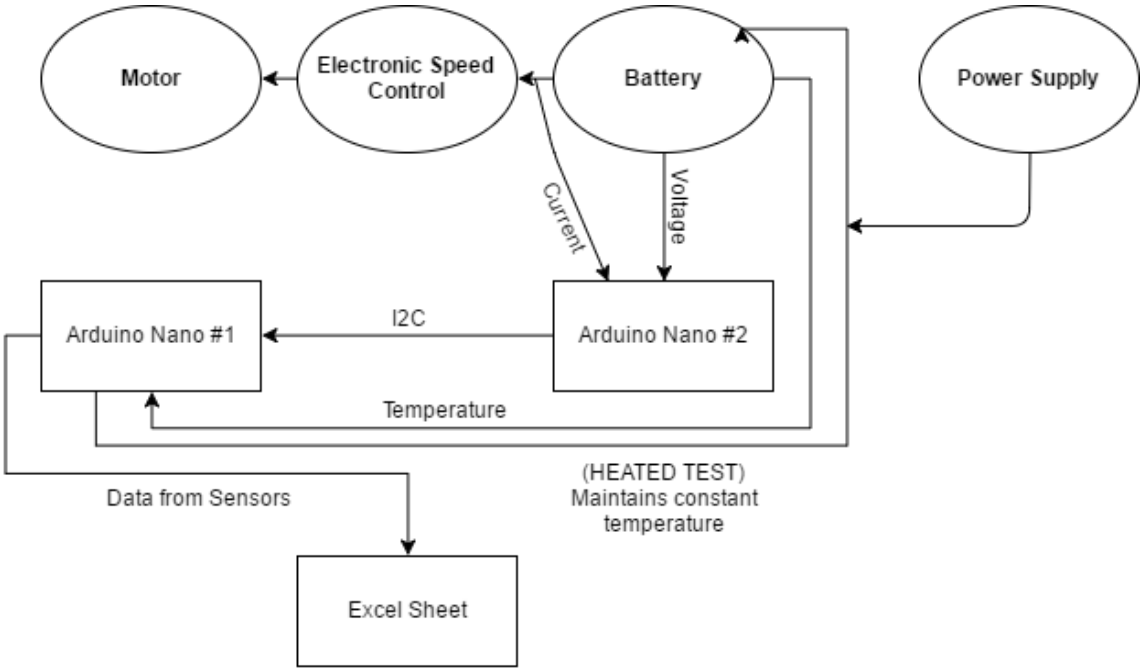

Figure 3.2 - Battery test experimental setup scheme.

3.1.2 Aerodynamics

3.1.2.1 Airfoil development

This part of the design affects the performance of the airplane as much as the propulsion system alone, great attention to design the most suited airfoil was given throughout the airplane development effort, starting from the beginning of the development works. Many purpose design airfoils were created using XFOIL [6] via XFLR5 according to the reasoning of reference [15] (mainly, delaying the transition for any lift coefficient throughout the lift curve) such that the lift coefficient for minimum drag was just below 0.4, as the expected lift coefficient during the flight competition legs was not expected to be any lower than this; the relative thickness was kept greater than 10% for comfortable accommodation of a wing spar; the trailing edge angle was sufficiently large to accommodate a Fowler flap and respective actuation mechanism; it was to have the highest possible maximum lift coefficient and to have a highest possible aerodynamic efficiency at a lift coefficient of about 1 for the airplane flying in tight turns, high load factor conditions.

3.1.2.2 Fowler Flap development

Considering the requirement of the speed flight task implemented in ACC15 and the lack of information concerning the use of high lift devices for low Reynolds number applications (60,000<Re<500,000), an MSc dissertation work [16] was carried out where low Reynolds Fowler flap design was studied based on the airfoil previously used in the airplanes of ACC11 and ACC15

UBI teams. For this flap design process, Computational Fluid Dynamics (CFD) Reynolds Averaged Navier-Stokes (RANS) and Unsteady RANS (URANS) methods were used. In total, 16 different combinations of flap gap, overlap, deflection angle and relative flap chord (see Figure 3.3) were simulated. The CFD calculations were performed using the k-ω SST turbulence model, for a Reynolds number of 2×10^5, with the open-source software OpenFOAM®. The computational model used in the study was validated through a mesh independence analysis and benchmarking tests without flap for the S1223 airfoil as well as the UBI_ACC11 airfoil. Although in certain conditions a reasonable discrepancy with experimental results was verified, in these cases the computational model was slightly pessimistic. Overall, the computational model was found to be adequate for estimation of the maximum lift coefficient with the Fowler Flap resulting two elements airfoils.

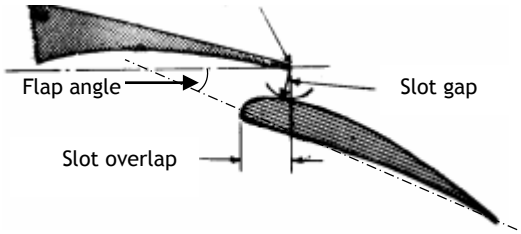

Figure 3.3 – Slot parameters, [17].

It was found that for the Fowler flaps configurations that were tested, the UBI_ACC2011 airfoil performed better with 25% chord flap with a 2.5% gap, 2% overlap and 30° flap deflection was the one with the most favourable performance, generating a Cl_{max} of 2.96 for a C_d of 0.081. With this flap, the aerodynamic efficiency of the basic airfoil was not damaged by the flap and even improved, with the $(L/D)_{max}$ reaching a value of 44 with the flap extended versus the original airfoil $(L/D)_{max}$ of 37 for the same lift coefficient. As expected, the absolute value of C_m greatly increased, going from a value of -0.251 without flap to -0.694 with flap.

3.1.2.3 Flight Testing

3.1.2.3.1 Fowler Flap Effectiveness

A prototype glider (see Figure 3.4) was tested to estimate the performance of a Fowler type flap. The Fowler flap on this glider was connected to the wing, and fixed in place, through balsa wood pieces. This flap did not have an extension/retraction mechanism. The glider was hand launched and performed a slope soaring flight. The data that was collected showed that with the Fowler flap, a C_{Lmax} or around 2.4 could be reached for the 3D glider wing. This indicated a 2D C_{lmax} of 2.95 for the wing geometry in use. The glider was instrumented with an

Arduino Nano, GPS static pressure and temperature sensor and differential pressure sensor. Figure 3.4 and Figure 3.5 show the glider being tested and the Fowler flap.

Figure 3.4 - Glider prototype for the Fowler flap flight-testing.

3.1.2.3.2 Roll Control with Spoilers

The usual design philosophy of UBI is to use rudder inputs for directional and roll control. This was usually done, among other factors, to allow the wing to remain "clean" (without the interference drag of the gap between ailerons and wing). It also allowed a lower weight since fewer servos are required.

However, the ACC competition now includes a flight task where the ability to manoeuvre the aircraft quickly and precisely is essential. The experience in the ACC 2015 has shown that this requirement was not easily met with rudder inputs alone.

To this end, tests were performed with the same glider of Section 3.1.2.3.1. to check different means of roll control. First, a new concept was tested with ailerons of just 3% of the wing chord (percentage of chord selected based on XFLR5). During the slope soaring flight test, this concept proved inadequate; the pilot stated that he had little authority over the aircraft and response time was too long.

After this, the use of roll spoilers and ailerons was tested. The major advantage of using spoilers is that these prevent the onset of adverse yaw by increasing parasitic drag on the wing that drops (compensating the increase in induced drag on the wing that is rising). This concept had satisfactory roll control authority and was eventually selected for the final aircraft.

Figure 3.5 - Glider prototype using spoilers in the Fowler flap wings to achieve roll control.

3.1.3 Construction Technology Preliminary Testing

3.1.3.1 Wing panels

To make a construction test of the wing panel, a 45cm span wing panel was laminated with epoxy and two layers of unidirectional carbon fibre cloth with $30\mathrm{g}/\mathrm{m}^2$ in a $\pm 45^{\circ}$ orientation on the upper and lower surface of a solid pultruded polystyrene foam (EPS) core that was cut in the 4-axis CNC hot wire cutting machine. The lamination was cured in a vacuum envelope using 0.35mm Mylar sheets in contact with the laminated surfaces to improve the surface quality (Figure 3.6a)). Then, after four of these panels were built, they were joined together with a mix of hollow glass microballoons and epoxy, with a consistency like peanut butter and the interface was reinforced using two layers of the same carbon cloth arrangement (Figure 3.6 b). The resulting 1.8m span wing was tested for flexural strength (Figure 3.6 c) and d)).

With a total weight of 9.5kg (the weight of a Lead Acid battery used as load and a lead plate weight) (Figure 3.6 d), the wing structure failed. The two layer CFRP stressed skins wing with a foam core was not enough to handle the flexural load expected for the ACC17 airplane. A possible solution would be to use a wing spar, but this was not possible to do without deforming the wing airfoil profile. It was, thus, decided to proceed with moulds technology to build the wings (Section 3.5).

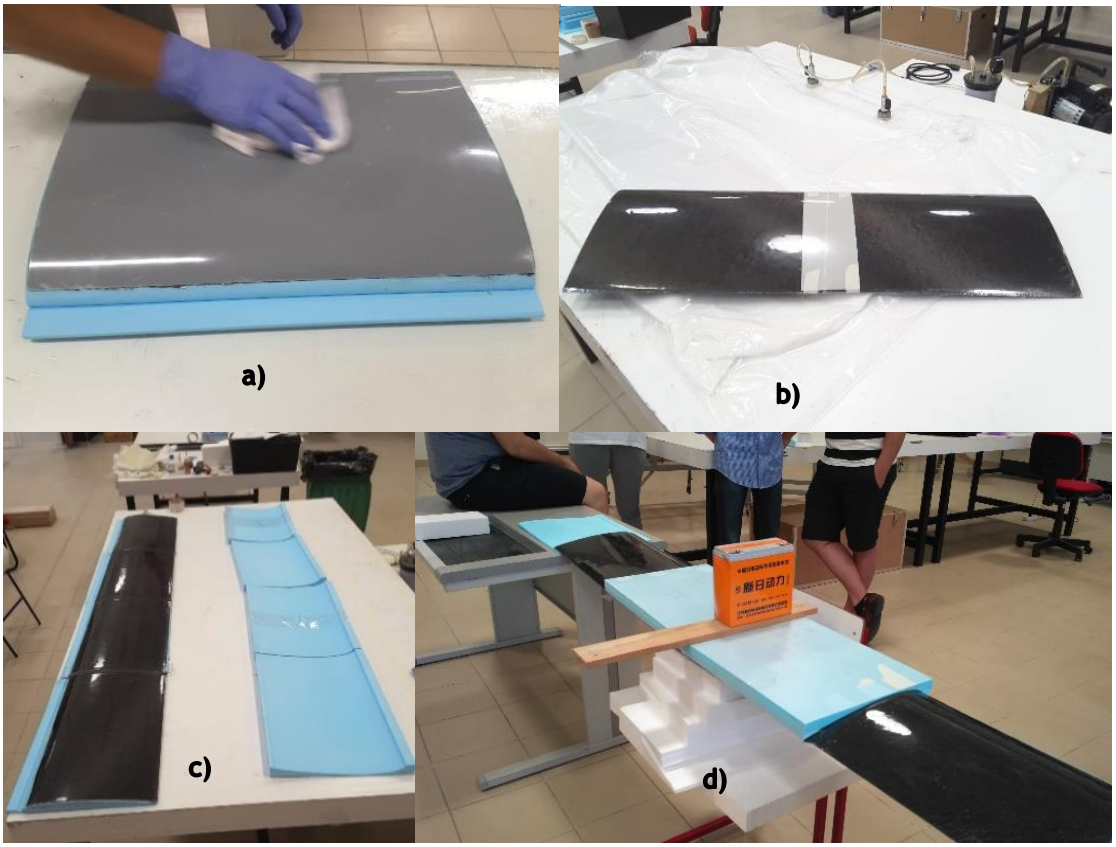

Figure 3.6 – Construction test of the wing panel, where in a) is one panel laminated, b) are two joined panels, in c) 1.8m of span are ready to construction test represented in d) with a 7kg battery.

3.1.3.2 Wing Panels Interfaces

One of the requirements of the ACC, is for the aircraft to fit inside a box with specific dimensions. On the other hand, the aircraft must pass on the structural test defined in the regulations (See Section 1.2). Therefore, it is necessary to define the structural interface between the wing panels, *i.e.*: how one wing panel is attached to the next wing panel. These must be light but sufficiently strong to resist the bending loads to which the wings are subjected.

One of the main aspects taken into consideration when developing the interfaces was to guarantee that they were common to all the panels connections to ensure that in the case one of these interfaces would be broken by a crash during the competition, it could be replaced taking a minimum of spare parts. The second aspect was the structural strength of the assembly. Several interface design concepts and structural tests were conducted to ensure the strength of the panels connection. To conduct the test, the interface part was loaded with the expected bending moment while connecting to two metal bars. A heavy battery was used to

bend load the connection. The value of the resisting bending moment was measured by a scale that was indicating how much weight of the load battery was being supported thus relieving the loading from the connection. Figure 3.7 shows the test just described. Several tests were performed until the interfaces had the strength.

Figure 3.7 – Interface strength test.

3.1.4 Zagreb Region Mean Wind Speed

Research [18] indicated a mean wind speed of 1.9m/s at the assumed default height of 10m in the region of Zagreb Airfield. This wind speed was accounted for the airplane preliminary design because a take-off in null wind condition is, in fact, not the general case. Table 3.1 shows the collected data.

Table 3.1 - Weather forecast in Zagreb region

August Weather - 7km from Zagreb Lucko Airfield [CWOP - EW6370] Latitude: 45.7669° ||| Longitude: 15.8486° ||| Altitude: 119 - 122 meters									
T[K]	p[Pa]	ρ[kg/m^3]	μ[Pa/s]	a[m/s]	T/T_0	p/p_0	ρ/ρ_0	μ/μ_0	a/a_0
287.37	99891.70	1.211	1.81E-05	339.83	0.997293	0.985854	0.98853	0.997849	0.998646

Year	Temperature			Pressure	Wind Speed			Humidity
	K			Pa	m/s			%
	Min.	Av.	Max.	Av.	Gust	Av.	Max.	Av.
2009	293.15	300.15	303.15	101730	2.995	1.922	2.816	67
2010	292.15	298.15	301.15	101430	2.593	1.609	2.503	77
2011	293.15	299.15	301.15	101540	2.190	1.296	2.101	81
2012	293.15	299.15	302.15	101690	2.414	1.520	2.190	77
2013	294.15	301.15	305.15	101620	2.906	1.788	2.593	61
2014	292.15	298.15	301.15	101420	2.816	1.699	2.682	80
2015	298.15	303.15	307.15	101560	4.292	2.682	4.202	55
2016	295.15	300.15	304.15	101870	3.979	2.503	3.889	64
AVERAGE	293.9	299.9	303.15	101608	3.023	1.878	2.872	70.25

3.2 Conceptual Design

The first stage of conceptual design is very important. Our professor in charge says:

"Only the best concept can result in the best optimum design"

Therefore, optimization is useless if performed on the wrong concepts. Concepts include the aircraft configuration, airfoil characteristics, building materials and construction techniques, *etc*. Conceptual design is the key moment of creation. To start the creative process, the objectives and requirements are analysed. Fundamental theory is reviewed and the state of the art is analysed, a basic theoretical model is established to quantify the performance of a possible concept. At the same time, materials with their impact in the aircraft geometry and their corresponding building costs and technology are surveyed. *E.g.*: full CFRP allows wings with smaller thickness or higher aspect ratio wings and composite materials allow double curvatures to be easily built.

The aircraft design will be defined by the competition objective, to carry the maximum possible payload while reaching the maximum average airspeed in the flight task and by the regulatory requirements and restrictions. The airplane development methodology used by our UBI teams over successive ACC editions relies on a meticulous analysis of the requirements to find limitations, risks and opportunity factors that can greatly affect the conceptual design, in not only the aircraft configuration, but also the type of structure, materials, *etc*.. Therefore, calculations are performed from the beginning of the design cycle to better define the problem in the light of the requirements. *E.g.* it is useless to equate a pusher-ducted propeller aircraft configuration if, from the beginning, a weight and balance calculation points out that the payload must be placed at a far forward position from the desired centre of gravity location, thus, making the unloaded aircraft to have an unacceptable rearward center of gravity (cg)

position and unsafe to fly. With the project spiralling towards the optimum objective, the best concepts appear naturally, without the subjectivity of the traditional trade studies.

Besides the competition regulations, any ACC UAV is a RC model aircraft. Therefore, in the present case, it must comply with the following basic restrictions, imposed by the Portuguese law, [19]:

R1 - Maximum Flying Mass with fuel: 25kg – Calculations for a conventional configuration fixed wing aircraft with the theoretical models described in Section 3.3.2, considering the propulsive system and requirements R11 (propeller), R12 (battery voltage), R14 (current), R15 (no reduction gear) and R16 (motor) - Described below, gave a rough estimative of the maximum take-off weight that could be flown in the limit as a function of the span with optimized wings mean chord. Figure 3.8 shows the results per these limitations, if the span is higher than about 3.3 m, there could be a chance that the aircraft weight had to be limited to 25kg by this legal requirement. These results do not account for the need to take off in 60m. It can be immediately concluded that the wingspan is the limiting factor for maximizing the airborne weight with the propulsive power involved. On the other hand, the take-roll length limit also limits the lift-off airspeed. Our team usually considers that headwind is present. Section 3.1.4 Zagreb Region Mean Wind Speed deals with getting rough estimate of how much wind to expect at Zagreb in August. However, it seems that Zagreb is much less windy than Stuttgart and Ota. Calculations in Section 3.3.2.2 also show the take-off in 60m aircraft weight limit is lower than the flying weight limit. This 2017 edition does not limit the span but for the flight task, the aircraft must handle effectively: with good roll rates. Additionally, the structural test is demanding (See Figure 1.1). So, the maximum span is expected from the beginning to not surpass the 4.5m value.

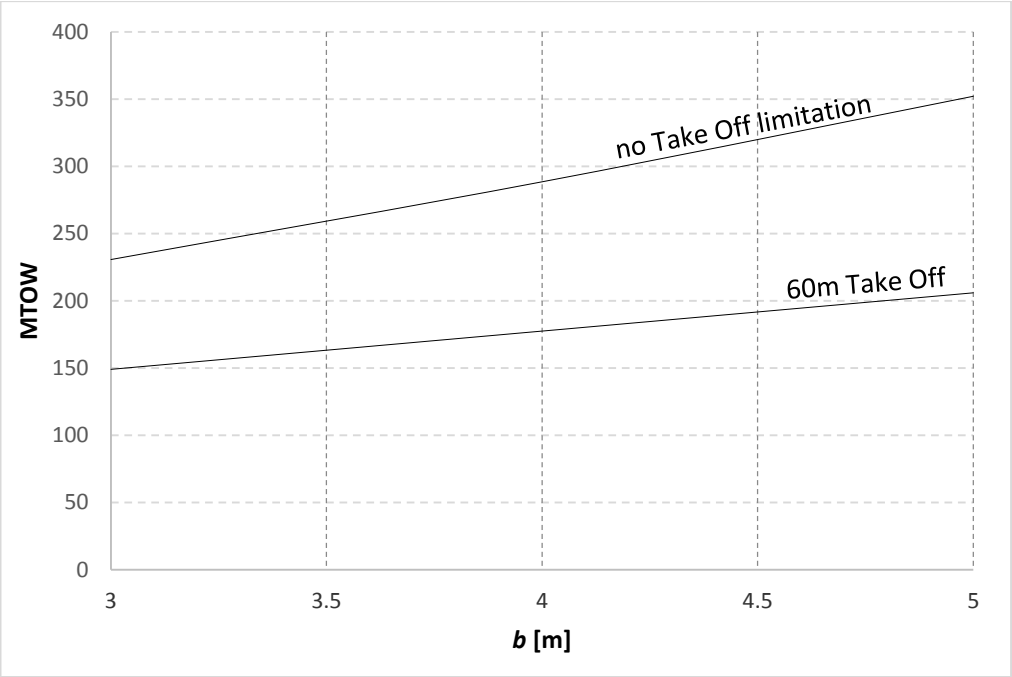

Figure 3.8 - Maximum flying weight with designs of chord optimized for maximum flying weight as function of span (above) and Maximum Take Off weight for the 60m TO run. Designs using a chord optimized for maximum flying weight as function of span considering the use of Fowler Flap (C_L is 2.51 for b=3m increasing to 2.71 for 5m span). A head wind of 1.9 m/s was considered (See Section 3.1.4).

R2 - Maximum Area of Lift Surfaces: 500dm^2 – With the results of calculations described in Section 3.3.2, it is seen that the wing chords involved, even for a 5m span result in a wings surface of about 165 dm^2, when optimized for minimum power required to fly. This is well below the 500dm^2 limit.

R3 - Maximum Wing Loading: 250g/dm^2 - Per this limiting requirement, if the aircraft were to be optimized for the maximum flying weight, the span would have to be greater than about 3.25m. This is a possibility but the take-off requirement and the need for an airplane that is flying with a comfortable excess power for agile turns during the speed task, point towards a much lower wing loading than the limit of 250g/dm^2.

R4 - Piston Engine Maximum C.C.: 250cm^3 – Not applicable requirements R13 mandates an electrical propulsion set.

R5 - Maximum Voltage for Electric Engines (open circuit): 72Volt. – The ACC 2017 regulation requirement that regards the batteries fits well within this limit (see requirement R13).

On top of these general restrictions the requirements imposed by this year's competition regulations were added:

R6 - No rotary wing. – A fixed wing aircraft concept is used.

R7 - Not lighter than air. – Although this requirement seems not to prohibit the filling of some internal volume with a lighter than air gas, e.g. the wing filled with helium, it was decided for the sake of a fair play competition spirit that this concept is not put into consideration.

R8 - No external assisted take-off power. No external assisted take-off power was used.

R9 - Maximum Take-off Distance: 60 m. – In a 60 m take-off run, limited energy can be supplied by the propulsive system. In fact, only 60m versus mean take-off thrust, taking all the losses that rolling friction and drag account for, the total kinetic energy that can be achieved is the limiting factor. If one wants to increase the mass, the take-off speed square, V_{to}^2, must decrease to do so. That is the same as increasing the lift coefficient at take-off because it is inversely proportional to V_{to}^2. Using a wing airfoil with the highest possible lift coefficient is the best way to go. A single element airfoil, for the minimum Reynolds number involved gets to a maximum lift coefficient of about 2.3. Since the present flight task demands a fast cruise and manoeuvring speed, an extra interest in increasing the wing loading is present. Therefore, a Multi-element airfoil was investigated (see Section 3.1.2). Having this in mind and analysing the requirement of 60m take-off for the set of designs corresponding to Figure 4.19 the calculations for the maximum take-off weight that satisfy the 60m, with zero head wind condition, show that this take-off requirement is a stronger limiting factor than the propulsive power available to fly. At the same time, confirms the span as a determining result factor. For the same conditions, the higher span aircraft will get the higher take-off weight. The highest possible span aircraft is a concept to go to and the span limit will be dictated by the empty weight function of span and by the flying qualities of the aircraft since a higher span lowers the roll rate, hence the turns at the ends of the 100m straight legs may be too sluggish with a 5m span aircraft.

One can notice also that the presence of head wind during take-off leads to a higher take-off weight and that this improvement gets more important with increasing span. Headwind during initial climb will also improve the climb angle, an important safety feature. Head wind is the general case not an exceptional one and is certainly a factor to consider. Note that these results correspond to designs with wings chord optimized for the previous condition of maximum flying weight for a given span. In this case the result would be designs that if with the weight limited to take-off in 60 m would climb at the fastest rate or would be able to sustain level flight with the maximum load factor during a turn. One important idea that comes out of the take-off limiting factor is that the propulsive system must be optimized to the maximum mean thrust during the take-off run. In our case, the propulsive set motor-propeller is prescribed so there

is not much to do for improving the take-off mean thrust. Even if the propeller were ducted, the gain would be marginal since the pitch is prescribed at 7 inches.

R10 – The aircraft must accomplish 10 legs of 100m length with 180 degree turns after each leg – his requirement mandates for an endurance of about 2 minutes for the 1000m course for an average speed of about 10m/s (not considering the length of the turn trajectories),

$$V = \frac{\Delta x}{t} = \frac{10 \times 100\ [m]}{2 \times 60\ [s]} \approx 8.3\ m.s^{-1} \qquad \textbf{(Equation 3.1)}$$

considering that, the turning trajectories are about the same order of lengths as the legs and that the aircraft will have a mean airspeed lower than 20m/s. This means that a minimum capacity of 1.5Ah must be used in the propulsion battery.

$$C_{Min_{Cap_{Battery}}} = A \times \Delta t = 45 \times \left(\frac{2}{60}\right) = 1.5\ Ah \qquad \textbf{(Equation 3.2)}$$

where $C_{Min_{Cap_{Battery}}}$ corresponds to the minimum capacity used in the propulsion battery, A is current and Δt corresponds to time in hours.

For the safe side, the capacity should be much higher. When a battery is almost completely discharged, there is a marked voltage drop. If the discharge process proceeds beyond the threshold voltage (if a full discharge occurs) the battery elements may be damaged, which would radically shorten the battery life. Even so, it was decided to not drain more than 70% of the battery charge per flight because it is a risk the battery condition. So, a battery capacity greater than 3Ah will be used.

$$C_{Min_{Cap_{Battery}}} = 1.5/0.70 = 2.55\ \approx 3\ Ah \qquad \textbf{(Equation 3.3)}$$

This requirement draws the attention to the need of being able to climb safely, to sustain flight at a load factor n>1 for banked flight during turns. For completing tight turns, a minimum of 30° bank turn is adequate for a low turning radius. In this case, $n \approx 1.155$ and a reserve excess power of 20% the required power is adopted to maintain the aircraft safe handling during flight speed task.

R11 – Use of an unmodified APC 13x7 Sport propeller. – It is mandatory to use a propeller with a 13 cm of diameter and 7 cm of pitch. This requirement together with R12, R15 and R16, prescribes the available thrust versus airspeed propulsion curve. This performance was measured in the wind tunnel and described in Section 3.1.1.

R12 - Electric propulsion with Lithium based secondary cells with a series of up to three elements. – This corresponds to a nominal voltage range of 6.4 to 7.4V, in series of 2 elements pack, or 9.6 to 11,1V, in a series of three elements, with the lower values corresponding to LiFe and the higher to Li-Ion and LiPo. To maximize propeller thrust at take-off and propulsive power during climb, assuming constant motor efficiency, the higher electrical power should be used. This means 40A current, from requirement R16, at the highest possible voltage. The LiPo batteries have higher voltage per cell for the same battery weight. So, a series of three Lipo cells will be used.

R13 – No prescribed minimum capacity for the propulsion battery.

R14 - Minimum battery discharge current rating of 45 A. – R15 and R16 are not limiting because, for the sake of maximum power, the current rating, proportional to the capacity should be as high as possible if the excess battery weigh will not reduce the payload more than it increases the relative voltage gain from a bigger capacity battery. Furthermore, a higher voltage, per the motor model described in section 3.3.2.4., increases the motor peak efficiency and, at the same time, makes the peak efficiency operating point occur at a higher current closer to the maximum 45A working condition. In Section 3.1.1.2 the battery capacity, weight and voltage under 45A discharge are experimentally investigated.

R15 - No reduction between the motor shaft and the propeller, *i.e.* propeller rpm equal to motor rpm.

R16 - Motor: Model Motors - AXI 2826/10. – Motor characteristics: K_v=920 rpm/V, R_i=42mΩ, I_o=1.7A, m=181g.

If the propeller was ducted, an increased take-off thrust could be achieved. This concept brings a mechanical complexity and losses as well as weight. The use of a duct was rejected from the start because of the weight, but, above all, the possibility of damage during the flight competition. A broken propeller issue is easy to repair in the field.

R17 – The aircraft must be able to perform the structure validation test: being supported by its wingtips. – This requirement demands for a very robust wing spar construction. Especially if one considers that, the speed flight task legs will be performed in a low lift coefficient. Thus, requiring an airfoil that has it minimum drag coefficient at low lift coefficients. Such airfoil is usually a small relative thickness one. Increasing the chord could be a solution for a strong and light wing spar but increases the parasite drag and specially the induced drag just after lift-off for a fixed span. This induced drag after lift-off is given by Equation 2.7.

According to our experimental research performed on the propulsion set (See Section 3.1.1), the maximum thrust at lift off is about 18N at about 8m/s. In the lift off-drag is about 1N. With Equation 2.7 and a flying weight of about 160N, K must be smaller than 0.05 for a lift coefficient of approximately three. According to the Fowler Flap development research study (Section 3.1.2.2), K_p is about 0.01. So, with Equation 2.4 with $K_i = 0.04$, A_R must be greater than eight. For a span limit of 4.5m, the mean geometrical chord should be smaller than 0.56m.

R18 - Maximum landing runway for the initial touchdown: 120 m – If the glide ratio is high, shallow final approach may be expected, making a precision landing a hard task. It may be necessary to use the propeller as a speed brake by setting the motor ESC brake OFF.

R19 - The payload distribution must not affect the stability characteristics. - The ratio of payload to empty weight is so high, about 5, that the payload must be almost coincident with the desired centre of gravity for the best compromise of stability and performance.

R20 - The payload material is steel in the form of plates. (Density of about 7800kg/m^3)

R21 - Prescribed payload volume: 160x80x80 (minimum height) mm^3. – This requirement, together with the previous R20 and the results for the payload call for a check whether a 80mm stack of steel plates can reach the payload value. Checking for the corresponding payload value, considering R20, an increase of the payload compartment height from 80mm to 140mm was chosen in order to be able to carry a 13kg payload.

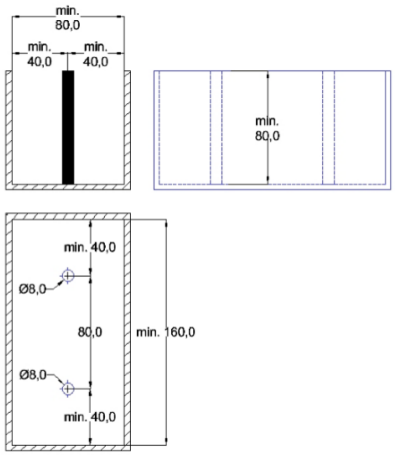

Figure 3.9 – Payload Volume

R22 – No auto pilot or control assistance systems. - I.e. Piloted manually via remote control. So, Good handling and stability must be achieved with the design. Thus, the centre of gravity position must be set for comfortable R/C piloting not for top performance.

A comfortable climb angle and a broad speed envelope for the fully loaded aircraft is an objective to keep a safe piloting condition and to obtain an agile aircraft for the speed flight task. In the speed flight task, the turns will be performed in dangerous flight conditions. A wing tip stall while turning near the ground can result in the loss of the aircraft. Thus, some extra care must be taken to ensure that the wing tips stall well after the wings' roots. This will be accomplished by washout and extra chord at the wing tips than the optimal elliptical chord distribution.

R23 - The aircraft must be loaded and ready for take-off in the least possible time. - Each 5 second will reduce 1 point to the total of 24 points maximum readiness bonus.

A fast payload loading, securing and closure in the aircraft must be conceived. One concept is to load the cargo bay outside the aircraft and supported in a table, then, the aircraft is fitted to the cargo bay as the later rests in the supporting table as in a previously used Aero@UBI ACC airplane design. That concept was used in ACC 2007 for the first time and proved well again in ACC 2011, where the body floor closure was supporting the cargo bay and the landing gear. (Figure 3.11).

R24 - Aircraft must fit in a transportation box that may not exceed the inside dimensions of 1000x500x400 mm³. - Considering the possible 4.5m span, the aircraft shall have interfaces in the airframe, at least between wing panels. Interfaces are always an extra and significant structural weight. In our case, this mandates the use of 5 wing panels.

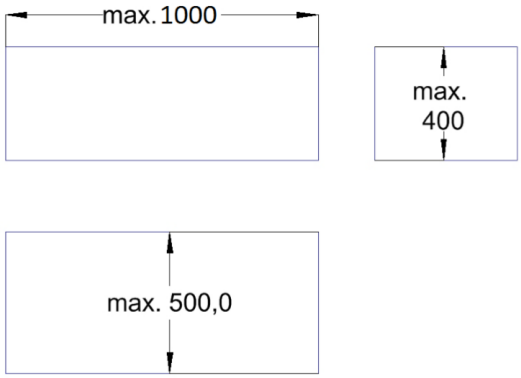

Figure 3.10 - Inside dimensions of the transportation box.

R25 - An Rx battery pack with C > 600mAh is mandatory. - A LiFeO4 2S 700mAh receiver battery will be used. It has a mass of 55g.

Figure 3.11 - Cargo Bay attached to the body floor in UBI's ACC 2007 Pegasus Team winner aircraft.

UBI has a long tradition in the Air Cargo competition. Ever since it started participating in the very first edition in 2003, UBI has a bit of everything: from radical experimental configurations, to more traditional ones. Although some of these experimental configurations were successful, others were not. Meanwhile the more conventional, sound configurations have usually had good results. Thus, the starting point for this year´s competition was our 2015 aircraft configuration. From this, it was decided that the ACC2017 aircraft would have the same general configuration of 2011 and 2015 aircraft with the difference that the tail cone would extend from the lowered payload body because the extended Fowler flap wing will have a small angle of attack for maximum lift coefficient of about 8 degrees. The parasol lifting surface concept.

Figure 3.14 shows the general configuration and main concepts adopted. A conventional tail surfaces configuration is preferred. The reasoning is simple. It does not suffer from the very low Re number problem found in a canard configuration at these airplane model size. Besides this, a canard cannot profit from the maximum lift coefficient of its main lifting surface, the wings. The canard must stall safely before the wing. It does not have the critical fore plane and after plane that the tandem wings configurations. It does not have such a low wing Re number as the multiplanes. A cruciform tail with the horizontal tail in the front of the vertical tail will be used. This design gives low tail boom torsion loads and low interference drag between the tail surfaces. The reason the vertical tail rests behind the horizontal tail is that the aspect ratio of the wing is high as foreseen by early design calculations. At the same time, the tail boom flexibility will act upon a smaller horizontal tail arm length to limit the dangerous change in the horizontal tail incidence due to tail cone flexibility.

The parasol wing configuration was chosen because of two main factors, one is that in the event of a crash the wings can separate from the cargo bay (where the payload and kinetic energy is concentrated) and the other factor is due to a Fowler flap action, because the connection of the right and left wing flaps allows an aerodynamic that is less disturbed by the presence of the cargo bay and demands a simpler actuation mechanism.

The wings will have, besides of taper, the geometric washout that optimizes the lift distribution at the design initial climb speed and prevents tip stall occurrence. An approximation to elliptical wing planform will be used to reduce the induced drag [20] but not reach a high torsion moment at the root. A slight negative wing pitching deflection proportional do the lift magnitude was considered a necessity to keep a bending load stable structure.

Weight and balance dictates that the motor rests well in front of the wing in a puller configuration. The fuselage consists of a CFRP tube for the motor, in front of the wings. An interface of this motor nose extension with the wings is used to allow transportation in the box according to the regulations. A lowered cargo compartment body is used as a way of raising the wings position to profit from the higher wind to shorten the take-off distance and help preventing wing tip strikes on the ground. The main landing gear will be attached to the cargo compartment. Three pylons will connect the lower body to the wing.

Regarding stability and control, pitch control is achieved through a flying tail elevator to maximize control authority with the 30% chord Fowler flaps (as found necessary in the early flight testing) while keeping the corresponding parasite drag at a minimum by the absence of a horizontal stabilizer to elevator gap. Roll control is achieved through rudder, ailerons and spoilers (see Section 3.1.2.3). Looking at the qualitative influence of the static stability proportions on the dynamic stability shown in Figure 3.12 and in Figure 3.13, one notices that since the wing has a negative speed stability because of the airfoil strong negative pitching moment, to minimize the risk of an unstable divergence dive, it is considered prudent to design for a negative lift contribution in the horizontal tail such that the horizontal tail cancels the wing negative speed stability. At the same time, to limit the performance penalty and prevent excessive downward deflection of the flexible tail boom, this negative lift must be kept in the smallest possible amount. Off course, this rationale can only be sustained with a precise centre of gravity location. The landing gear plays an important role for this matter. It is located such that the loaded aircraft will balance on the main wheels. So, a nose up attitude on the ground: the aircraft falls on its tail. A nose down attitude and the nose will remain stable on the ground. Another purpose of this concept is to minimize the load on the horizontal tail needed for rotation during take-off, minimizing the corresponding loss of lift. Regarding the directional stability, Figure 3.123 suggests that even with a high positive dihedral effect due to high wing

and raised wing tips (like winglets), the static directional stability can remain with a modest value.

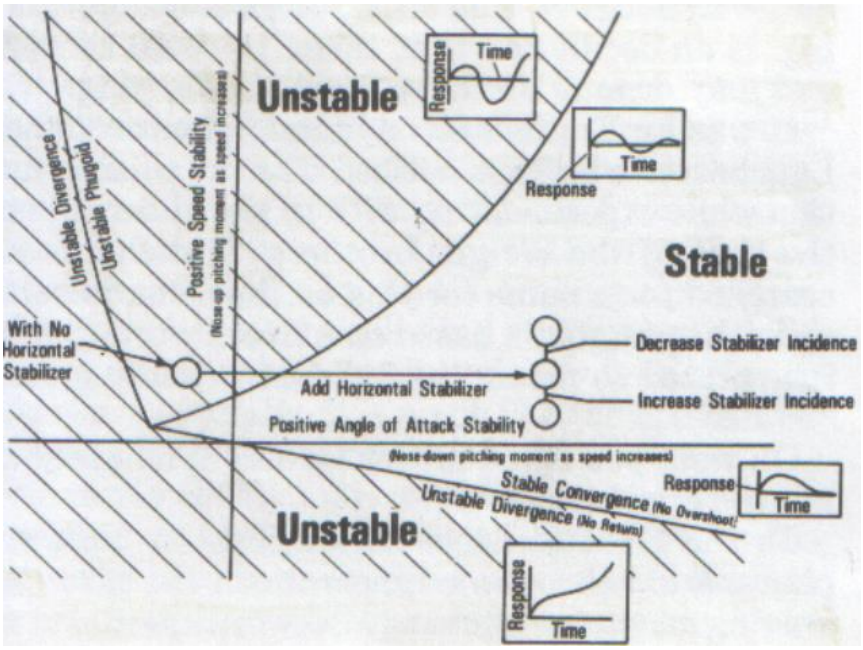

Figure 3.12 - Typical Longitudinal Stability Map, [21]

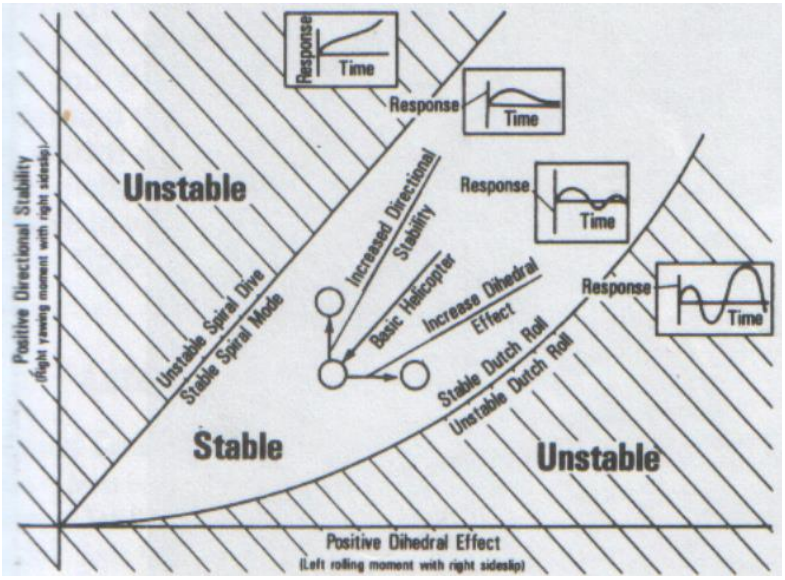

Figure 3.13 - Dutch Roll Action (Slightly Unstable), [21]

Regarding the lateral stability and control, initially it was decided not to use ailerons. Such practice has long been UBI philosophy of design for the Air Cargo Competitions because ailerons are prone to wing tip stall while prematurely taking off when trying to comply with the 60m run limit. However, given the different nature of the pylon racing, the need for installation of ailerons did arise. This was because early research testing glider prototypes in the mountain slopes revealed that the airplane did not have sufficient control authority for fast turns.

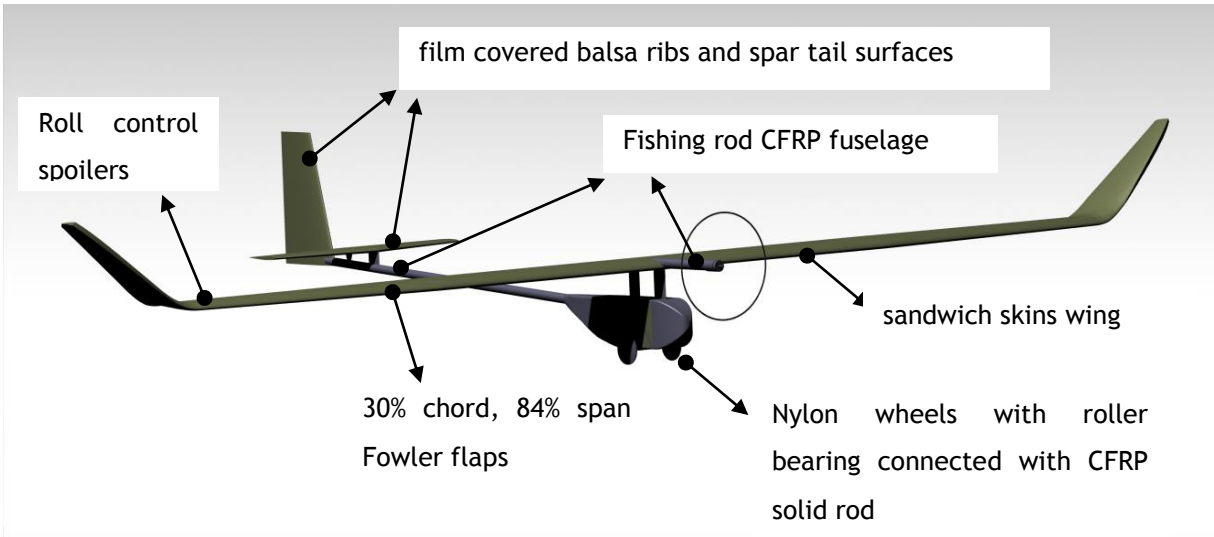

Figure 3.14 - General configuration and main concepts adopted.

3.2.1 Structural Design

To start an initial study to insure a high torsional stiffness because of the massive pitching moment, because of the implemented $0.3c$ and $0.85b$ Fowler flaps, the wing structure concept is based in 30 kg/m^3 EPS foam cores sandwich panels with CFRP skins, corresponding to the wing upper and lower surface. Each skin uses two ±30º orientation layers of unidirectional 30g/m^2 high strength carbon fiber in epoxy matrix with an outer ±45º bidirectional 30g/m^2 glass fibre. Unidirectional high strength carbon fibre roving reinforces the maximum thickness region in the upper and lower wing surface to resist the structural wing-bending test. Close to the wing root, an internal C shaped ±45º bidirectional high strength is joining those unidirectional spar caps. Figure 3.15 shows this structural concept. This initial structural concept was later modified on the final aircraft. The final concept used is shown in Figure 3.16.

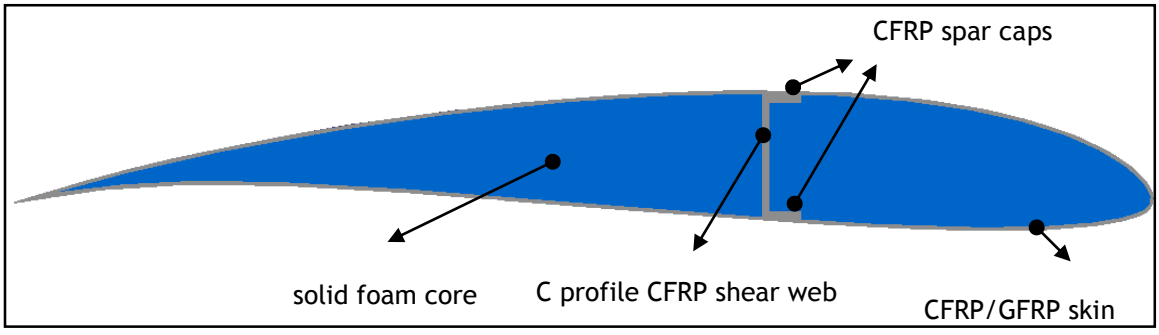

Figure 3.15 – Generic Wing section structure.

Our landing gear, just like our 2011 aircraft, will consist of only 2 wheels connect through a unidirectional CFRP solid rod. Fairings made from simple foam and or iron on film will be made to reduce parasitic drag from the circular shaped rod. The wheels shall be large enough to reduce rolling resistance. In the rudder, a skid will provide limited directional control.

This solution is extremely lightweight and provides very low rolling resistance. One disadvantage though is that during take-off, full power cannot be applied immediately from the start. The aircraft must start rolling slowly and only then can full power be applied, otherwise the static friction of the wheel is so large that a full power setting will generate a nose down moment causing the aircraft to tip face first on its nose. Such was the case during the first takeoff in Stuttgart in 2011.

The solution used was shown in

Figure 3.16, the upper and lower skins of the wing structure concept is in Balsa Wood 1 mm thickness core sandwich panel with CFRP bidirectional $\pm 45º$ of 80 g/m^2 skins. The main and unique spar, 0.3c, is in unidirectional Carbon Fiber.

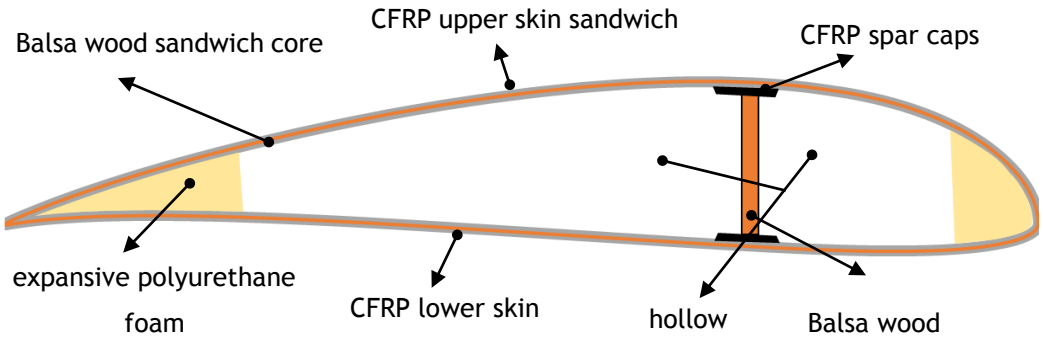

Figure 3.16 – Wing Section structure used in ACC17.

3.3 Preliminary Design

3.3.1 Design Variables

For the design process, a Microsoft Excel spreadsheet was implemented to incorporate the formulation for the aerodynamic, flight task performance, take-off performance, structure weight, propulsion and International Standard Atmosphere (ISA) models. This spreadsheet uses CG position (h_{cg}), horizontal tail arm (hh), horizontal tail area (Sh), vertical tail arm (hv), vertical tail area (Sv), and C_L. Most importantly, the chord *(c)*, span *(b)*, and mass *(m)* are used in the parametric study.

3.3.2 Theoretical Models

3.3.2.1 Airplane Aerodynamics Model

Equation 3.4 is used to calculate the wing lift coefficient by applying a correction factor to the airfoil lift coefficient.

$$C_{Lmax} = \frac{C_{l\ max\ Re_{Ref}} \left(\frac{Re_{Cl_{ref}}}{Re}\right)^{Exp_{Re}}}{1+\frac{C_{l_{max\ Re_{Ref}}} \left(\frac{Re_{Cl_{ref}}}{Re}\right)^{Exp_{Re}}}{\pi e A_R}} + C_{Lh}\frac{S_h}{S} \quad \Leftarrow Re < Re_{Ref}$$

$$C_{Lmax} = \frac{C_{l_{max\ Re_{Ref}}}}{1+\frac{C_{l_{max\ Re_{Ref}}}}{\pi e A_R}} + C_{Lh}\frac{S_h}{S} \quad \Leftarrow Re \geq Re_{Ref} \qquad \textbf{(Equation 3.4)}$$

Just like C_L, C_D also has a profile correction factor to the Reynolds number of 1.5 as given in equation 3.5.

$$C_D = \frac{C_l}{\frac{C_l}{C_d}}\left(\frac{300000}{Re\sqrt{Cl}}\right)^{1.5} \qquad \textbf{(Equation 3.5)}$$

The theoretical model used to estimate the performance (the required thrust and power in level flight and airspeed envelope at sea level) consists of the following equations (all in the International System of Units):

$$L = W = \frac{1}{2}\rho V_\infty^2 C_L S \qquad \textbf{(Equation 3.6)}$$

Where,

ρ is the ISA (International Standard Atmosphere) air density;

V_∞ is the airspeed;

S is the reference area;

C_L is the aircraft lift coefficient;

$$C_L = \frac{S_h}{S}C_{L_h} + C_{L_W} \qquad \textbf{(Equation 3.7)}$$

With the subscript h denoting horizontal tail and w for wings.

For the wings lift coefficient:

$$C_{L_W} = C_l \cos(\alpha_i) \quad \textbf{(Equation 3.8)}$$

Where,

C_l is the wing´s airfoil lift coefficient

α_i is the wings induced angle of attack correction:

$$\alpha_i = \frac{C_{L_W}}{\pi A_R}(1+\tau) \quad \textbf{(Equation 3.9)}$$

With, $\tau = \frac{1}{e} - 1$ and e is the Oswald´s efficiency factor which can be derived from analytical models available at [22] or from results in XFLR5.

The horizontal tail lift coefficient is calculated according to

$$C_{L_h} = \frac{S\left[C_{m_W} + C_{L_W}(h_{cg} - 0.25)\right]}{S_h(h_h + 0.25 - h_{cg})} \quad \textbf{(Equation 3.10)}$$

This results from the equilibrium of pitching moment condition about the center of gravity.

For the drag,

$$D = T = \frac{1}{2}\rho V_\infty^2 C_D S \quad \textbf{(Equation 3.11)}$$

Where T is the required propeller thrust for level flight (assuming the thrust line is at a small angle relative to the longitudinal axis);

C_D is the aircraft's drag coefficient:

$$C_D = C_{D_p} + C_{D_i} \quad \textbf{(Equation 3.12)}$$

With the total parasitic drag coefficient:

$$C_{D_p} = C_{D_p} + \frac{S_h}{S} C_{D_{p_h}} + \frac{S_V}{S} C_{D_{p_V}} + C_{D_{p_{other}}} \quad \textbf{(Equation 3.13)}$$

Considering:

$C_{D_p} = f(C_l)$ is the predicted wings airfoil polar function based on XFLR5;

$C_{D_{p_h}} = C_{D_{p_V}} = 0.011$ as the value for the tail airfoil drag representative of the assumed NACA0009 at low lift coefficient.

In the calculations, the wing airfoil parasite drag coefficient was corrected for the Reynolds number according with the function:

$$C_{D_{p_i}} = C_{D_{p_{i_{Re_{ref}}}}} \left(\frac{Re}{Re_{ref}} \right)^{Re_{exp}} \quad \textbf{(Equation 3.14)}$$

Where, $C_{D_{p_{i_{Re_{ref}}}}}$ is an airfoil parasite drag coefficient at a known Reynolds number Re_{ref}, Re_{exp} is a suitable correction exponent in our case taken as -0.4.

For the remaining parasitic drag coefficient (which includes the fuselage parasitic and induced drag, wing-fuselage interference drag, tail interference drag, cooling drag, landing gear drag, *etc*...), a value was assumed. With, $C_{D_{p_{fus}}} = 0.03$ for a thick airfoil shaped body fuselage concept and $S_{fus} = 0.06m^2$.

$$C_{D_{p_{other}}} = C_{D_{p_{fus}}} \left(\frac{S_{fus}}{S} \right) + 0.25 C_{D_{p_w}} \quad \textbf{(Equation 3.15)}$$

The total induced drag coefficient is:

$$C_{D_i} = C_{D_{iw}} + \frac{S_h}{S} C_{D_{ih}} \quad \textbf{(Equation 3.16)}$$

where, $C_{D_{iw}} = \frac{C_{L_w}^2}{\pi A_R e}$ is the wings induced drag coefficient and $C_{D_{ih}} = \frac{C_{L_h}^2}{\pi A_R e}$ is the horizontal tail induced drag coefficient.

The horizontal tail Oswald coefficient was assumed as $e = 0.975$. The horizontal tail lift coefficient is calculated with the equilibrium condition around the center of gravity position by,

$$C_{L_h} = \frac{S\left(C_m + C_{L_w}(h_{cg} - h_w)\right)}{S_h(h_h + h_{cg} - h_w)} \quad \textbf{(Equation 3.17)}$$

Where,

h_h is the wings aerodynamic center longitudinal distance from the datum in number of wing mean geometric chords, h_{cg} is the aircraft's longitudinal distance from center of gravity to the datum in number of wing mean geometric chords, h_h is the longitudinal distance from the horizontal tail's 0.25 chord to the datum in number of wing mean geometric chords.

The required level flight propulsive power is,

$$P_R = TV_\infty \quad \textbf{(Equation 3.18)}$$

3.3.2.2 Take-off Performance Model

The theoretical model used to estimate the performance in the take-off considers the ground run acceleration as,

$$\frac{dV}{dt} = \frac{T - D - \mu_R N}{m} \quad \textbf{(Equation 3.19)}$$

Were μ_R is the rolling friction coefficient. The normal ground reaction:

$$N = W - L \quad \textbf{(Equation 3.20)}$$

and D has a Reynolds number correction factor:

$$D = \frac{1}{2}\rho V^2 S C_D \left(\frac{\frac{\rho V c}{\mu}}{200000} \right)^{-0.4} \quad \textbf{(Equation 3.21)}$$

and the rolling friction, that was determined experimentally as $\mu_R = 0.055$.

$$\frac{dV}{dt} = \frac{dV}{ds}\frac{ds}{dt} = V\frac{dV}{ds} = \frac{1}{2}\frac{dV^2}{ds} \quad \textbf{(Equation 3.22)}$$

Considering $W = mg$,

$$\frac{1}{2}\frac{dV^2}{dS} = \frac{g[T - D - \mu(W - L)]}{W} \quad \textbf{(Equation 3.23)}$$

Finally,

$$ds = \frac{W dV^2}{2g[T - D - \mu(W - L)]} \quad \textbf{(Equation 3.24)}$$

The integration of this last relation gives the total take-off run distance s_{acel} as a function of the velocity increase necessary for taking-off, which is V_{to} minus V_{Wind}.

$$s_{acel} = \frac{W(V_{LO} - V_\infty)^2}{2g[T - D - \mu(W - L)]_{0.70V_{LO}}} \quad \textbf{(Equation 3.25)}$$

See Reference [23] for further insight on the implementation and use of the current formulation.

The Lift-Off Speed, V_{LO}:

$$V_{LO} = 1.1\sqrt{2 \times \frac{\frac{W}{C_{Lmax}}}{\frac{cb}{\rho_0}}} \qquad \textbf{(Equation 3.26)}$$

The distance of take-off, X_{TO}:

A different model, that takes into account the static thrust available on take-off, is given by X_{TO}:

$$X_{TO} = \frac{\frac{W}{g}}{F_{TO}}\left(\frac{(V_{LO} - V_{wind})^2}{2}\right) \ (m) \qquad \textbf{(Equation 3.27)}$$

where V_{LO} is the lift-off speed, g=9.81m/s and V_{Wind} is the windspeed.

The take-off force is given by:

$$F_{TO} = T_{static}\frac{V_T - V_{LO}}{V_T} - \frac{\left(\frac{1}{2}\right)\rho_0 V_{LO}^2 cb\frac{C_{Lmax}}{10}}{3} - 0.025W \quad (N) \qquad \textbf{(Equation 3.28)}$$

where V_T is thrust at a set velocity and $(V_T - V_{LO})/V_T$ is a velocity correction factor.

3.3.2.3 Structure Weight Model

The design point is determined by evaluating multiple design point solutions using the formulation above in a spreadsheet. Firstly, the performance of the design is evaluated by setting the weight at the value that allows to take-off in 60m. The empty weight is modelled as a function of span and chord by

$$W_0 = wW_{pay}W_{0_{ref}}\left(\frac{b}{b_{ref}}\right)^{e_b}\left(\frac{c}{c_{ref}}\right)^{e_c} + W_{sys} \qquad \textbf{(Equation 3.29)}$$

Where, w is a proportionality function of the empty weight to the payload mass;

W_{pay} is an arbitrated payload weight for each design point;

$W_{0_{ref}}$ is a reference airplane weight with similar structure concept (including material and building technology) and b_{ref} =2.5, reference span and c_{ref} =0.2, reference mean chord;

W_{sys} is the systems weight (motor, propeller, ESC, battery, receiver, etc);

e_b=1.3 and e_c=1 are exponents that reflect the nonlinearity of the empty weight function with the actual airplane span and chord. The constants e_b, e_c, b_{ref} and c_{ref}have been determined through structural construction tests.

3.3.2.4 Propulsive Model

The equations that describe the propulsive model are Equation 3.30 and Equation 3.31:

$$T_{available} = -0.57V_{\infty} + 22 \quad \textbf{(Equation 3.30)}$$

$$T_{available} = (-0.57V_{\infty} + 22\ )I/45 \times 0.95 \quad \textbf{(Equation 3.31)}$$

where V_{∞} is the airspeed, I is the current of the battery and 45 is the minimum battery discharge current rating of 45 A as described in requirement 14 of Section 3.2. These models described the linear reduction in *T* with airspeed and provide a correction for the battery voltage.

3.3.2.5 Stability and Control Modelling

Aircraft must have a certain amount of inherent stability and controllability to be flyable. It is therefore important to consider these characteristics when designing a new aircraft. Accurate evaluation of the stability characteristics of any given aircraft is a complicated process, and is not well suited for preliminary or intermediate design. Fortunately, an alternative criteria that gives reasonable estimates and is vastly simpler to apply can be used. Such estimate is based on static margin, which is given by:

$$\text{S. M.} = \frac{\mathrm{x_{np}} - \mathrm{x_{cg}}}{\mathrm{c}} \quad \textbf{(Equation 3.32)}$$

$$\frac{x_{np}}{c} \approx \frac{1}{4} + \frac{1 + \frac{2}{A_R}}{1 + \frac{2}{A_{R_h}}}\left(1 - \frac{4}{A_R + 2}\right)V_h \quad \textbf{(Equation 3.33)}$$

Where x_{np} is the location of the neutral point, x_{cg} is the cg position and c is the MAC, A_{Rh} the horizontal stabilizer aspect ratio and V_h the tail volume coefficient. Recommended values for the static margin vary between +0.05 and +0.15.

3.3.2.6 Performance Estimation

3.3.2.6.1 Available and required power versus airspeed

A rather complete analysis of performance can be obtained once one has the available and required level flight power curves (see Figure 4.20). The available power was measured in the wind tunnel tests of the propulsive set (Section Propulsion 3.1.1). The levelled flight required power curve was obtained from the flight mechanics model described in Section 3.3.2.1 with 16kg maximum take-off weight at 0m altitude. It is seen that an ample margin was left for achieving good climb performance and execute high load factor g's turns in the speed flight task.

Rate of climb is given by:

$$RC = \frac{P_a - \mathrm{P_R}}{W} \qquad \textbf{(Equation 3.34)}$$

Where P_a is the available propulsive power and $\mathrm{P_R}$ is the required propulsive power.
Then, the terrain climb angle is given by;

$$\gamma = arcsen\frac{RC}{V_\infty - V_{wind}} \qquad \textbf{(Equation 3.35)}$$

3.3.2.6.2 Flight Task Points Estimation

This following model considers a flight task flown in a straight line with semi-circle turns. The length of a turn is given by:

$$L = \pi r + 100 \qquad \textbf{(Equation 3.36)}$$

The flight task points (FTP) is estimated by:

$$FTP = 2m_{payload}\left(\frac{100}{L(0.67V_\infty + 0.33V_{\max})}\right) \qquad \textbf{(Equation 3.37)}$$

where the payload mass ($m_{payload}$) is the total mass of the aircraft (m_{total}) minus the mass of batteries ($m_{batteries}$) minus the empty weight of the aircraft (m_{EMPTY}).

$$m_{payload} = m_{total} - m_{batteries} - m_{EMPTY} \qquad \textbf{(Equation 3.38)}$$

3.3.2.7 Parametric Studies

Multiple airplanes (or design points) are calculated having different spans, chords and lift coefficients using the described formulation (Section 3.3.2). In this way, a parametric study is performed; producing the results presented in Section 4.3 .

3.3.2.7.1 Design Point

Table 3.2 shows the aircraft design point with the most important dimensions.

3.3.2.8 Weight and Balance

Weight budget and the weight and balance results are shown in

Table 3.3. The total mass is expected to be about 16kg and the maximum payload at sea level, 12.75 kg.

Table 3.2 - Design Point

Variables	Value	Variables	Value
h_{CG}	30% MAC	S_V	0.06 m^2
h_H	1.2 m	S_H	0.12 m^2
h_V	1.5 m	b_{Wing}	4.2 m
C_{Lmax}	2.7	b_V	0.65 m
$MTOW$	160 N	b_H	0.72 m
MAC_{Wing}	0.26 m	$A_{R_{Wing}}$	17.6
MAC_{EV}	0.17 m	A_{R_V}	3.28
MAC_{EH}	0.17 m	A_{R_H}	4
S_{Wing}	1.00 m^2	λ_{Wing}	4.8

Table 3.3 - Airplane weight and balance

Nº	Components	Weight [g]	Quantities	Total Weight [g]	dXcg* [mm]	W*dXcg [gfmm]
1	Wing Root Panel	450	2	900	-139	-125100
2	Tip Wing Panels	350	2	700	-127	-88900
3	Winglets	200	2	400	-99	-39600
4	Tail Horizontal Surface	80	1	80	1199	95920
5	Tail Vertical Surface	70	1	70	1438	100660
6	Motor Boom	35	1	35	-404	-14140
7	Cargo Bay Body	250	1	250	-149	-37250
8	Cargo Bay	35	1	35	-189	-6615
9	Tail Boom	100	1	100	685	68500
10	Motor	181	1	181	-517	-93577
11	Propeller	10	1	10	-559	-5590
12	Prop Hub/Spinner	10	1	10	-559	-5590
13	Battery	220	1	220	-365	-80300
14	Electric Speed Controller	50	1	50	-460	-23000
15	Receptor Rx	15	1	15	-249	-3735
16	Receptor battery	60	1	60	-420	-25200
17	Landing Gear	129	1	129	-189	-24381
18	Wing Servos	9	not defined	50	-70	-3500
19	Tail Servos	9	2	18	1320	11880
21	Servo Wires and Servo Plugs	35	1	35	0	0
22	Battery/ESC/Motor Connectors	10	4	40	-460	-18400
23	Payload	12750	1	12750	-205	-2613750
	Structure Weight [g]	2699			**Total Dw**	-2931668
	Systems Weight [g]	689			**CG**	-181.6624117
	Total Empty Weight [g]	3388			**%mac**	30.1
	Take Off Weight [g]	16138				

* Datum Line is the Wing Root Trailing Edge. Positive direction of X is from trailing edge to the tail.

3.4 Detailed Design

3.4.1 Wing Design

The wing chord, sweep, dihedral, incidence and sweep distributions along the span were studied using an iterative study using XFLR5. Tiny changes to the overall shape of the wing were systematically made, having the maximum lift to drag ratio and the drag versus airspeed results as the optimization drivers. To reduce the induced drag, it was decided to use winglets. With a trial and error approach, where the relative span, dihedral angle, sweep back and chord distribution were iteratively changed until the results were not getting better, the final wing was designed.

3.4.2 Propulsion

3.4.2.1 Motor controller – ESC

The team decided to use a speed controller with data logging to make the aircraft's flight tests an easier task. Besides that, a lightweight ESC with very low internal resistance are the concepts that guided the search for the ideal hardware. The selected ESC is the Castle Creations Phoenix Lite 100 that was purchased by UBI for the ACC 2011 edition because of the data collection of the motor rotational speed, current and voltage that it allows.

3.4.2.2 Battery

As shown in Section 4.1, from the set of purchased batteries, the Basher 2800 mAh 3S is the correct choice for us.

3.4.3 Detailed Wing design

Through XFLR5, with the chosen airfoils and wingspan, an iterative process was used to set the final shape of the wing. Taper, dihedral and sweep were systematically changed to obtain the maximum possible efficiency (L/D) over the speed range and in particular: push the lower level flight drag to the highest possible airspeed, such that the maximum level flight airspeed is maximized to perform the flight task legs in minimum time.

One big concern is the flight characteristics when the airplane stalls. The wing must have washout at the wingtip to prevent a wingtip stall, a linear washout distribution along the entire wingspan was tested against washout only at the wing tip panels, this last option can provide the flight characteristics that are needed without a significant penalization in the wing efficiency.

3.4.3.1 Fowler flap mechanism

To design the Fowler Flap mechanism, the software SolidWorks was used to aid with the design. Figure 4.15 shows the work environment Sketch of the Dassault Systems SolidWorks software. The motion and dimensions of the bars was iterated so that the motion was perfect and the bars did not interfere with each other. The bars are the components represented by dashed lines and the circumferences are hinges. The circumferences with a circle inside are fixed position hinges. The circumferences with a cross are hinges that connect the bars and are free to move according to the bars motion. It was essential to guarantee that for both the extended and retracted positions, none of the mechanism´s bars interfered with each other. After the design was ready on SolidWorks, a 3D printer was used to "build" all the components. A total of 9 different components were printed for each single flap mechanism set.

The flap was first designed on SolidWorks. An STL file is then created and exported to a software in order to validate the scale and orientation of the part. Finally, a G-code is produced to print the parts on the 3D printer. After printing, the components will be assembled. The time of assembly is quite long due to the size of the components and the material that is used. The material used in the 3D printing, polylactic acid (PLA) is quite resistant, but with pieces measuring about 1 cm, these can be easily bent or broken when doing the perforations for the assembly (a hole diameter study was performed to allow a reliable assembly with an appropriate hole diameter. However, when the mechanisms were printed for the different stations of the wing, the hole diameter that should have been kept constant was changed due to scaling effects. This meant that the smaller mechanisms near the wing tips had small holes that required perforations to be enlarged, and the mechanisms near the roots had holes that were too large). Pins were used to keep the connections in place.

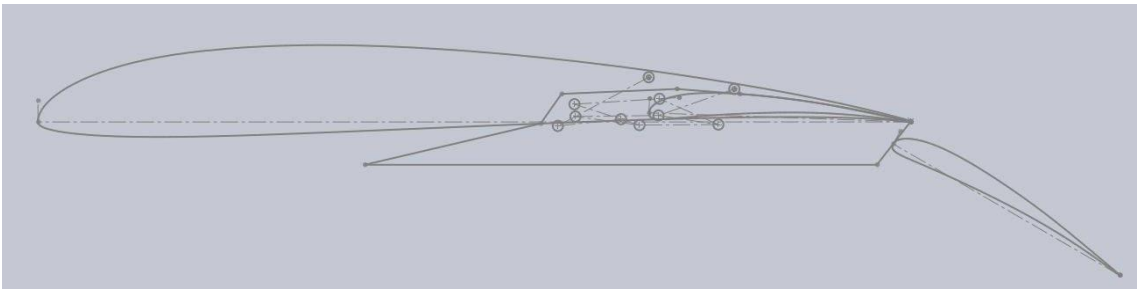

Figure 3.17 - Design of mechanism in Dassault Systems SolidWorks software.

3.5 Airplane Construction

3.5.1 Wings

For the manufacturing of the wing moulds, first it was decided to manufacture a wing mould plug (also called wing master). Foam cores were cut in the hot wire cutting 4-axis CNC machine, sanded with 80 grit sandpaper, the pores and dents were filled with hollow glass microballoons-epoxy, (Resin Biresin CR92 and Biresin CH92 of Hardener mix ratio 100:28) and two layers of bidirectional glass fibre 120g/m^2 ±45° were wet layed up and allowed to cure. A thick layer of hollow glass microballoons-epoxy was then applied and sanded after cure. After sanding with increasing higher sanding paper grit (up to 600 grit), a coat of paint two component polyurethane paint was applied; this coat was carefully sanded. This was done to ensure the surface was smooth to guarantee that the final aircraft has minimal skin friction drag. Figure 3.18 shows the process. Figure 3.19 shows the resulting upper surface on one of the wing mould plug. The reflection shows the smoothness of the surface.

The Epoxy, Biresin CR92 and Hardener Biresin CH92 will be used in all constructions.

The next step was to build the mould using the wing plug. As seen on Figure 3.20 a), wooden planks were placed to create the parting line and small pieces of wax were applied as alignment dowels (red dots on the mould). Then, on a dust clean environment (see Figure 3.20 b)), a layer of PVA is applied and allowed to dry for demoulding the master from the future mould. The mould structure started by a layer of tooling epoxy gel coat (a mix Biresin S15 A:B = 100:7) and then left to cure. The gel coating is used to give the mould a hard and smooth finished surface. Before drying, a layer of fibreglass (chopped strand mat 450 g/m^2) and epoxy resin was applied and allowed to cure, see Figure 3.20 d). To provide rigidity to the to the mould structure, a plank of MDF (medium density fibreboard) was attached to the mould back side with polyurethane foam. In a previous attempt, a mixture of sand and polyester resin was used to reinforce the moulds but it proved unsuccessful as the polyester resign delaminated from GFRP, allowing for the remaining GFRP mould structure to warp beyond repair. For this reason, the moulds construction took place twice, delaying the airplane construction in a crucial manner. For the other half of the wing mould, the same process was repeated, but with a small difference. Since a gel coat layer is applied on top of the male mould, to demould it is necessary to apply PVA (Figure 3.20 c) to the existing half of the mould too. This layer must have as few imperfections as possible and as few air bubbles and dust particles as possible, otherwise the mould replicates all those imperfections to the produced parts. The technique used was to apply the PVA with a paint air gun inside an improvised clean room. Nevertheless, applying the PVA proved to be extremely difficult because it was very prone to run off the mould surface making the PVA film uneven.

Once both halves of the mould were done, demoulding is easy with the use of PVA, both the lower and upper surface sandwich skins of the wings could be built. The advantage of using moulds is that it is possible to build the whole wing in a single procedure, with precisely the desired geometry and size.

Figure 3.18 – Male mould fabrication process. The figure shows the application of hollow microballoons a), glass fibre layers b) another layer of hollow microballoons c), and coat of paint d).

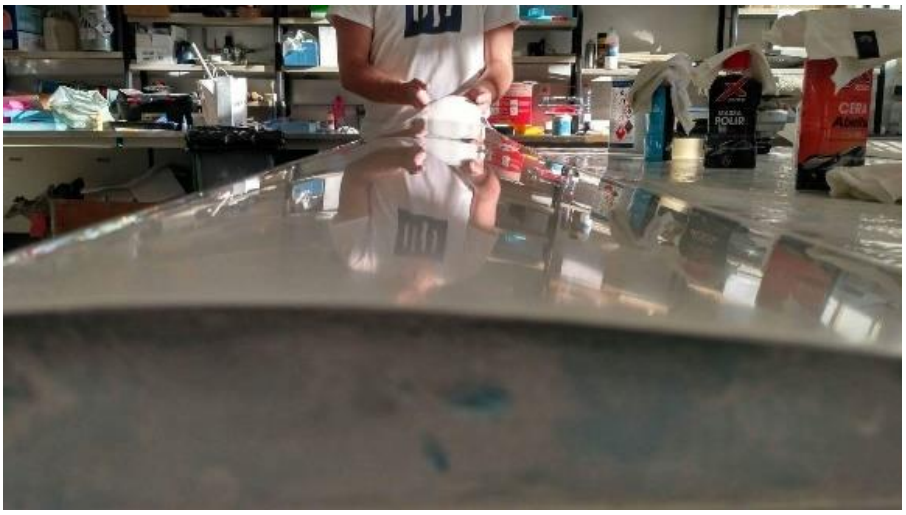

Figure 3.19 -- Wing mould plug fabrication process.

Figure 3.20 – Wing mould manufacturing.

Figure 3.16, in Section 3.2.1, shows the conceptual design of the wing shell; this is how the wing was built using the moulds. To build the wing skins shells, each wing surface outer contour and important characteristics like fibre reinforcements limits were drawn on a clear flexible plastic sheet with a permanent marker first, see in Figure 3.21 a). Then, 1mm medium density balsa wood pieces were cut for the sandwich skin cores as well as the bi-axial fibre ± 45 degree 80 g/m^2 carbon cloth pieces that made up the sandwich skins. The carbon cloth was impregnated with epoxy resin using a roller and laid up between two sheets of the clear plastic sheets before it was laid on the mould surface; the amount of resin was kept to a minimum to keep the weight in check. One of the advantages of producing laminates by hand is that the person doing the job can judge the necessary amount of resin while the job is performed. Putting the carbon fibres cloth between two clear plastic sheets made spreading the resin easier, thus helping to control the weight. Nevertheless, the biaxial carbon cloth may well absorb more resin than the spread tow bidirectional carbon fabric because the first seems to build a thinner skin for the same cloth weight per square meter. The impregnated carbon Cloth was trimmed cut to the limits of the clear plastic sheets to make it easier to place it in the mould without dealing with excess fabric, see in Figure 3.21. The whole process must be performed within the epoxy resin working time; otherwise, the resin will harden, making it impossible to use the material. In this manner, the mould that was previously coated with PVA, a sandwich wing consisting in faces of one layer of bi-axial CFRP and 1mm balsa wood core is built. Hollow microballoons were used to fill the voids. At the same time, great care is taken to leave sufficient space between two balsa core sheets in the correct position for the spar caps (see Section 3.5.1.1.). After placing the spar caps that were also hand laid up from unidirectional carbon roving, the outer layer of wet bi-axial carbon cloth is applied.

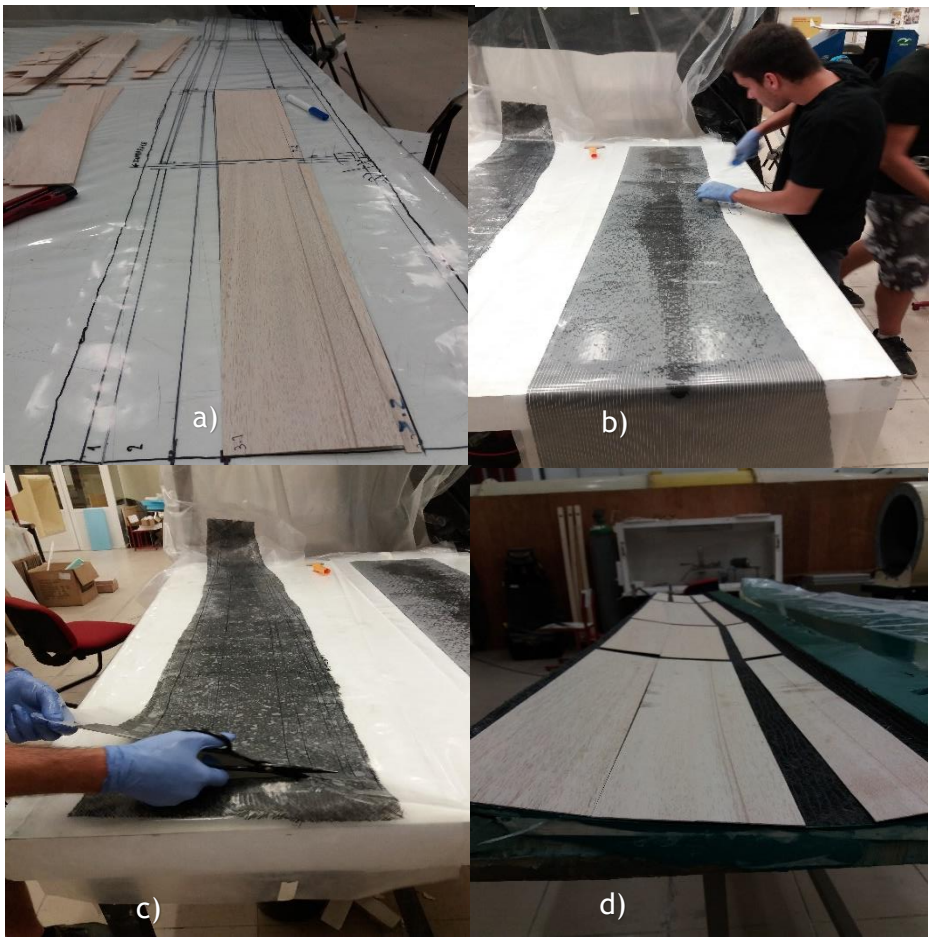

Figure 3.21 – Wing shell manufacturing a) drawing the wing skins structure on clear flexible plastic sheet and cutting the balsa wood core sheets to size; b) laying up the bi-axial carbon fibre cloth with epoxy resin; c) cutting the carbon fibre to measure according to the clear plastic sheets markings; d) applying balsa wood on the carbon fibre (note the gap for the unidirectional carbon fibres spar cap on the lower right).

3.5.1.1 Spar

This part of the work had to be performed at the same time as the wing shells/skins. The spar resists most of the most demanding loads imposed on the wing. If this step is not performed properly, the wing's structure may be compromised leading to serious structural failure and the loss of the airplane. Unidirectional carbon fibre roving were cut (Figure 3.22 a)), carefully impregnated with epoxy resin and placed in the gaps between the 1mm core balsa sheets reserved for the wing (Figure 3.22 b)). In Figure 3.22 c), the wing spar cap is carefully placed. The spar cap thickness is constant at 1mm to conform with the wing shell balsa core but the width is substantially increased near the root, starting from 5mm near the wing tip increasing linearly to 50 mm at the wing root. In Figure 3.22 d), the result can be seen; it is also possible to see the mixture of epoxy and hollow microballons filling any region prone to voids or to starve the impregnated fibres cloths by capillary resin absorption in the wing shell structure,

including the balsa wood core sheets pores. This procedure is performed at the same time for the four moulds: 2 upper surfaces of the wing and 2 lower surfaces of the wings. This was performed during a single night.

Figure 3.22 – Wing shell manufacturing.

3.5.1.2 Vacuum Bag

After lamination, the curing process is done in a vacuum bag. Figure 3.23 shows the vacuum bag. It was allowed to cure for 12 hours only due to the strict schedule at the moment but no problem was encountered due to the rather low curing time.

Figure 3.23 – Improvised vacuum bag.

The next step was to join the wing halves. The limits of the Fowler Flap were delimited with a barrier wall of plasticine so that both the leading edge and trailing edge of the wing could be filled with polyurethane foam as seen on Figure 3.24 b) without the foam invading the Fowler flap region. At the same time, the 6mm medium density balsa wood spar web was placed with a bidirectional $200 g/m^2$ carbon cloth impregnated with epoxy at ± 45 degree orientation. Figure 3.24 c) shows how the panels were joined while still in their respective mould half. The alignment dowels initially defined by wax pins during the mould construction of Figure 3.20 a) were now used since they guarantee that the panels fit in the right place for the perfect match between the wing lower and upper surfaces.

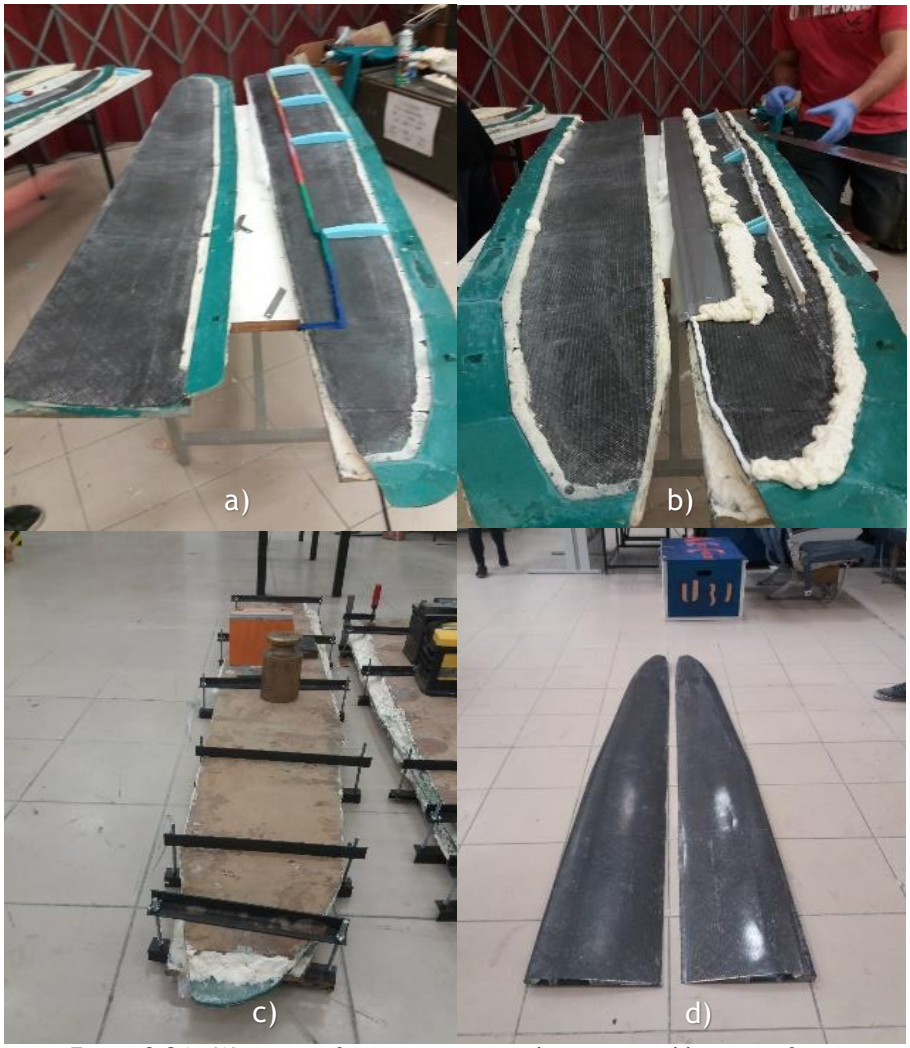

Figure 3.24 – Wing manufacturing, joining the upper and lower surfaces

3.5.1.3 Wing Panels Attachment Interfaces

The four interfaces that joined the wing panels together were made from segments of rectangular solid pultruded CFRP with attachment pins on the extremities tied with ultra-high-molecular-weight polyethylene (UHMWPE, UHMW) Dyneema® strings and cyanoacrylate glue. The reinforcement of the pin for the interfaces was thoroughly tested. First, unidirectional carbon fibres were used, but these proved inadequate. Then, with UHMWPE; the number of reinforcement turns was estimated and tested successively to determine the necessary amount. These interfaces in Figure 3.25 were built in series and were all lookalike such that if any single one would fail during the competition, it could be replaced readily (see Figure 3.26).

Clamps were used to join the moulds halves but they were overtightened in the region of the root of the left wing producing a significant dent in the upper surface of the root panel of the left wing.

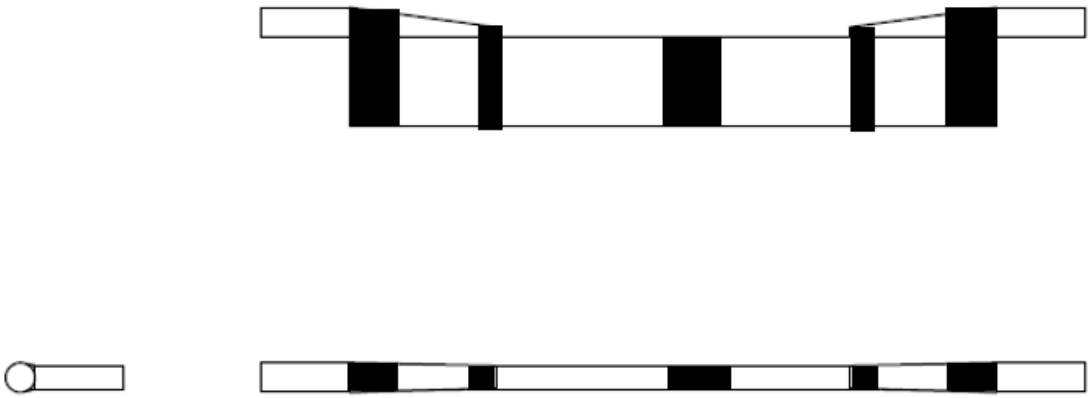

Figure 3.25 -2D drawing of an interface. The black bands correspond to the Dyneema®

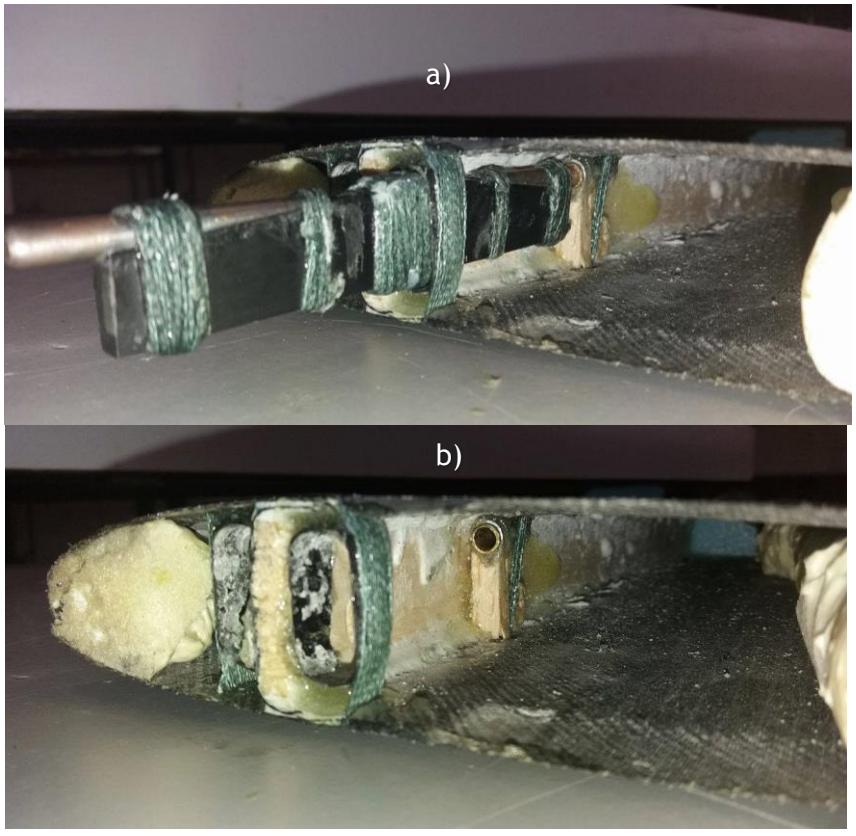

Figure 3.26 – a) The connection between wing panels showing the interface part: a); and the hard-points in greater detail: b).

3.5.2 Tails

A tail boom supporting cone made of solid 30 kg/m^3 Expanded Polystyrene (EPS) foam was used just after the cargo bay compartment. The tail surfaces will be built with conventional ribs and heat shrink film covering using balsa wood cap spars and EPS cores. Figure 3.27 a) final tail and b) tails on CATIA V5.

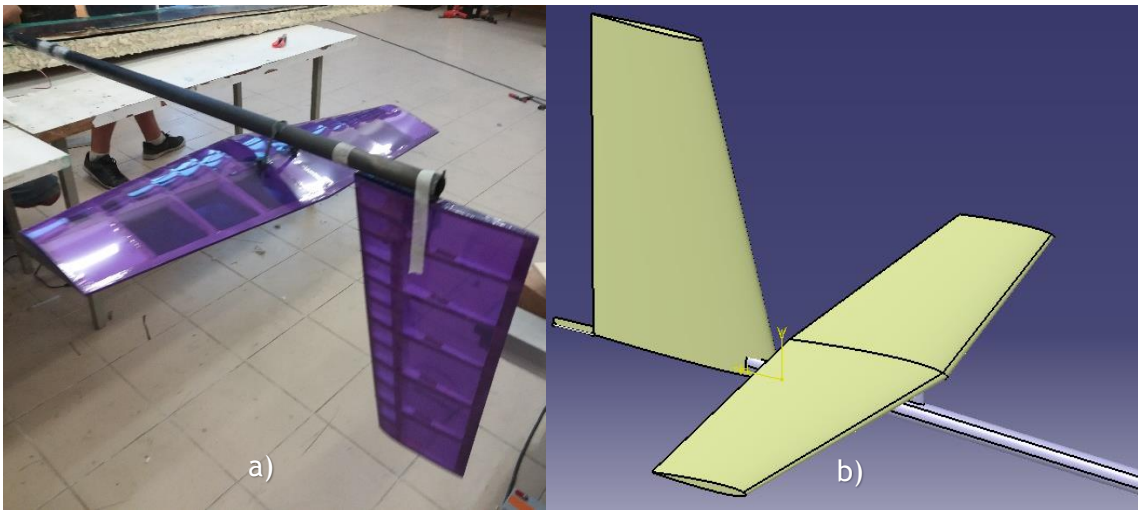

Figure 3.27 – Tail surfaces.

3.5.3 Cargo Bay

CATIA V5 image of the cargo bay is shown in Figure 3.28. The three connection links were made of rectangular solid pultruded with balsa wood cores and the extremities had pins covered with Dyneema®.

3.5.4 Fuselage

Fishing rods CFRP tubes were used to support the motor and the tail surfaces. These are off-the-shelf light-weight structural components that offer a great compromise of price-weight-strength-rigidity. The fuselage will be a CFRP tube (fishing rod) with a support for the motor on one of the ends and the connections to the tail surfaces on the other end.

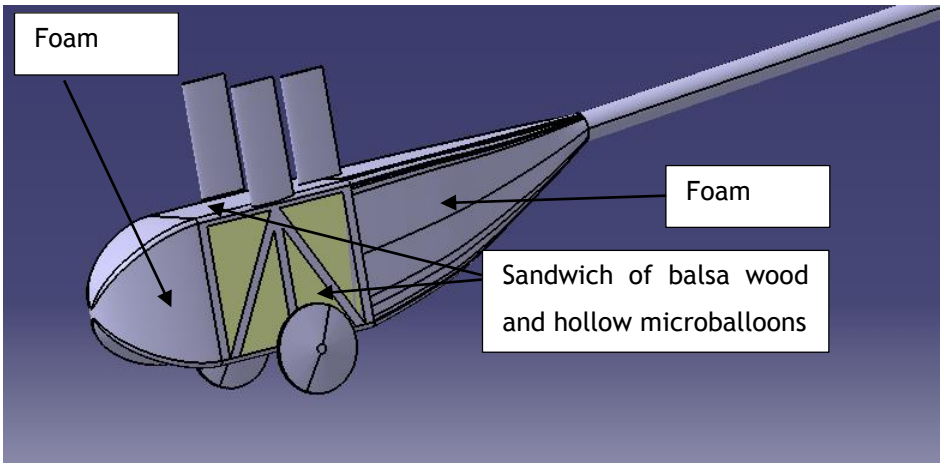

Figure 3.28 – Cargo bay image on CATIA V5.

4 Results

4.1 Propulsion

After collecting the experimental data from the batteries with the test rig described in Section 3.1.1.2, the results confirm that significant supply voltage difference occur in the final of the flight (about 200 seconds) that according to the battery pack in use, thus confirming the importance of battery choice in the performance of the propulsion system, see Figure 4.3. The higher the voltage supplied by the battery, the higher will be the motor speed, that is proportional to the supply voltage for the same load, and the higher will be the current to the motor (note that motor torque is proportional to the current) thus, an even higher useful power will be available, giving more performance to the airplane.

Figure 4.1 shows the instantaneous voltage of the worst and the best batteries. The worst is Tattu 1300 mAh and the best one is Basher 2800 mAh 3S HV.

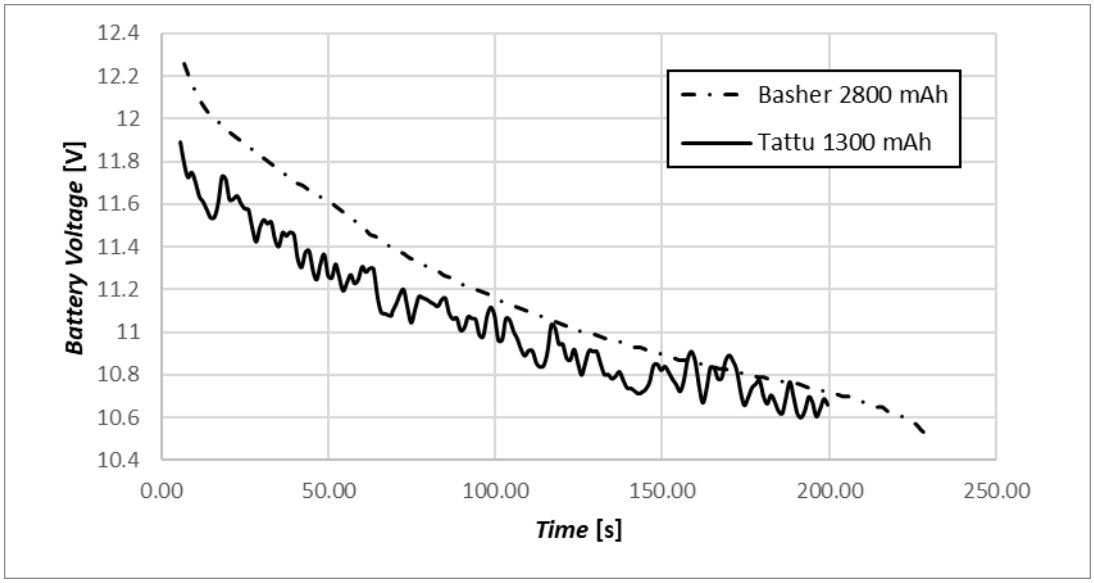

Figure 4.1 - Instantaneous voltage of the worst and the best batteries.

The experiments show that heated batteries at 40º Celsius to have higher voltage under load and during the flight than the ones that room temperature. Thus, heated batteries give more performance. (See Figure Figure 4.2)

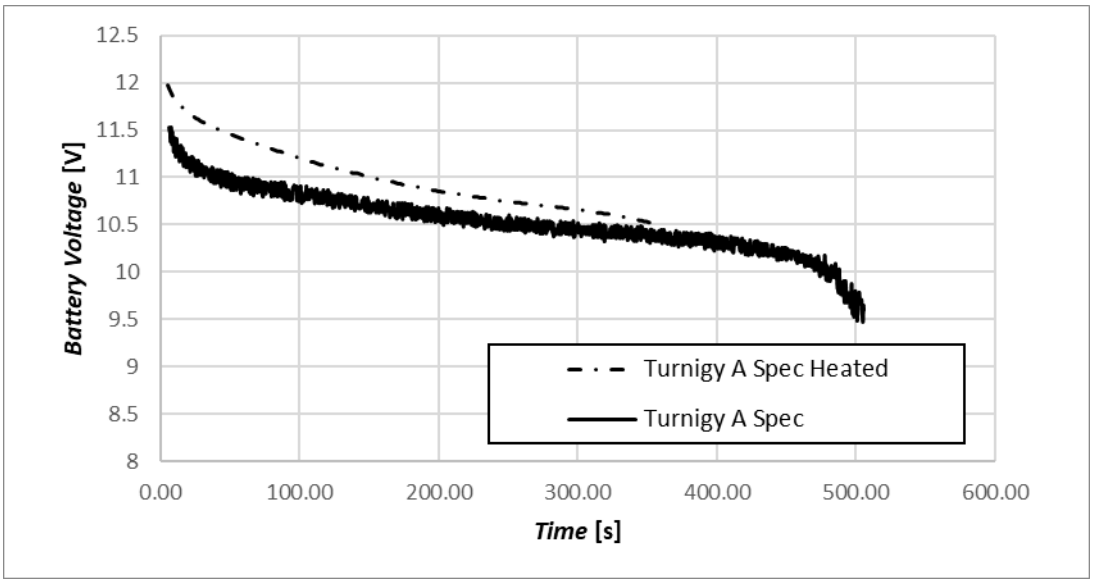

Figure 4.2 -Comparison of a heated versus a cold Turnigy A Spec 4500 battery.

The data from heated batteries tests are presented in Figure 4.3. The best battery, considered to be the best choice for the current ACC17 airplane was the Basher 2800 mAh 3S HV, because it can hold more voltage in the initial take-off and climb, giving a higher performance to the airplane. This can be explained by the high voltage (HV) characteristic of this battery. Meaning that it can be charged to 4.35V against 4.20V of the regular LiPo batteries. Battery Ultimate 6400 mAh 3S seems to have a better performance from the middle of the flight duration onwards, but it was not the best choice for the airplane because this battery has much more capacity and weight than all the others, so it is far from the final stage of the discharge in a flight of 200 seconds.

Another important factor to know about the batteries is their weight. So, the specific energy was measured for a 150 seconds flight, based on current, voltage and time (See Figure 4.4). The points located further upwards and to the left correspond to the better-suited batteries for our airplane, because those deliver more energy to the airplane while their smaller weight waist less energy to be carried on bord during the flight. According to this last comparison chart, the best battery to our model is confirmed to be the Basher 2800 mAh 3S HV, the Lithium High Voltage (LiHV) battery can hold the highest voltage throughout the flight and has the highest specific energy.

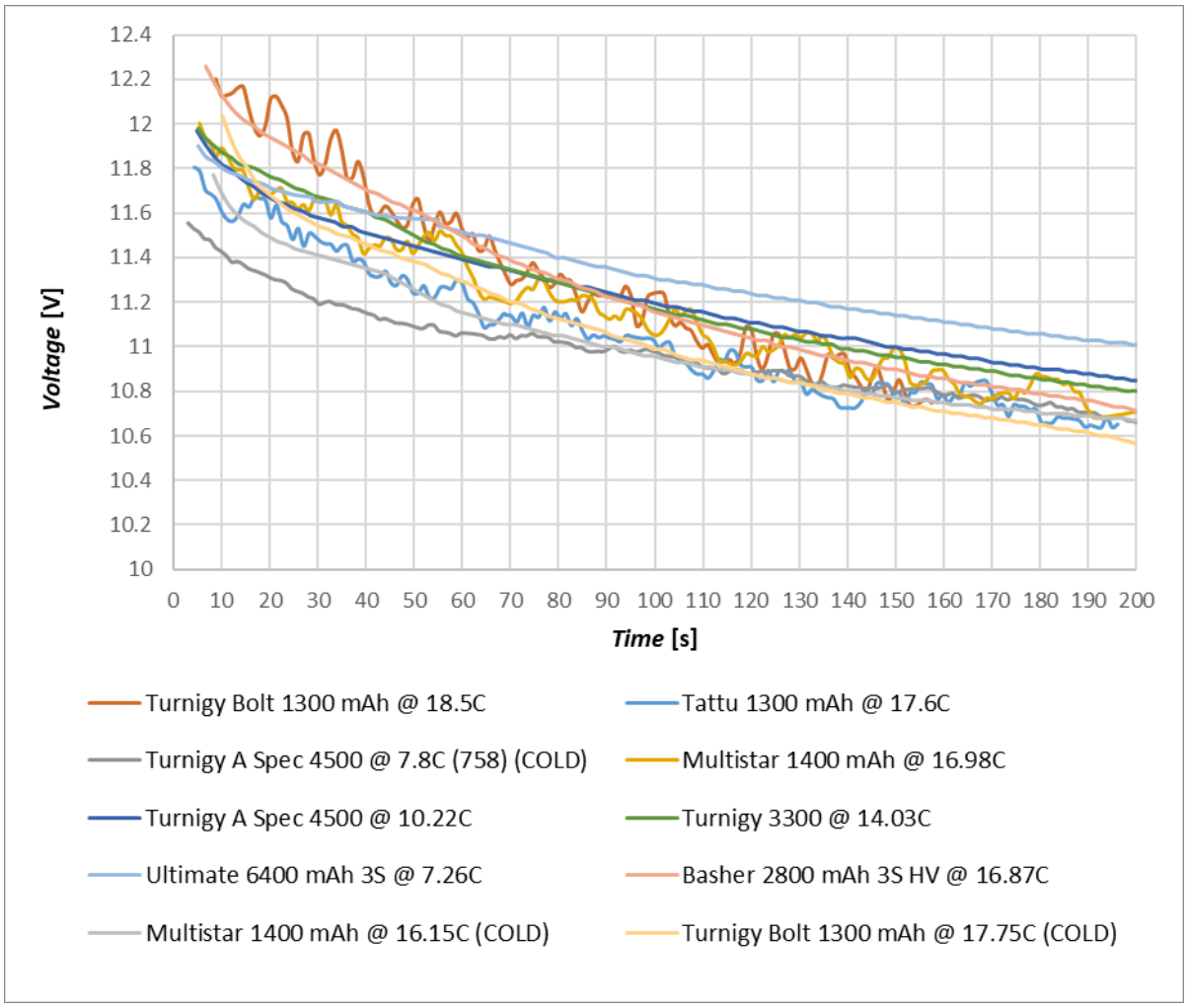

Figure 4.3 - Batteries performance data.

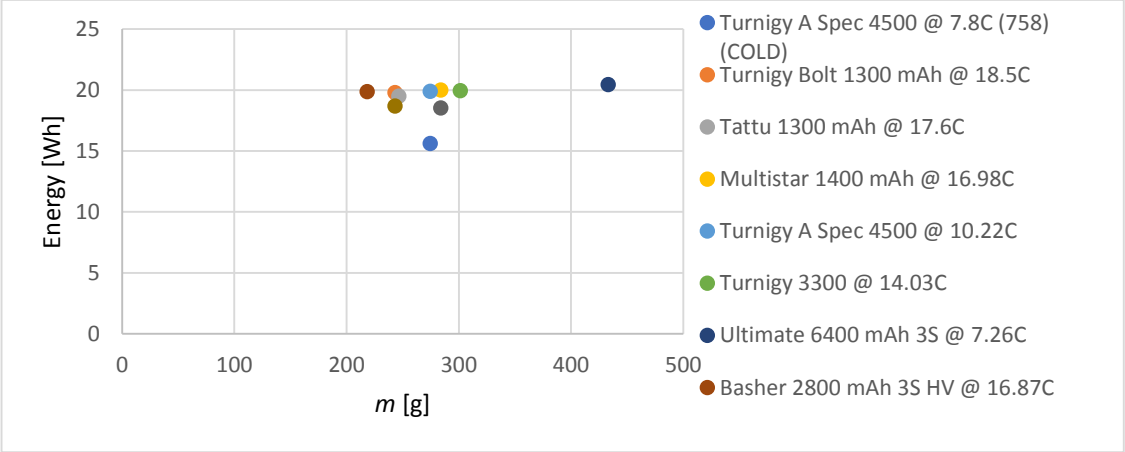

Figure 4.4 - Comparison of the specific energy of all batteries with the time of flight of 150s.

4.2 Aerodynamics

4.2.1 Designed Airfoils

Figure 4.5 shows the final airplane main wing airfoil used in the competition (full line). The airfoil with the dashed line is the initial airfoil MS115_437, used in the Fowler flap design. Note that the final airfoil has a larger trailing edge angle. This allows an easier installation of the Fowler flap and respective mechanism. Figure 4.6 shows the Wing tip airfoil.

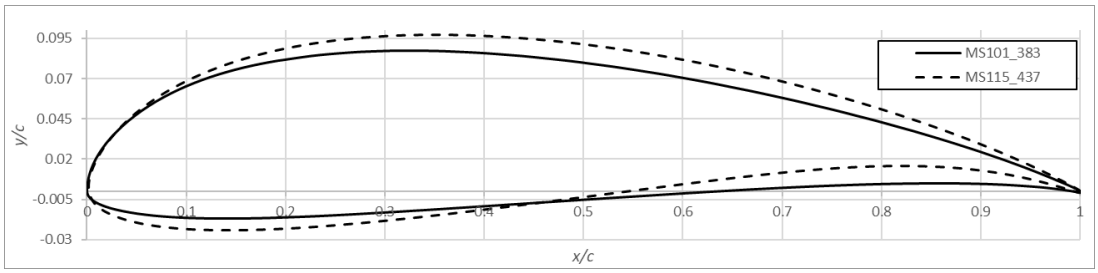

Figure 4.5 – Airfoils: MS115_437 initial airfoil; MS101_383 final airfoil used in the UBI ACC17.

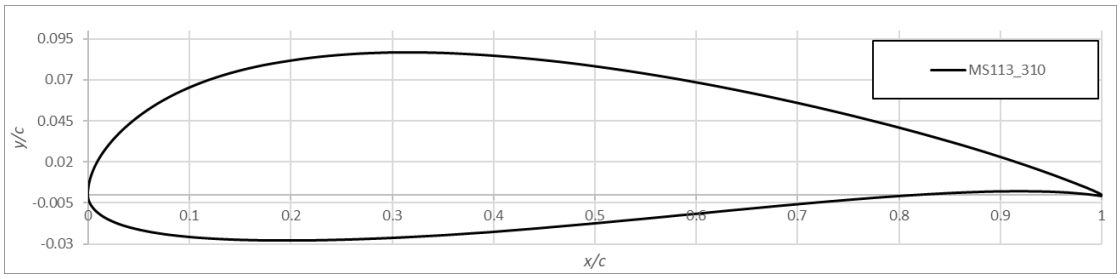

Figure 4.6 -MS113_310, wing tip airfoil

The flight task speed legs, according to the calculations using the theoretical models described in Section 3.3.2.1 for the airplane design (Table 3.2) is performed at a Cl value of 0.4. Iterative changes to the airfoil geometry through the inverse design tool allowed the design of an initial airplane airfoil later improved to a main final wing airfoil and a tip airfoil. The airfoil nomenclature follows a designer-thickness-camber reasoning. The airfoil designed for the airplane is the MS 115_437, thus meaning Miguel Silvestre (designer), 11.49% relative thickness and 4.37% camber. MS101_383 is the final airfoil design for the UBI ACC17 airplane and has 10.10% relative thickness and 3.83% camber. While designing these airfoils, the objective was to maximize the aerodynamic efficiency (C_l/C_d) around that lift coefficient. This is the reason why, according to Figure 4.7, the final airfoil is expected to have a maximum C_l/C_d that is not impressive at a value of near 80 at $Re\sqrt{C_l}$=200,000, against 85 of the initial airfoil, and near 60 at $Re\sqrt{C_l}$=100,000, but, on the hand, has a remarkable C_l/C_d value at the 0.4 lift coefficient of about 65 at $Re\sqrt{C_l}$=200,000, compared to just below 50 of the initial airfoil, and 40 at $Re\sqrt{C_l}$=100,000. The tip airfoil, MS113_310, was developed to behave similarly as the main

airfoil, but it was important that the C_l/C_d would not deteriorate for lift coefficients because the tip effectively works at lower lift coefficients and, also, to not stall before the main airfoil. In Figure 4.7, the tip airfoil data performance prediction is presented only at $Re\sqrt{C_l}$=100,000 and is seen to have a slightly even higher C_l/C_d value of 42 against the final main wing airfoil at the 0.4 lift coefficient and increasingly smaller C_d value as the lift coefficient drops way from 0.4 (clearer in Figure 4.8).

It is seen that the aerodynamic efficiency in the Figure 4.7 for the initial airfoil. MS115_437 peaks at 85 for a lift coefficient of 1 and holds a value above 50 from 0.5 to 1.5 Cl. The pitching moment coefficient is quite low at -0.16 and the maximum lift coefficient is expected to reach 1.6.

Figure 4.8 also shows that MS 101_383 has a lower drag coefficient at lower lift coefficients. For the flight task lift coefficient, has a lower drag at a Cl below 0.4., this is ideal since the wingtip is operating at a lower lift coefficient. The Cl/Cd of MS101_383 is also higher. Despite having an overall slightly lower maximum Cl/Cd, at lower lift coefficients, the Cl/Cd is also slightly higher for the MS 101_383 and better distributed over the whole C_l range.

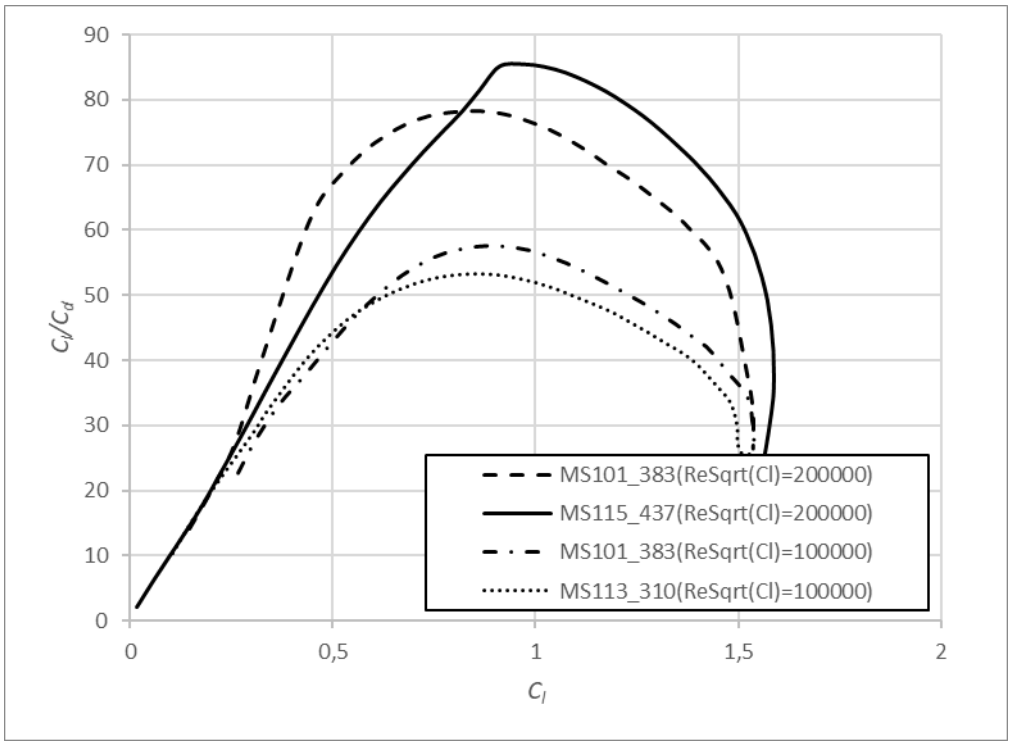

Figure 4.7 - Airfoil lift to drag ratio comparison. MS115_437 is the airfoil initially developed; MS101_383 is the final airplane airfoil; MS113_310 is the wingtip airfoil.

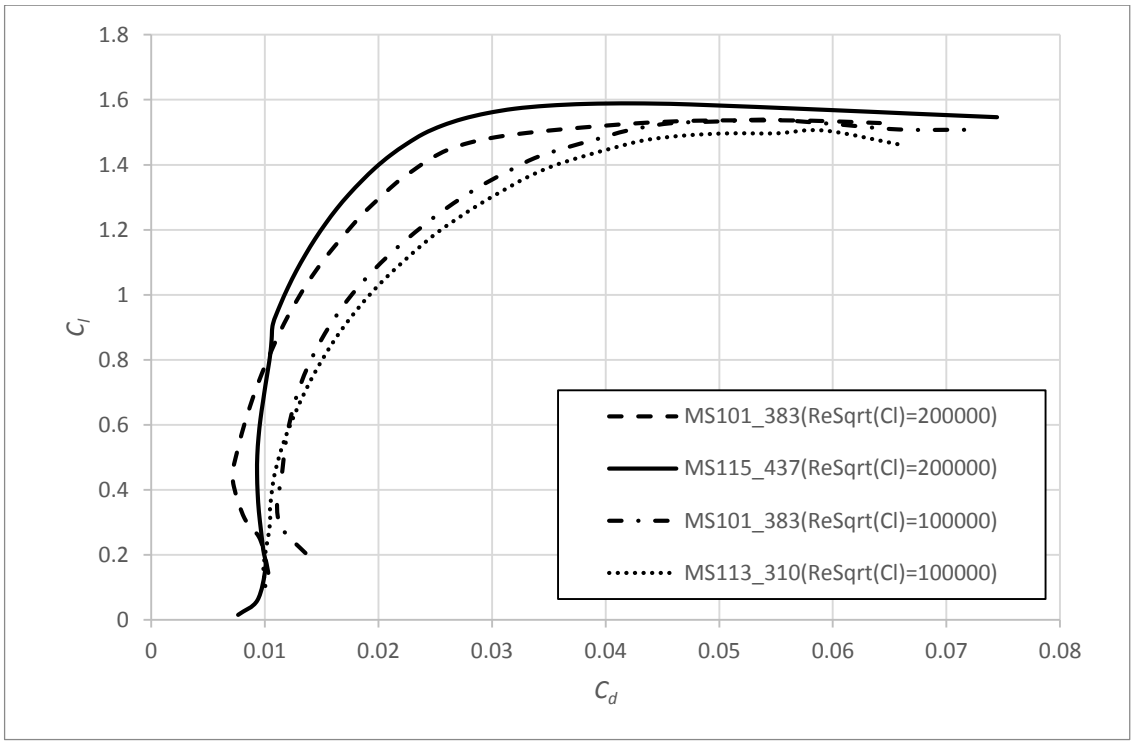

Figure 4.8 – Airfoils drag polars.

Figure 4.9 shows MS101_383 has a slightly lower maximum lift coefficient occurring at approximately the same angle of attack of the other airfoils.

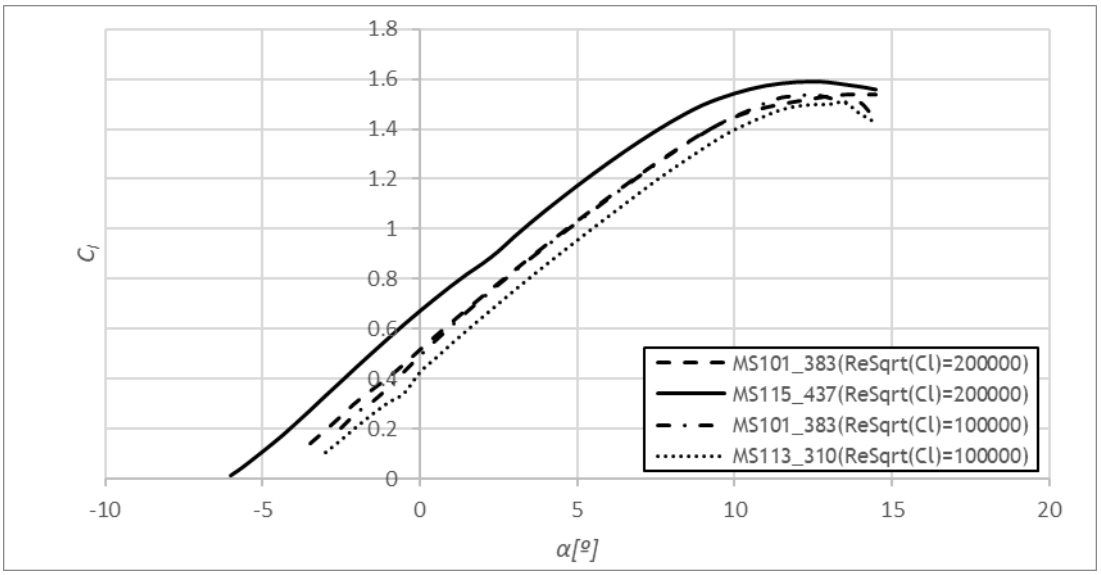

Figure 4.9 – Airfoils lift curves.

Figure 4.10 and Figure 4.11 show the transition point on the airfoil from laminar to turbulent flow. On the underside of the airfoil, Figure 4.10 shows that the airflow remains attached for a $Cl = 0.4$ (laminar) throughout the entirety of the airfoil chord.

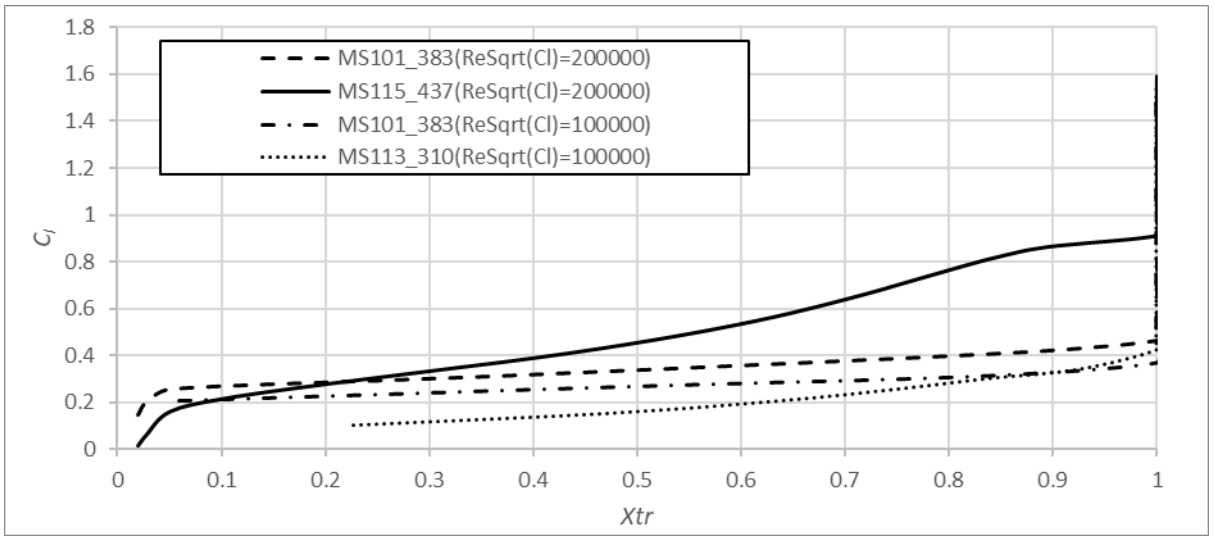

Figure 4.10 – Lower surface transition curves.

On the upper side of the airfoil, Figure 4.11, it is shown that the airflow remains laminar until 90 % of the chord at a lift coefficient of 0.4. After this, the airflow transitions from laminar to turbulent. It is desirable to delay the airflow separation as much as possible since laminar flows have less overall drag. Sometimes, in a low Re number a reattachment bubble may form, that is, the airflow will separate from the surface and then become reattached further downstream.

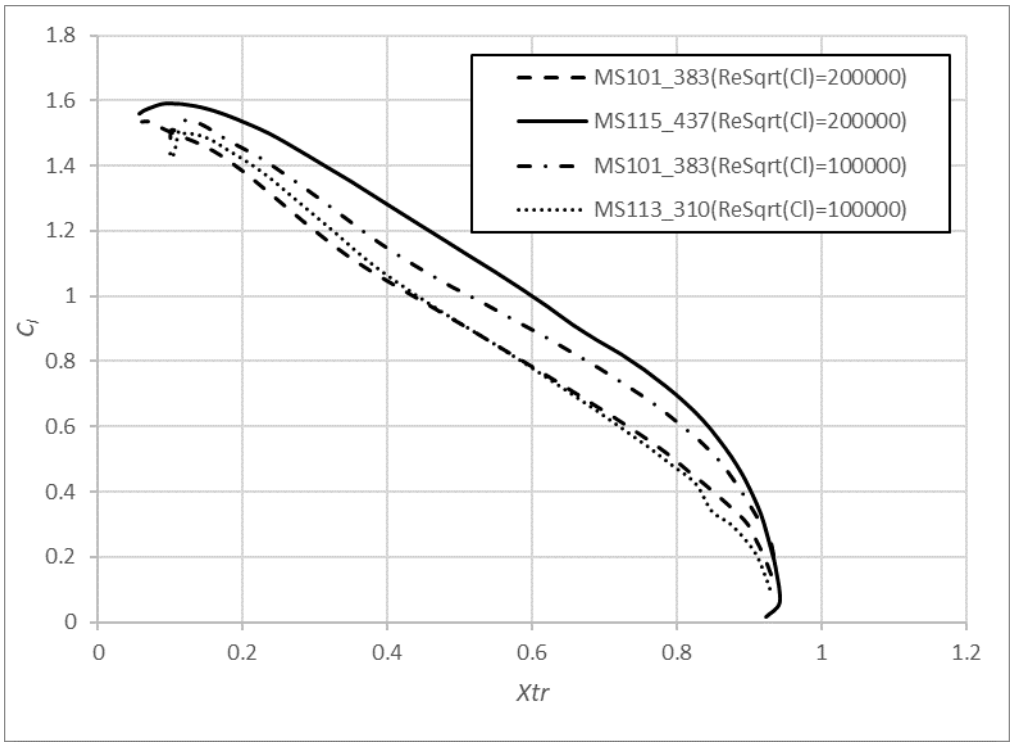

Figure 4.11 – Upper surface transition curves.

MS115_437 has a higher Pitching moment in Figure 4.12 than MS101_383.

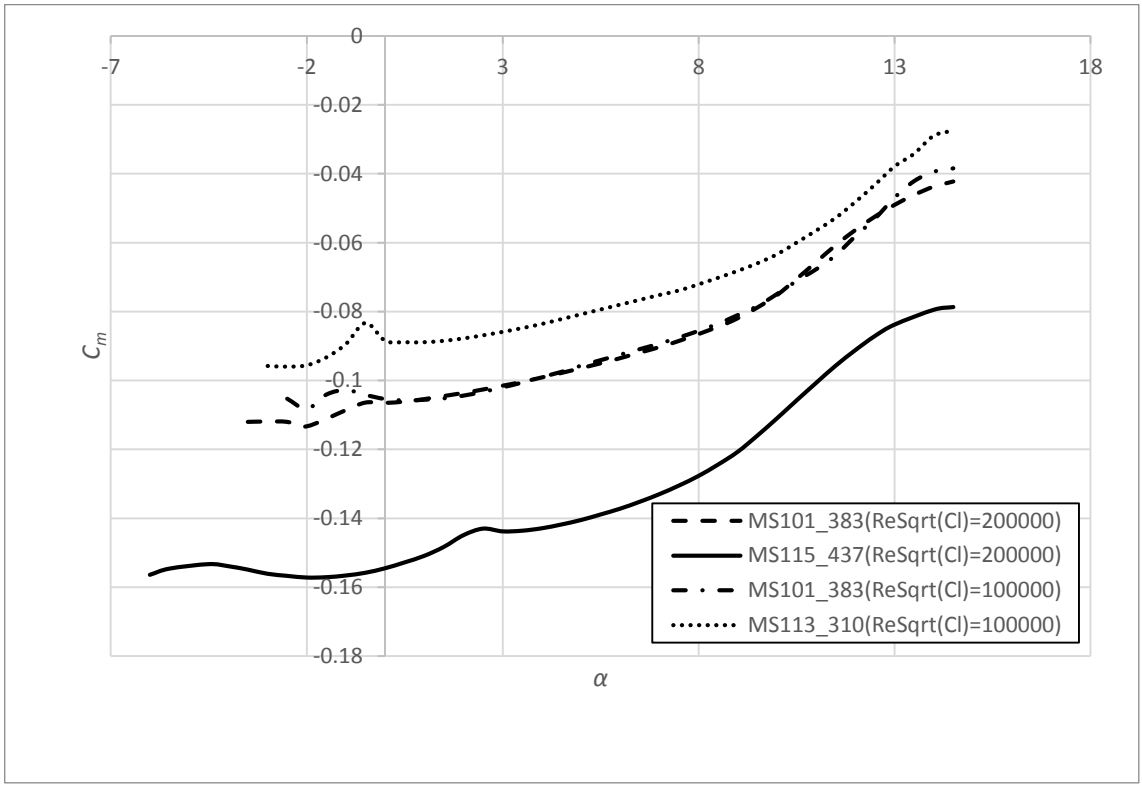

Figure 4.12 – Airfoil pitching moment comparison.

4.2.2 Fowler Flap

With the preliminary version of the airfoil designed for the current ACC airplane, Figure 4.13 shows the geometry of the $0.3c$ Fowler Flap to use with a maximum lift coefficient flap design condition of -0,025 gap, $0{,}02c$ overlap, 30º deflection. Figure 4.14 shows the results obtained according to the methodology described in reference [16]. It is seen in the top left graph the lift curve showing a maximum lift coefficient of about 3. In the top right, the drag polar shows a reasonable profile drag in the lift coefficient interval of 2 to 3. In the lower left, the aerodynamic efficiency versus lift coefficient shows values of about 30 for the same lift coefficient interval (although the simulations seem to over predict the drag coefficient because they do not predict the transition position correctly). In the lower right, the pitching moment coefficient versus lift coefficient shows a mean pitching moment coefficient of about -0.6 demanding for a high value of horizontal tail volume coefficient.

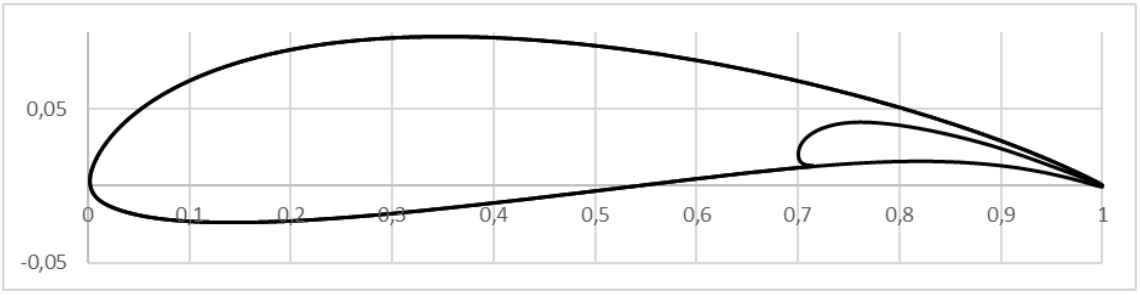

Figure 4.13 - MS115_437 with the 0.3c Fowler Flap.

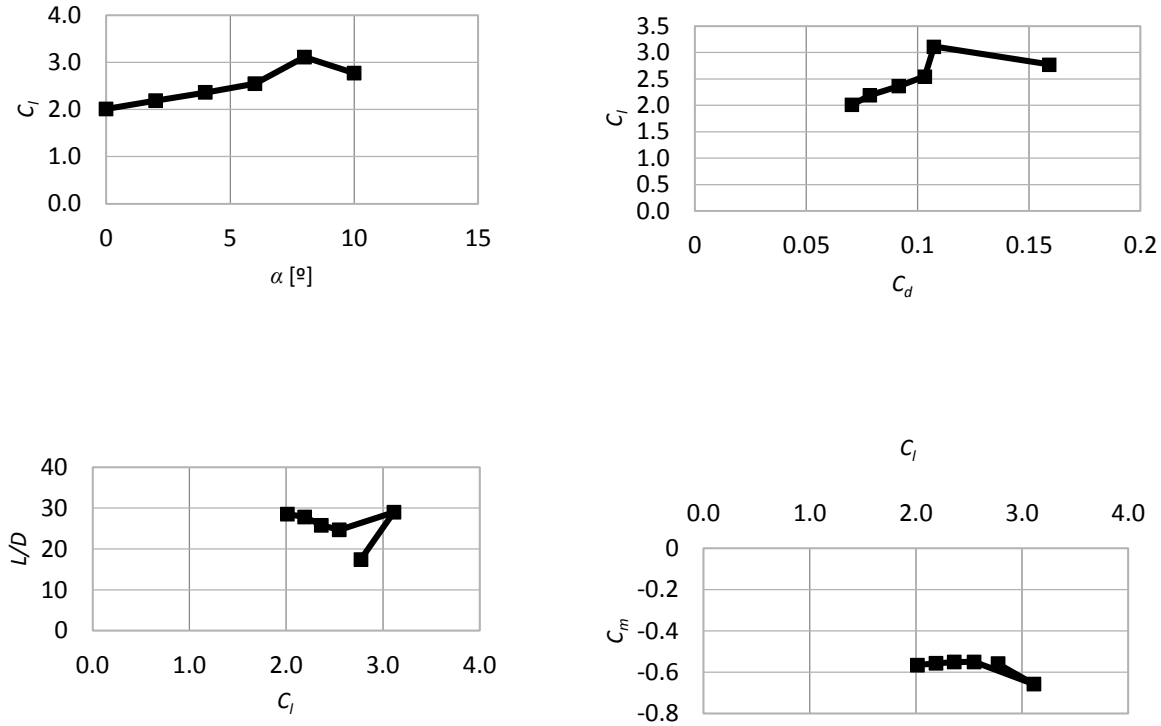

Figure 4.14 - MARS_UBI_ACC2017 Airfoil and 0.3C Fowler Flap geometry with -0,025 gap, 0.02C overlap, 30º deflection angle. Top left: lift curve. Top right: drag polar. Lower left: aerodynamic efficiency versus lift coefficient. Lower Right: pitching moment coefficient versus lift coefficient.

Figure 4.15 and Figure 4.16 show the final mechanism design. Figure 4.15 shows the design of the mechanism in the Dassault Systems SolidWorks software for one reference position along the wing span, with the dimensions of the bars. Figure 4.16 shows the Fowler flap motion from the retracted position up to the designed flap extension: initial retracted position a), intermediate position b) and final extended position c).

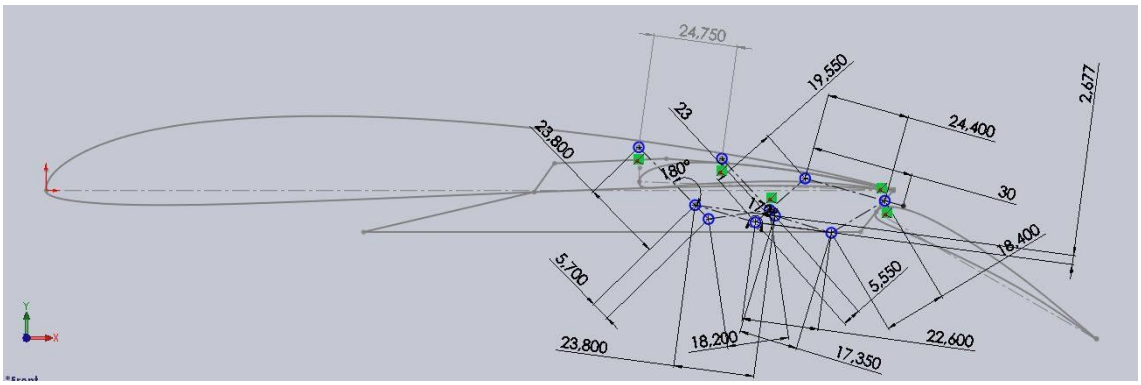

Figure 4.15 - Design of mechanism in Dassault Systems SolidWorks software.

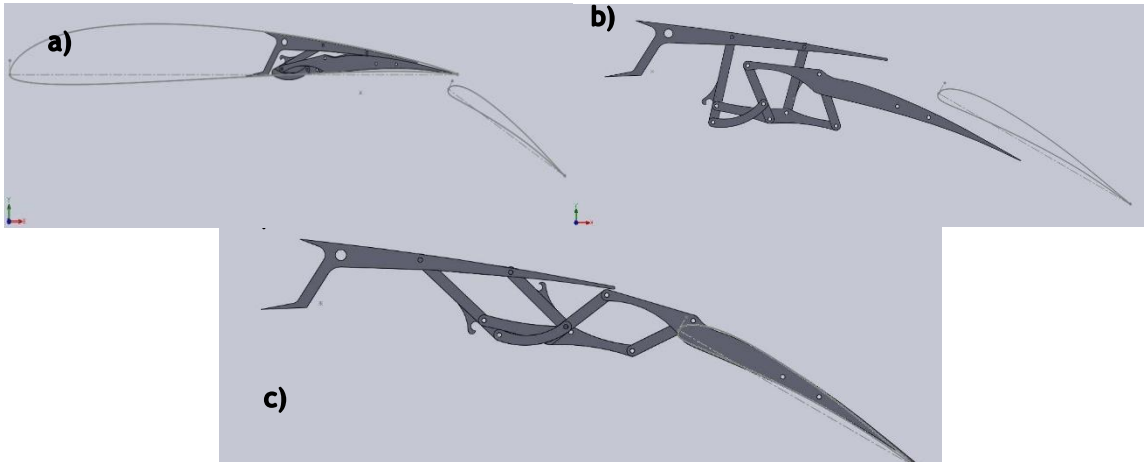

Figure 4.16 – Final design of the Fowler flap extension actuation mechanism. a) initial position, b) intermediate position and c) final extended position.

The finished Fowler flap mechanism has a weight between 20 to 24gr, once assembled, depending on the wing span position. The lighter (around 20 gr) corresponds to those placed towards the tips of the wing while the heaviest one (24 gr) is placed at the root of the wing.

Elastic bands ensure that the Fowler flap returns to the retracted position. (See Figure 3.14). The actuation of full the Fowler flap mechanisms set was meant to be performed by a high torque servo placed in the wing root region pulling Dyneema® strings, one for each span position flap mechanism. One of the difficulties to implement the actuation system was the difference of the extension length according to the span position of each flap mechanism. This was overcome by pulling each string by a dedicated pulley with the correct diameter for the corresponding extension mechanism span position.

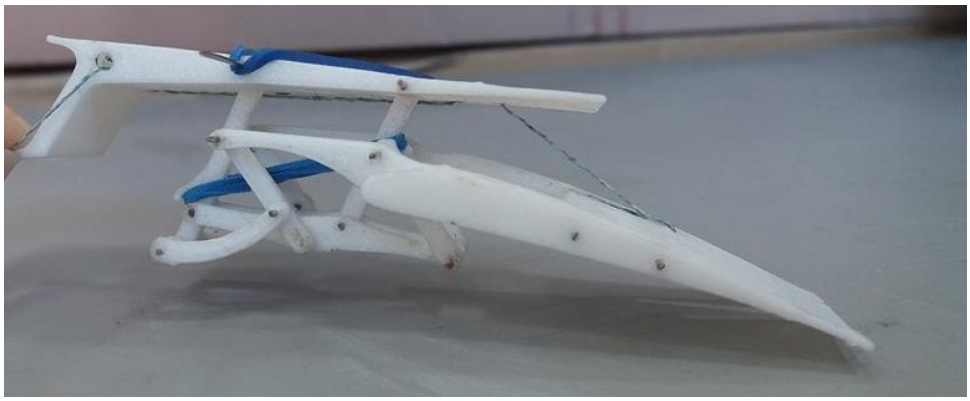

Figure 4.17 -Built 3D print Fowler flap actuation mechanism.

4.3 Parametric Studies

Figure 4.19 shows the study of the chord influence on the flight task points. It is seen that there is an optimal chord at 0.22m, but this is too small from a structural standpoint. So, as in most engineering problems, since the formulation is not perfect, there is never a perfect multidisciplinary optimization and a good compromise must be chosen as a design point.

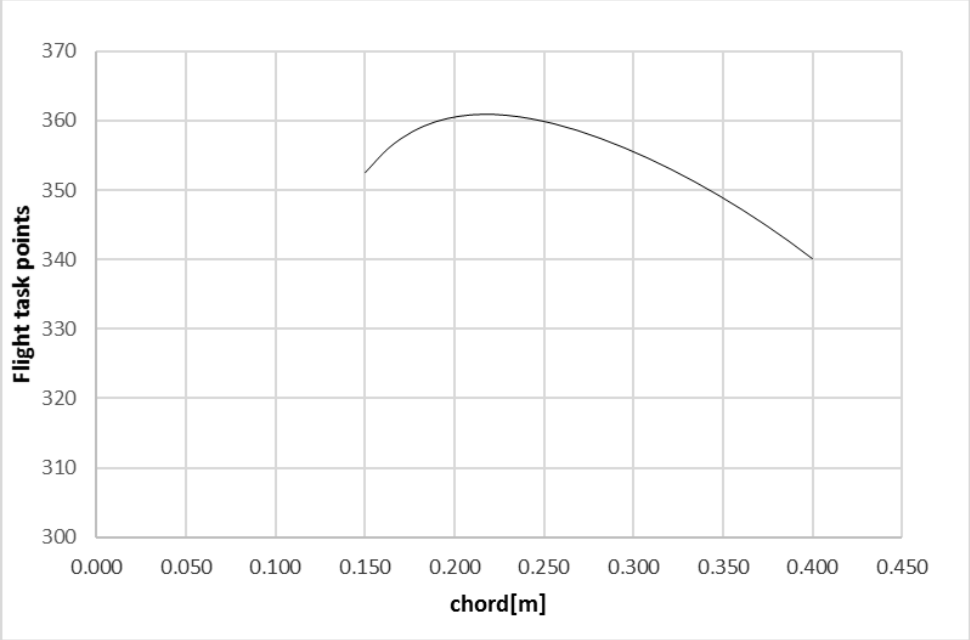

Figure 4.18 - Parametric study results regarding the chord influence on the flight task points. (b=4.26m) considering a constant TOW.

Figure 4.19 shows the parametric study results regarding the chord influence on the flight task points for different spans considering the TOW is limited by the 60m TO run. Greater chords for the same wingspan will naturally result in both higher takeoff weight as well as more flight task

points; but it is obvious that for each combination, there is an optimum compromise between increasing the chord and getting more points.

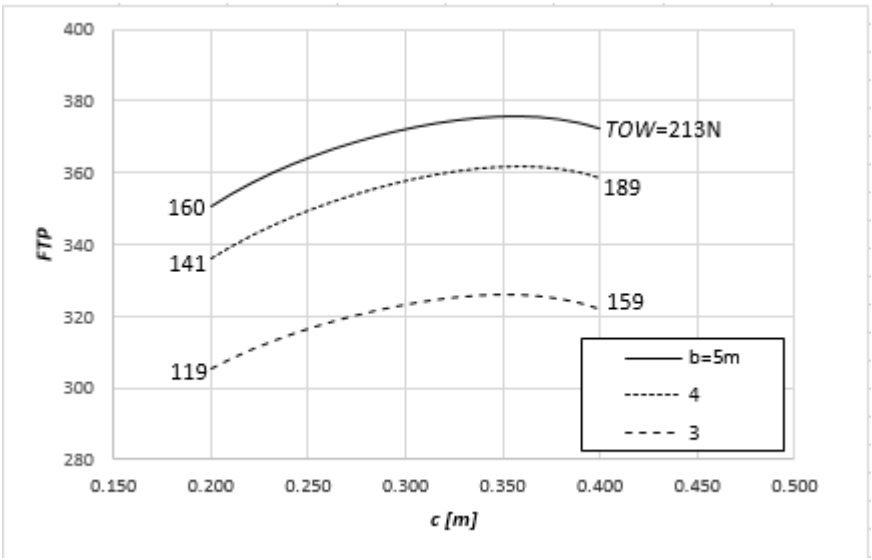

Figure 4.19 - Parametric study results regarding the chord influence on the flight task points for different spans considering the TOW is limited by the 60m T/O run.

4.4 Performance

A rather complete analysis of performance can be obtained once we have the available and required level flight power curves (See Figure 4.20). Nevertheless, only a basic flight performance prediction was performed. The required power curve for level flight versus airspeed was obtained from the flight mechanics model described in Section 3.3.2.6 with 16kg maximum take-off weight at 0m altitude. The available power versus airspeed corresponds to the propulsion system experimental data. It is seen that an ample excess power margin was left for achieving good climb performance and execute the high load factor turns in the speed flight task.

Through the model used in Section 3.3.2.6.1, a stall speed of about 9m/s is obtained, the best climb airspeed is estimated to be 16m/s with a climb rate, RC, of about 0.8m/s, the best climb angle, γ, is about 3.7º at 13m/s. Maximum level airspeed is about 24m/s.

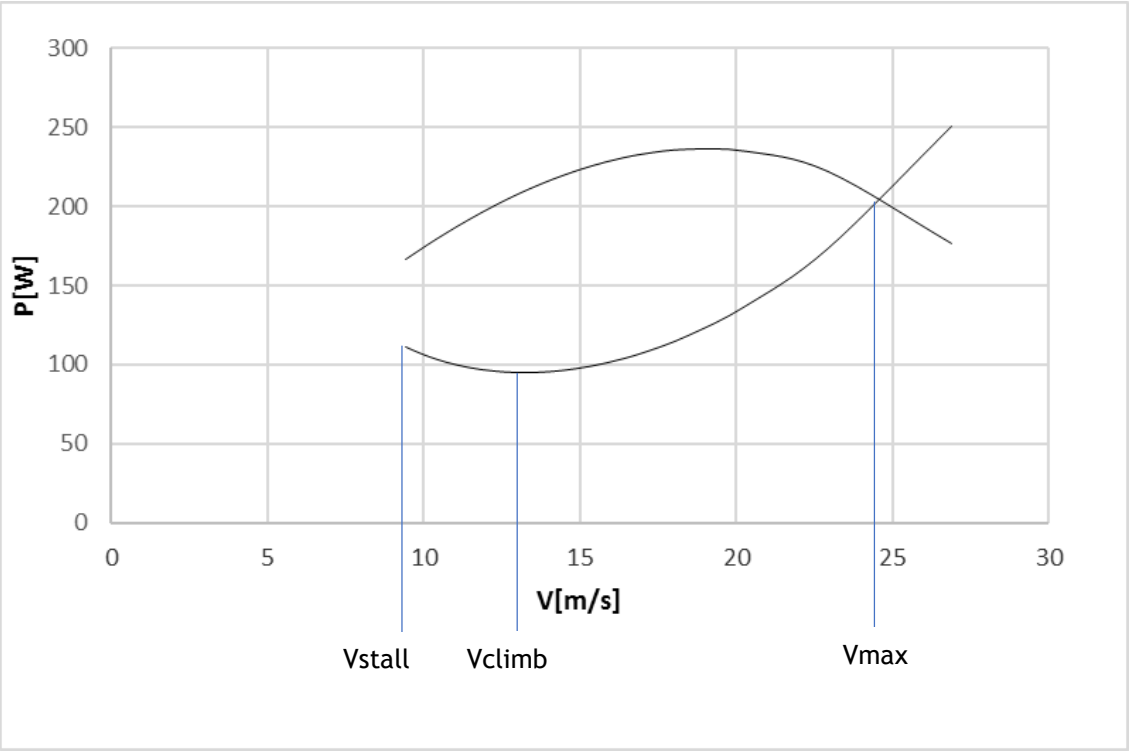

Figure 4.20 - Available and required power versus airspeed.

4.4.1 Estimated Payload Versus Altitude

The ACC17 regulations require that a payload versus density altitude prediction chart is presented for the aircraft. The variation of the payload that the aircraft can carry as a function of altitude is shown in Figure 4.21. To obtain these results, the calculation method presented in Section 3.3 was used; the altitude changed while the payload was the value adjusted such that the take-off 60m distance requirement was met. These results are optimistic prediction because the propulsive model was not corrected for the altitude change.

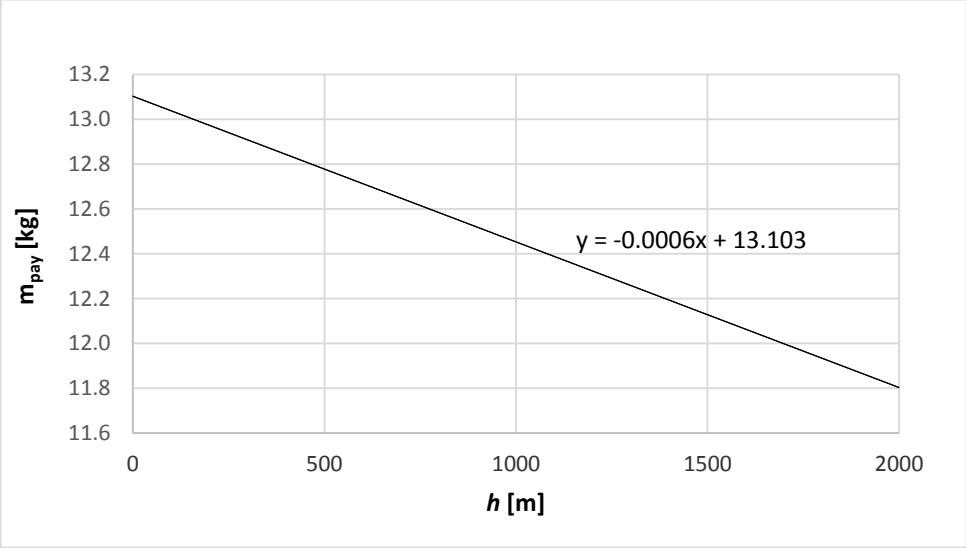

Figure 4.21 – Payload versus altitude prediction.

4.4.2 XFLR5 Final Design Wing Performance

The final wing design point is 4.2m for the span and the mean aerodynamic chord is 0.26m, with one central panel, and two panels on the tips. Small wingtip panels are used do accommodate the wingtips dihedral.

Figure 4.22 shows the initial design and the final design wings drag polars. The final wing design is seen in Figure 4.23. It is clear that the final wing drag polar has been shifted to the right and down corresponding to a faster and aerodynamically cleaner final wing design. This means that there will be a higher excess thrust and that the maximum airspeed will also be higher since the available thrust curve will intercept the graph at a higher airspeed

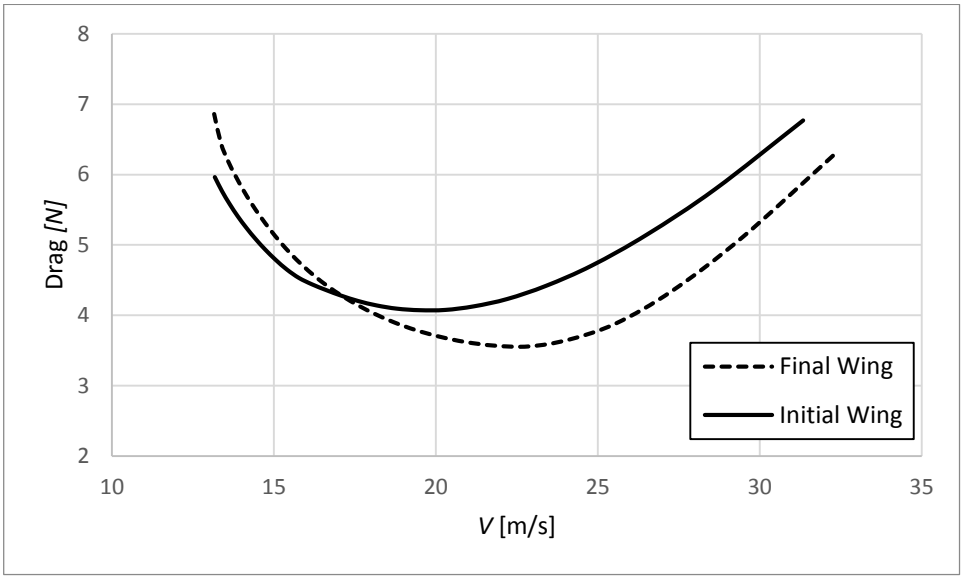

Figure 4.22 -Wing Drag polar comparison.

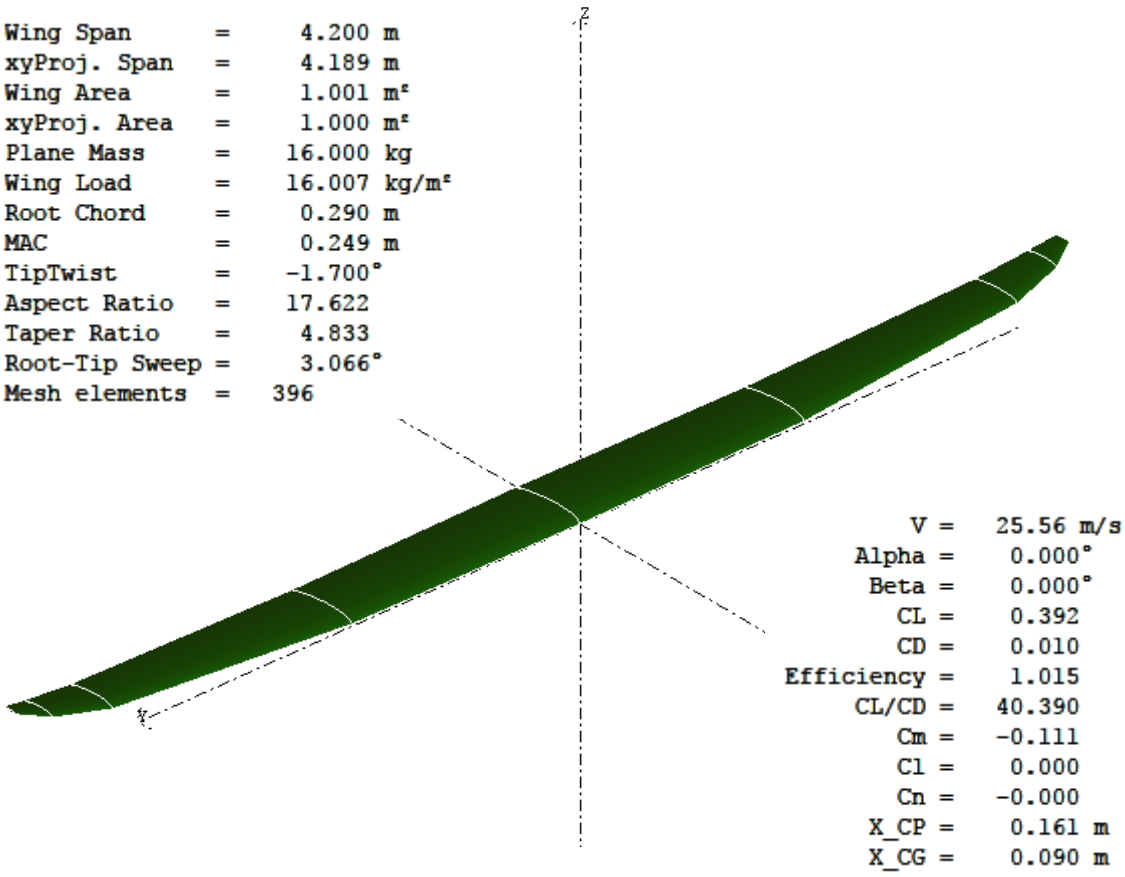

Figure 4.23 - Final wing design prediction data obtained with XFLR5 (b=4.2m).

Table 4.1 shows the final dimensions of the wing panels and the airfoil of each panel. The wingtip wing panel airfoil is different from the central wing panel airfoil.

Table 4.1 - AERO@UBI_MARS measures of final wing in XFLR5.

Y [m]	chord [m]	Offset º	Dihedral º	Twist º	Airfoil
0	0,29	0	0	0	MS101_383
0,9	0,27	0,01	2	0	
1,8	0,19	0,07	8	-0,75	
2	0,13	0,115	14	-1,4	MST113_310
2,1	0,06	0,17	-	-1,7	

4.5 Stability and Control

Using the model described in Section 3.3.2.5, the ACC17 aircraft has a static margin above +0.15, thus guaranteeing adequate level of static longitudinal stability. The actual airplane proved stable in all axes during the final test flights before the competition but the Fowler flaps were never deployed.

4.6 Final Airplane

4.6.1 Final Airplane 3D CAD

The final aircraft was drawn on DS CATIA V5, see Figure 4.24.

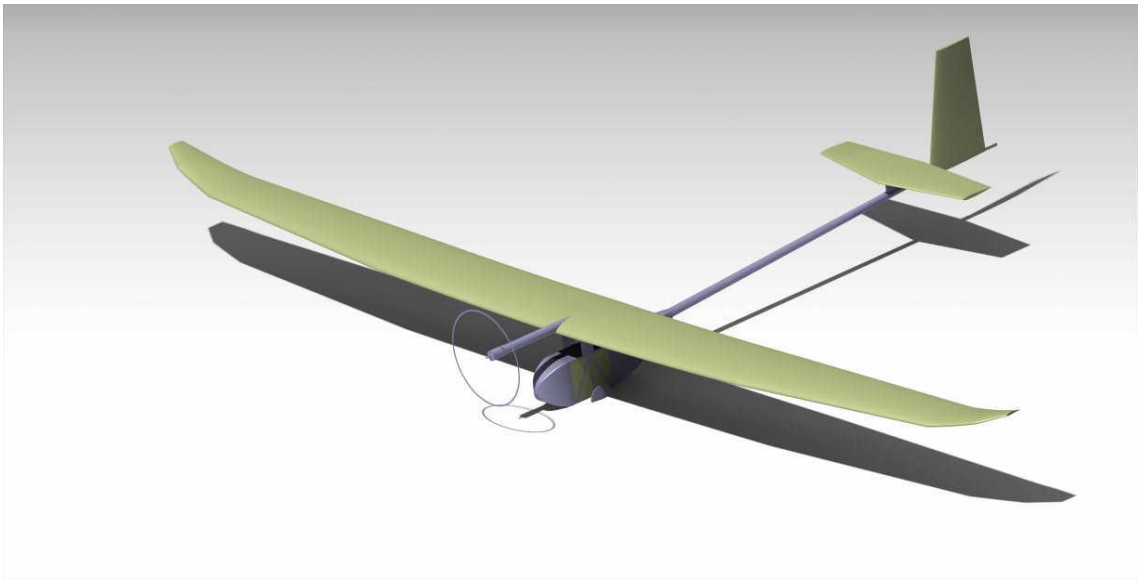

Figure 4.24 – Final aircraft, designed in CATIA V5.

Once the design was finished in CATIA V5, we obtained the 3 view drawings of Figure 4.25.

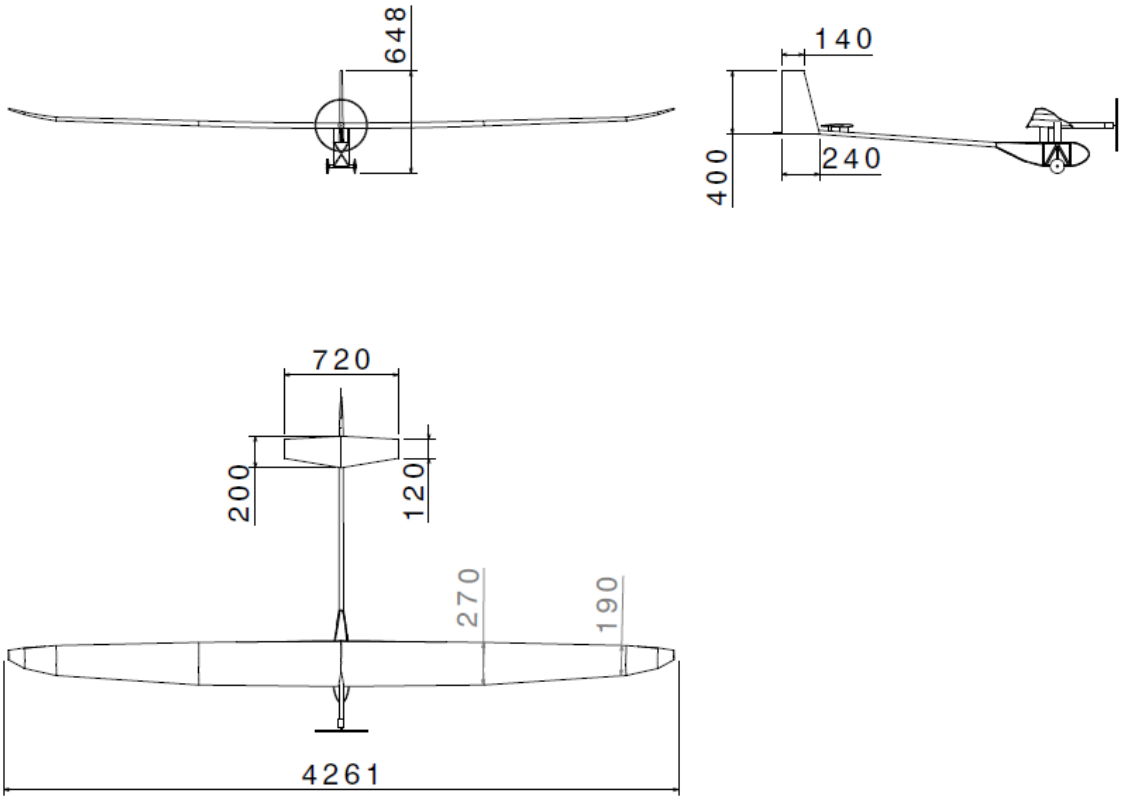

Figure 4.25 – 3 View drawings of the ACC 2017 plane.

To draw the fixed wing aircraft in CATIA V5, the dimensions of Table 4.2 were used. This table shows additional and detailed information regarding the wing and tail panels.

Table 4.2 - AERO@UBI_MARS airplane dimensions.

	Vertical Tail	Horizontal Tail	Wing
b [m]	0.4	0.72	4.2
c_{Root} [m]	0.24	0.2	0.29
c_{Tip} [m]	0.14	0.12	0.06
Area [m^2]	0.04	0.1152	1
Airfoil	NACA0009	NACA0009	MS101_383 and MST113_310

4.6.2 Flight Test Aircraft

Figure 4.26 shows the aircraft before one of the flight tests. The major problem that was faced was the lack of time, which prevented the team from being able to implement the Fowler flap actuation system and to complete the flight intended testing program and pilot training required for the ACC competition. The initial test flight was a slope soar in the mountain with tail surfaces that belonged to the ACC15 UBI's airplane. Only one take-off was performed with 3.5 kg payload (the <60m distance was met) and the actual airplane tail surfaces but vertical

tail flutter was encountered because the hinge was placed behind the one quarter position of the mean vertical tail chord and the actuation servo was attached to the rear of the rudder in a special actuation mechanism. This problem was corrected for the competition.

Figure 4.26 – The finished aircraft.

4.6.3 Wing Structure Testing

A structural test was performed to simulate the 160N (equivalent to two lead-acid batteries used as load). Figure 4.27 shows two people lifting the wings by their tips as defined in the ACC17 regulations. Only after this wing bending structural test that validated spars, the separation of the panels was performed such that the airplane could fit inside the transportation box. The wing panels interfaces hard points should have been placed when the two wing halves were joined. Unfortunately, despite being ready to be used, they were forgotten outside in the pressure of the delayed construction. This proved impossible to overcome before the competition deadline preventing the airplane from flying in ACC2017.

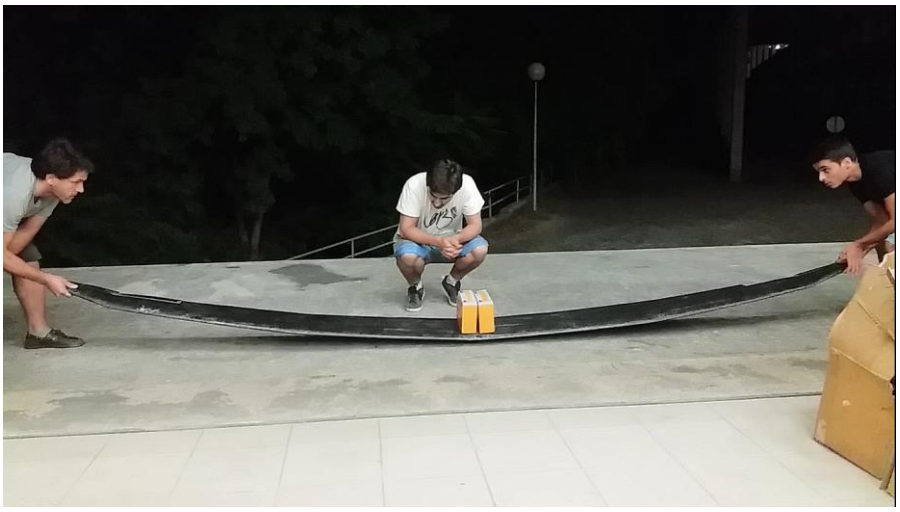

Figure 4.27 – Wing structural test.

The final wings weight was about 2.3kg (a value that exceeded the prediction) but test flights proved that the sandwich construction employed was perhaps too resistant (thus too heavy) since the aircraft crashed several times but the wing remained intact, except for one flight, in which the wing struck directly a rock and damaged the leading edge of one of the panels on the left wing. The repairs with carbon and resin were quick and easy to perform.

4.7 ACC17 Participation

During the first day of the contest, the oral presentations were performed, as well as the technical inspections. Since AERO@UBI_MARS was team number one, they performed the oral presentation first (as well as showing the flight test video). In this part of the contest, the team got 85.5 points.

During the second day, the team worked to finish the wing panel interfaces, which had not been placed in the wing at the right time. The team tried to glue the interfaces hardpoints with 15-minute epoxy but without success because the access to the inside of the wing to place the glue was almost impossible.

On the third day, the team glued the interfaces and passed the technical inspection. The team tried to perform a flight with 5 kilograms payload. Since we were unable to install the Fowler flap mechanism, maximum lift coefficient was severely reduced and thus takeoff performance was hampered. Although the team passed the structural test, the aircraft was unable to take-off in 60 meters and the flight was declared invalid. The attention of UBI for the last flight round turned exclusively to the second UBI airplane because it had flown 3 times but none valid and was in a better position to obtain a valid flight.

The team AERO@UBI_MARS in Figure 4.28 finished in 23rd place with only 85.50 points. The second UBI ACC17 airplane, Team AERO@UBI_PVG Figure 4.29 got the 20th place, with the valid flight in the 5th flight (and last) round of the competition. This was the worst result UBI got in an ACC edition so far, but the lessons learned will surely strike home and help to succeed in the future.

Figure 4.28 - AERO@UBI_MARS ACC team.

Figure 4.29 - AERO@UBI_PVG ACC team.

5 Conclusion

This Dissertation documented the development and participation of UBI's AERO@UBI_MARS team in the Air Cargo Challenge competition thus archiving the accumulated know-how over many participations in ACC editions. An analysis of previous competitors allowed the identification of technologies that increase the competitiveness of the aircraft.

Using a combination of low fidelity models (Excel), medium fidelity models (XFOIL/XFLR5) and high-fidelity models (OpenFOAM®), new low Reynolds number airfoils have been developed, as well as a Fowler flap. The flap that was developed has an innovative extension mechanism that should prove useful for UAV applications. Propulsion system tests have shown that heated LiPo batteries and a carefull choice of the battery model can have a significant impact for higher performance.

Flight tests with purpose built gliders have proved the effectiveness of roll spoilers for roll control as well as the actual effectiveness of a low Reynolds number Fowler flap.

3D printing technologies and moulds have been used to build the wing shells and flap. The construction of the wings with moulds has proven to be a challenge. The setbacks arising from the lack of experience with this technology are part of the reason why the participation of UBI in the ACC 2017 was not as successful as intended.

As future work, further research and experience with the mould construction technology should be accumulated to ensure that UBI teams remain competitive in the ACC competition.

Bibliography

[1] Wikipedia, “Air Cargo Challenge,” 2017. [Online]. Available: https://en.wikipedia.org/wiki/Air_Cargo_Challenge. [Accessed: 06-Sep-2017].

[2] Euroavia Stuttgart, “Regulations for the Air Cargo Challenge 2015,” no. October 2014, 2014.

[3] A. C. Challenge, “Requirements , Rules and Evaluation for the Air Cargo Challenge 2017,” 2016.

[4] S. GUDMUNDSSON, *General Aviation Aircraft Design : Applied Methods*, 2014th ed. UK, 2014.

[5] M. Sadraey, *CHAPTER 5 WING DESIGN*. .

[6] M. Drela, “Low-Reynolds-number airfoil design for the M.I.T. Daedalus prototype- A case study,” *J. Aircr.*, vol. 25, no. 8, pp. 724–732, 1988.

[7] M. S. Selig, “Low Reynolds Number Airfoil Design Lecture Notes - Various Approaches to Airfoil Design,” *Low Reynolds Number Airfoil Des. Lect. Notes - Var. Approaches to Airfoil Des.*, no. November, pp. 24–28, 2003.

[8] A. Deperrois, “XFLR5: a tool for the design of airfoils, wings and planes operating at low Reynolds numbers,” *Softw. Packag.*, 2010.

[9] J. McArthur, “AERODYNAMICS OF WINGS AT LOWREYNOLDS NUMBERS: BOUNDARY LAYER SEPARATION AND REATTACHMENT,” no. May, 2008.

[10] A. Stuttgart, “Air Cargo Challenge 2013 Project Report,” no. 27, 2013.

[11] J. Andrašec, M. Balaško, J. Čulina, and I. Knezović, “Projekt letjelice HUSZ Tern,” 2016.

[12] “AkaModell München e.V.,” 2015. [Online]. Available: https://www.facebook.com/akamodell/photos/ms.c.eJxFjskNAwEMAjuKbHz331gUe8N~_RzCgWaGWwFhXQj76AD2gBEgJR9cfmKEg40Ygm6hhpS~;RTPgBEORV6HDZWWHCbROZBHdMeMz9B2K44nWV1zE7C14P20rzaZyj~_wXriCA4aVCachV8AS~;4QW0~-.bps.a.1673960789505164.1073741830.1473247536243158/167. [Accessed: 11-Sep-2017].

[13] “EUROLIFTER Team,” 2015. [Online]. Available: https://www.facebook.com/Eurolifter-316214115167287/. [Accessed: 11-Sep-2017].

[14] M. A. R. Silvestre, J. P. Morgado, P. J. Alves, P. M. Santos, P. M. Gamboa, and J. C. Páscoa, “Propeller Performance Data at Low Reynolds Numbers,” *Int. J. Mech.*, vol. 9, no. January, pp. 1–18, 2015.

[15] P. V Gamboa and M. A. R. Silvestre, “Airfoil Optimization With Transition Curve As Objective Function,” *VI Int. Conf. Adapt. Model. Simul. ADMOS 2013*, no. June 2013, pp. 1–12, 2013.

[16] A. Oliveira, “Low Reynolds Number Fowler Flap Design,” 2017.

[17] H. H. Wentz, W; C. Seetharam, “Development of a Fowler Flap System for a High-

Performance General Aviation Airfoil," no. December 1974, 2017.

[18] "Weather Study," 2017. [Online]. Available: https://www.worldweatheronline.com/. [Accessed: 10-Sep-2017].

[19] FPA, "Federação Portuguesa de Aeromodelismo," *Agenda do Aeromodelista*, p. 60, 2014.

[20] C. P. Van Dam, "Induced-Drag Characteristics of Crescent-Moon-Shaped Wings C.P.," vol. 24, no. 2, pp. 115–119, 1987.

[21] P. Raymound W., *Helicopter Aerodynamics. Rotor Wing International*. 1985.

[22] T. Abramowski, "NUMERICAL INVESTIGATION OF AIRFOIL IN GROUND PROXIMITY," *J. Theor. Appl. Mech. 45, 2, pp. 425-436, Warsaw 2007*, vol. 45, pp. 425–436, 2007.

[23] P. Albuquerque, P. Gamboa, and M. Silvestre, "Parametric aircraft design optimisation study using span and mean chord as main design drivers," *Adv. Mater. Res.*, vol. 1016, pp. 365–369, 2014.